A MULTI-PROXY STUDY OF THE KALKKOP IMPACT CRATER LAKE DEPOSITS IN SOUTH-CENTRAL SOUTH AFRICA: IMPLICATIONS FOR LATE NEOGENE CLIMATE EVOLUTION

Ponani Mthembi (BSc Hons)

Submitted in fulfilment of the requirements for the degree of

Master of Science

Department of Geological Sciences

UNIVERSITY OF CAPE TOWN

May 2014

Supervisors:

Professor Chris Harris

Dr Dave Roberts

Council for Geoscience

PLAGIARISM DECLARATION

I know the meaning of plagiarism and declare that all of the work in the thesis, save for that which is properly acknowledged, is my own.

ABSTRACT

The Kalkkop Crater Lake deposit formed as a result of a meteorite impact, and is situated ~51 km southwest of Graaff-Reinet in the Southern part of South Africa. The structure is about 650 m wide, and contains 90 m of lake deposits that are mainly carbonate precipitates. A 90 m sediment core from the Kalkkop Crater Lake was investigated using sedimentology, palynology and geochemical analysis. The KK1 core, along with the other two boreholes (KK2 and KK3), comprise of finely laminated and massive, structureless carbonates interrupted by debris flows from the crater rim.

All samples of the KK1 borehole have the same Zr/Y (~5.3) and Zr/Nb (~10) ratios which suggest that composition of the non-carbonate component dust remained constant throughout deposition. There is a good positive correlation between $\delta^{18}O$ value and $^{87}Sr/^{86}Sr$ ratio in the carbonate sediments. Evaporation is the most likely process that caused an increase in $\delta^{18}O$ value, and it is suggested that evaporation was related to dry conditions and an increase in the addition of dust. The dust would have contained easily dissolved radiogenic Sr, therefore there is a relationship between the degree of evaporation and an increase in Sr-isotope ratio There is a strong positive correlation between $\delta^{13}C$ and $\delta^{18}O$ in the lower half of the core (>45 m depth). This is ascribed to a rapid loss of CO_2 from solution which resulted in non-equilibrium kinetic fractionation between the HCO_3- and CO_2. These data have no palaeoclimate significance, other than indicating that evaporation was effective, and in turn implying a dry climate. Above 45 m depth (upper section of the core), there is less correlation between $\delta^{13}C$ and $\delta^{18}O$, which means that it is possible to use these data as a climate proxy. The observed increase in $\delta^{13}C$ may be influenced by lake salinity, decomposition and respiration of plants/cyanobacteria, groundwater and runoff (isotopically heavier CO_2 under arid conditions), equilibration of atmospheric CO_2 with the lake and oxidation of lacustrine and terrestrial organic matter. Cyanobacterial mats preferentially extract CO_2 from the lake water (enriching them in ^{13}C), and are favoured by hypersaline conditions formed in arid settings.

Besides the overall core samples from borehole KK1, small interval samples at 47.4-47.76 m (B1-B19), and at 66.83-67.47 m (A1-A24), showed variation significantly greater than the analytical error.

Previous unpublished palynological work which was incorporated into the present study, showed the presence of humid sub-tropical to tropical arboreal species at some depth intervals, as well as the moist, more temperate genus *Podocarpus*, -indicating a climate contrasting with the present semi-arid conditions. Other intervals are more dominated by grasses and sclerophyllous *fynbos* taxa, suggesting fluctuating wetter and drier periods, confirmed by stable isotopes which, along with mineralogy, also illustrate an overall aridification through time.

Previous studies, using radiometric dating methods, suggested that the age of the Kalkkop was ~250 ka. However, it was observed that the crater rim has been almost entirely eroded and by analogy with other similar size impact craters, it became evident that it must be much older than this. The present-day diameter of the lacustrine carbonate deposits of the Kalkkop crater is ~650 m, which is the size of the impact structure as quoted in the literature. This diameter is similar to the present day to diameter of the Tswaing Crater Lake located near Pretoria, but whose rim-to-rim diameter is 1130 m. From eroded remnants of the crater rim at Kalkkop and by analogy with Tswaing, the original rim- to -rim diameter of the Kalkkop crater would have been ~1,200 m rather than 650 m. Given that the rim is for practical purposes completely eroded, and was originally ~50 m high, this suggests an age of ~6.3 ±1.6 Ma, i.e. latest Miocene, as calculated from the estimated rate of erosion of the rim. The geochemical data therefore fits with other proxies in this study and it is concluded that the Kalkkop Crater Lake was deposited during dry conditions.

DECLARATION

I, Ponani Mthembi, hereby declare that the work on which this thesis is based is my original work (except where acknowledgements indicated otherwise) and that neither the whole work nor any part of it has been, is being, or is to be submitted for another degree in this or any other university.

I empower the university to reproduce for the purpose of research either the whole or any portion of the contents in any manner whatsoever.

Name: Ponani Mthembi

Date: May 2014

ACKNOWLEDGEMENTS

First of all I would like to thank the Almighty God, for giving me the ability and strength to do this project.

My supervisor Professor Chris Harris and co-Supervisors Dr Dave Roberts as well as Dr Roger Smith for their guidance and assistance throughout, thank you.

Secondly, to my sponsors InkabaYeAfrika especially Professor Maarten De Wit, thank you so much for giving me this opportunity, for all the funding and the exposure. To the Council for Geoscience, Dr Luc Chevallier, thank you for your patience and time given to me to complete this project. Also to thank my colleagues who helped me with graphics and support, Dr Chiedza Musekiwa, Ms Claire Browning and Mr Ishaam Davids.

And many thanks to Mr Ian Newton, Archaeology department (UCT) and Ms Fayrooza Rawoot, Geology Department (UCT) for their assistance in the Stable Isotopes lab. Thanks to Professor Louis Scott, Department of Plant Sciences, University of the Free State for his input on the pollen study. I would also like to thank Dr Heinz Wilkes, Helmholtz-Zentrum Potsdam (GFZ), for assisting at the beginning of the project and providing most of the references.

To my partner Mr Dinga Mnisi thanks for your love and support. To all my friends Hadjira, Melissa, Winnie, Chido, Dawn and Lettie, thank you so much for your kind words of encouragement.

And lastly, to my family (including Mushwana family), thank you for the support and the love throughout my studies, especially mom Mhlavasi, my brother Oscar, my sister Sharon, and my niece Kimberly.

TABLE OF FIGURES

TABLE OF CONTENTS

1. INTRODUCTION

1.1. GENERAL INTRODUCTION

The Kalkkop impact crater is situated ~51 km southwest of the town of Graaff-Reinet on a low relief plain, in the semi-arid Karoo biome of southern South Africa. The crater palaeo-lake deposits are about 0.6 km in diameter at surface and 90 m in thickness, potentially providing a long and detailed record of palaeo-environments during the time span of deposition. Since the discovery of the site in the 1940's, several exploratory boreholes have been drilled through the succession in the search for oil and diamonds, it was previously thought to be an explosive diatreme (Koeberl, 1994; Reimold *et al.,* 1998). The last boreholes were sunk in the 1990's and their interpretation conclusively demonstrated the impact origin of the crater (details in Chapter 2.2).

Sand and dust are blown and washed into crater lakes, which along with the lacustrine chemical precipitates, constitute the lacustrine lithofacies. The study of crater lakes is important because they can be used as terrestrial dust and geochemical archives and they preserve high resolution sedimentary records of fluctuating palaeo-environments, climatic and records. Crater lakes are closed systems and their hydrochemistry is archived in the geochemistry of the palaeo-lake precipitates (Zolitschka *et al.,* 2006). Organic remains representing sspecialized faunas and floras thrive in the lakes, supplemented by pollen blown in from the surrounds become preserved in the lake sediments, providing a direct record of contemporary biodiversity. In palaeoclimate research, stable isotopes, strontium isotopes and trace elements in sedimentary carbonates provide significant sources of information of depositional environments (Zhao *et al.,* 2009). Thus analysis of the lithofacies and palaeontology, along with the stable isotopes, mineralogy, and trace elements of the various lithofacies components should record regional and local fluctuations in the atmosphere, lithosphere, hydrosphere and biosphere in the timescale of lacustrine deposition (Colman, 2007).

At the commencement of this study, the later Pleistocene age (~250 ka) of the Kalkkop Crater Lake deposits as inferred by U-series dating on palaeo-lake carbonates (Reimold *et al.,* 1998) was accepted as being correct.

It was on the basis of this time frame that Mazus, (1999) compiled a preliminary (unpublished) internal report for the South African Council for Geoscience, that included the palynology, sedimentology and stable isotopes of the finely laminated, carbonate dominated palaeo-lake deposits. The intention of this study was to complement the previous study with more data from the longest core and present the combined information on late Quaternary environments in a form accessible to the scientific community. However, a visit to the site in 2010 revealed the highly degraded nature of the crater rim and the positive weathering relative to the surrounds of the crater fill sediments. In contrast, the Tswaing impact crater (Fig 1 and 2 (A-C)) some 900 km to the northeast which is also dated to ~250 ka is relatively pristine and contains an extant saline lake (Partridge, 1987). These observations, allied with palynoforms indicating periodic presence of sub-tropical forest (Mazus, 1999) in the presently semi-arid Kalkkop environs, suggest a Neogene age (6.3 ±1.6 Ma) rather than Quaternary age. Furthermore, the original estimate for the crater diameter is based on the surface diameter of the crater lake deposits (Fig. 1) in the absence of the (eroded) crater rim. However, it is evident that this represents a major underestimate of the original rim- to -rim crater diameter (the normal crater size metric), as shown for example by comparison with the well preserved Tswaing impact crater (Fig. 1).

Neogene fluvio-lacustrine records from the winter rainfall region of the southwestern Cape are characterized by the presence of palms and other tropical /sub-tropical taxa. This flora is in stark contrast with the Quaternary summer-dry adapted floras (Coetzee, 1980), representing a major upheaval in climate and ecosystems. The Neogene Knysna lignites are situated within the humid year-round rainfall zone of the southern coast, where temperate rain forest presently flourishes. Whereas the pollen record for the Knysna lignites suggest a past warmer/ wetter climate (Carr *et al.,* 2010), the contrast between the Neogene and Quaternary ecosystems is far less pronounced than in the winter rainfall region. Perusal of the literature showed that there is currently no Neogene record for the remaining major ecosystem of southern South Africa, namely the (semi-arid) summer rainfall region of the eastern Karoo and the intensity of the Neogene to Quaternary climate shift are unknown.

It has been shown that remote ocean /atmosphere phenomena such as El Nino/La Ninja currently affect rainfall in the summer rainfall region of southern Africa (Tyson, 1999), and it has been suggested that under the warmer Neogene climate regime a permanent El Nino may have existed in the east Pacific (Philander and Fedorov, 2003). However, the extent to which this may have influenced Neogene climate in the summer rainfall region of southern South Africa in the past is unclear-and the high resolution record offered by Kalkkop can potentially shed light on this issue. In view of the considerations discussed above, the chief aims of the study are to:

- reconstruct the original dimensions of the Kalkkop impact crater (prior to erosion) and provide a new age model;
- measure various palaeo-environmental parameters in the crater lake core
- use chemical-stratigraphy as a high resolution proxy record of fluctuating climates and ecosystems during the deposition of the finely laminated crater lake sediments;
- compare the Neogene climate/ecosystems in the summer rainfall region with adjacent year –round and winter rainfall regimes;
- tie the proxy data to the marine record to investigate correlations with global events and climate forcing mechanisms.

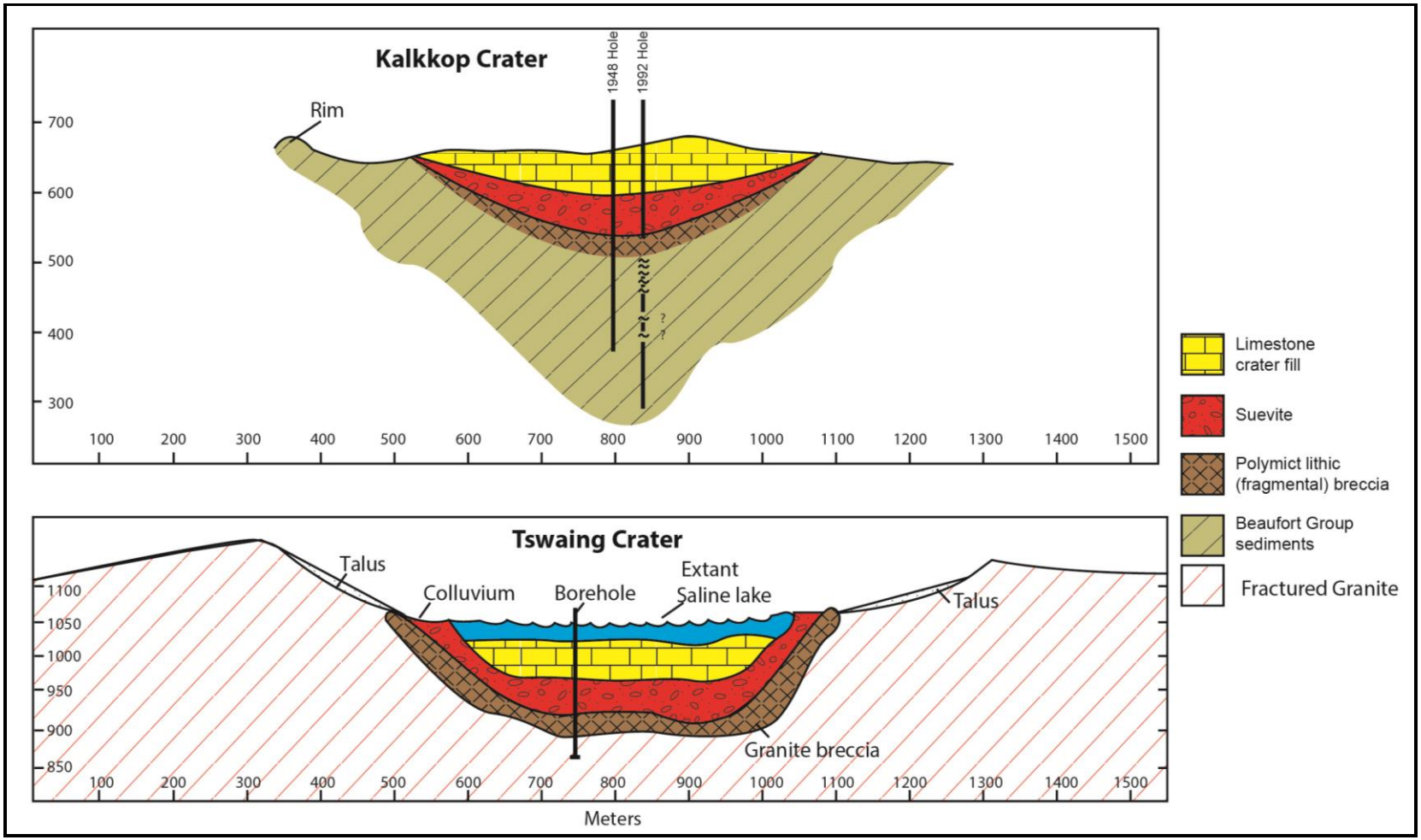

Figure 1: Cross section of Kalkkop and Tswaing craters showing the highly eroded Kalkkop rim (from Reimold *et al.*, 1998, redrawn by P. Mthembi).

1.2. CARBONATE LAKES

Lacustrine carbonates are mostly dominated by biogenic or bio-induced precipitates and these preserved sediments usually provide valuable information on the present state of a lake and its catchment environment, its history and past climate changes (Platt, 1991., Li *et al.,* 2012). According to Platt (1991), most work/literature that has been done on the description of modern carbonate lakes and their deposits has been based mainly on small lakes with varied geological histories. Meanwhile, most ancient lake deposits are thick and laterally extensive, recording deposition in very large, long lived, tectonically controlled lake basins (Platt, 1991). Most commonly lake carbonates comprise thin, 10-30 m thick, upward-deepening cycles. The sequence usually starts with fluvial, deltaic, or shoreline quartz sandstones overlain by carbonates of variable facies depending on the stage of the lake (Sarg *et al.,* 2012). The facies that follow may include molluscan coquina layers, rudstone or oolitic grainstone, and then followed by high salinity lake deposits as well as a few meters of thick stromatolites (Sarg *et al.,* 2012). It is still unclear what the palaeoenvironmental importance of lacustrine stromatolites is since their varying contexts suggest a range of possible lake salinities and chemistries. Platt, (1991) mentioned that fresh water to brackish water stromatolites, oncoids and algal travertines were found in Plio-Pleistocene of the East African rift and the Triassic of Greenland. Freshwater to mesohaline stromatolites with cyanobacterial layers were noted from the Oligocene of Southern France, the Eocene Green River Formation in the USA and the Cambrian of South Australia. Fresh water tufas and travertine may provide very good paleoclimatic and paleoenvironmental information with high temporal resolution, up to seasonal, monthly or even daily in resolution (Liu *et al.,* 2009). Several factors can influence carbonate precipitation by impacting physicochemical processes such as in/outgassing of CO_2 (Liu *et al.,* 2010). The endogenic carbonate (varves) have chronologic precision and biogeochemical sensitivity of annual layers which makes them an ideal archive for recording shifts in seasonal climate (Wittkop *et al.,* 2009). The study of isotope composition in carbonates has been used to interpret paleoenvironmental factors, because it is one indicator of environmental change in lakes, (Li *et al.,* 2012).

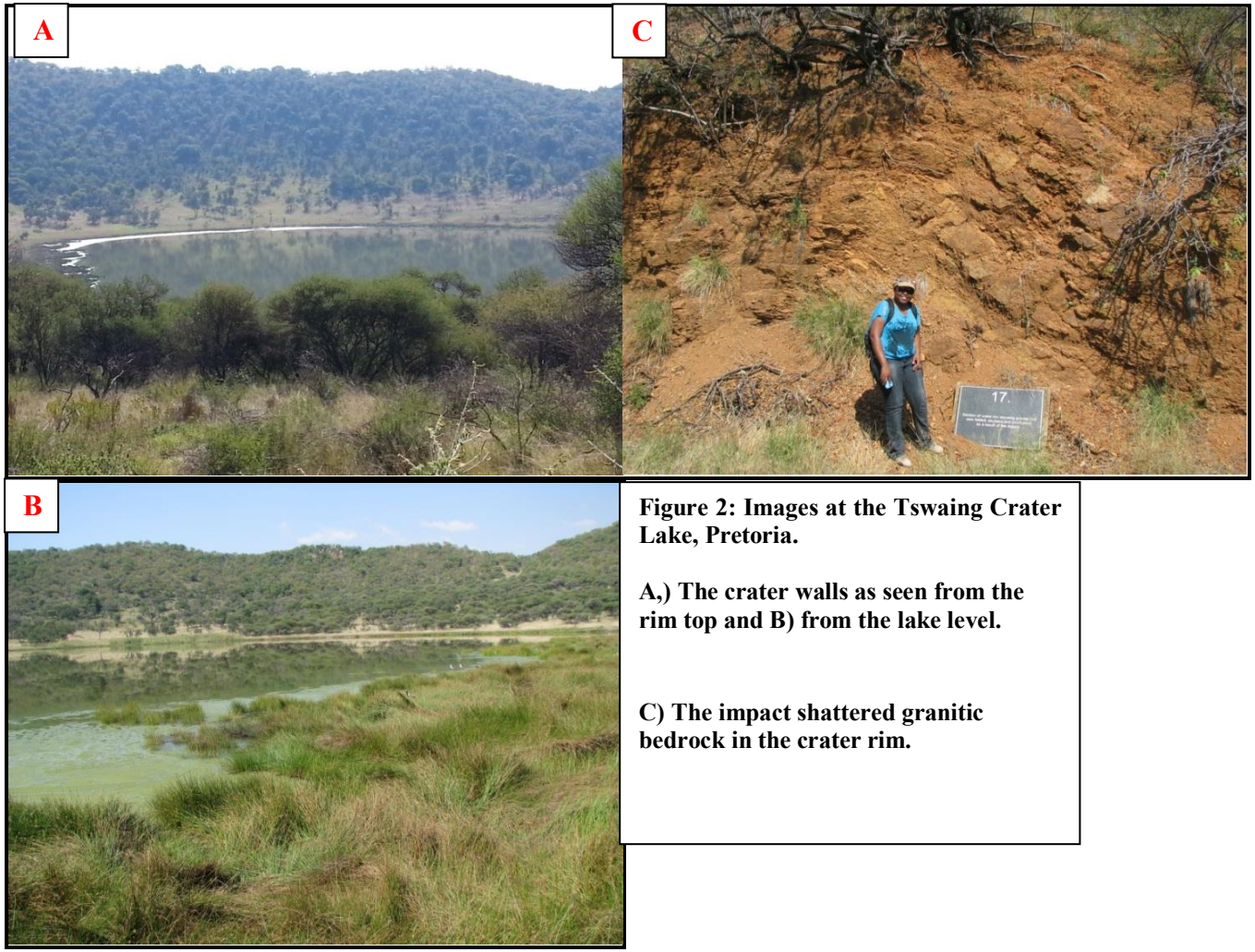

Figure 2: Images at the Tswaing Crater Lake, Pretoria.

A,) The crater walls as seen from the rim top and B) from the lake level.

C) The impact shattered granitic bedrock in the crater rim.

1.3. GEOCHEMISTRY

Stable isotopes have been used in palaeoclimate reconstruction since the 1950's (e.g. Maier and Titschack, 2010). The $\delta^{13}C$ and $\delta^{18}O$ ratios are reported as the relative deviation from a standard expressed in per mil (‰), (Talma and Netterberg, 1983). PDB (Pee Dee Belemnite) is a standard that is generally used in carbonates while SMOW (Standard Mean Ocean Water) is used to report the $\delta^{18}O$ values of rocks in most cases (Lee-Thorp and Talma, 2000; Talma and Netterberg, 1983), but the value of δ can be converted between the two standards (δ^{18} SMOW = 1.03 δ^{18} PDB + 30.4‰). The $\delta^{13}C$ value is a standard method for distinguishing the photosynthetic pathways of C3 and C4 plant groups (Kristen *et al.,* 2010, Lamb *et al.,* 2005). Evaporation has a major influence on the O isotope ratios of large closed lake systems, especially those in dry/arid regions, where water loss is mostly due to evaporation (Leng and Marshall, 2004).

Presumably, in an environment such as the saline Kalkkop crater lake, oxygen isotope ratios in the precipitating carbonate minerals are influenced by changes in temperature and hence evaporation, whereas carbon isotope values are controlled by the isotope composition of the dissolved carbon which in turn relates to the composition of the atmospheric CO_2, dissolved sediment influx and the ratio of C3/C4 plants in the biomass. It is therefore difficult to measure the isotope composition of carbonates and to be able to interpret the values into complete or even relative temperature variation without making assumptions or to resolve the proportions of C3/ C4 plants. A consistent problem in understanding geochemical proxies for climate in ancient lakes is the fact that it is only possible to measure the isotope composition of carbonate and not of the water from which it precipitated. This means that it is not possible to estimate directly the temperature of formation of the carbonate (Leng and Marshall, 2004). Carbon isotope composition of lake carbonates depends on the C-isotope composition of the biomass in the crater and the C-isotope composition of the atmosphere. The latter is unlikely to have changed significantly during formation of the lake sediments. Most terrestrial plants are C3, with all forest communities and most temperate zone plant communities of all kinds being dominated by C3 plants.

1.4 GEOLOGY AND GEOGRAPHICAL SETTING

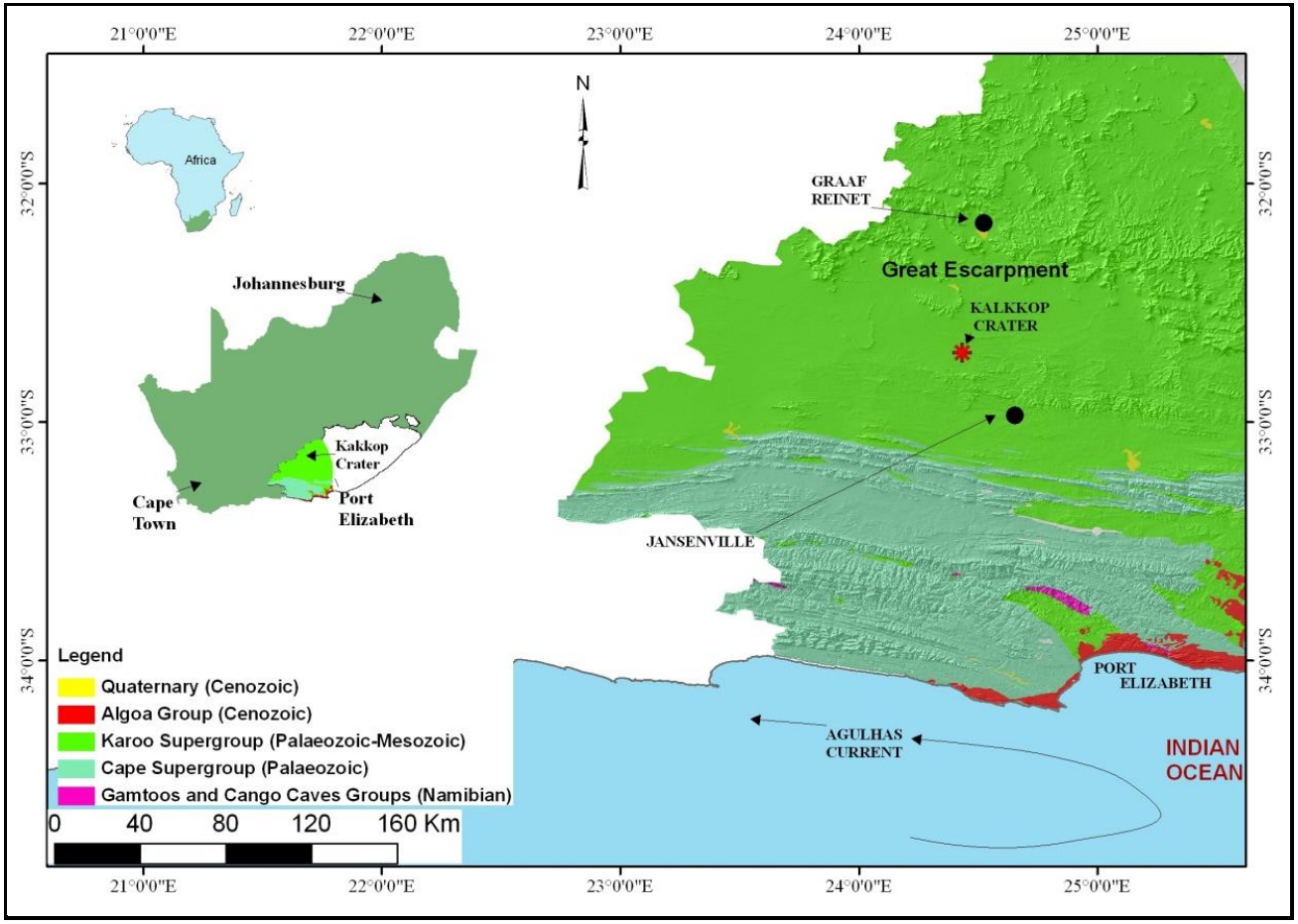

Figure 3: Geology and locality map of the Kalkkop Crater (data from Council for Geoscience 1:250:000 map)

1.4.1 Geology and topography

The Kalkkop impact crater is located on Uitgeleide Zeekoegat 508 farm (coordinates 32^0 42'30"S and 24^0 25' 57"E), ~50 km south-southwest of the town Graaff Reinet in southern South Africa (Fig. 3). The immediate surrounds of the site, which is at an elevation of ~650 m above sea level (ASL), comprise a low relief plane. The plane is bounded by the Great Escarpment ~40 km to the north, which is thought to have been initiated at the onset of the (Mesozoic) dismemberment of Gondwana and is incised into the Permo-Triassic lower Beaufort strata of the Karoo Supergroup. The escarpment separates the coastal platform from the elevated interior in southern South Africa (Partridge and Maud, 1987). The Cape Fold Belt Mountains binds the plain in the south, chiefly comprised of Palaeozoic quartzites which form the divide between the humid coastal belt and more arid interior. The Triassic Koonap Formation (Beaufort Group) formed the target rocks of the impact and consists of intercalated mudrock and sandstone, with minor chert lenses (Koeberl, 1994; Reimold, 1998). A schematic stratigraphy of the area is shown in Figure 4.

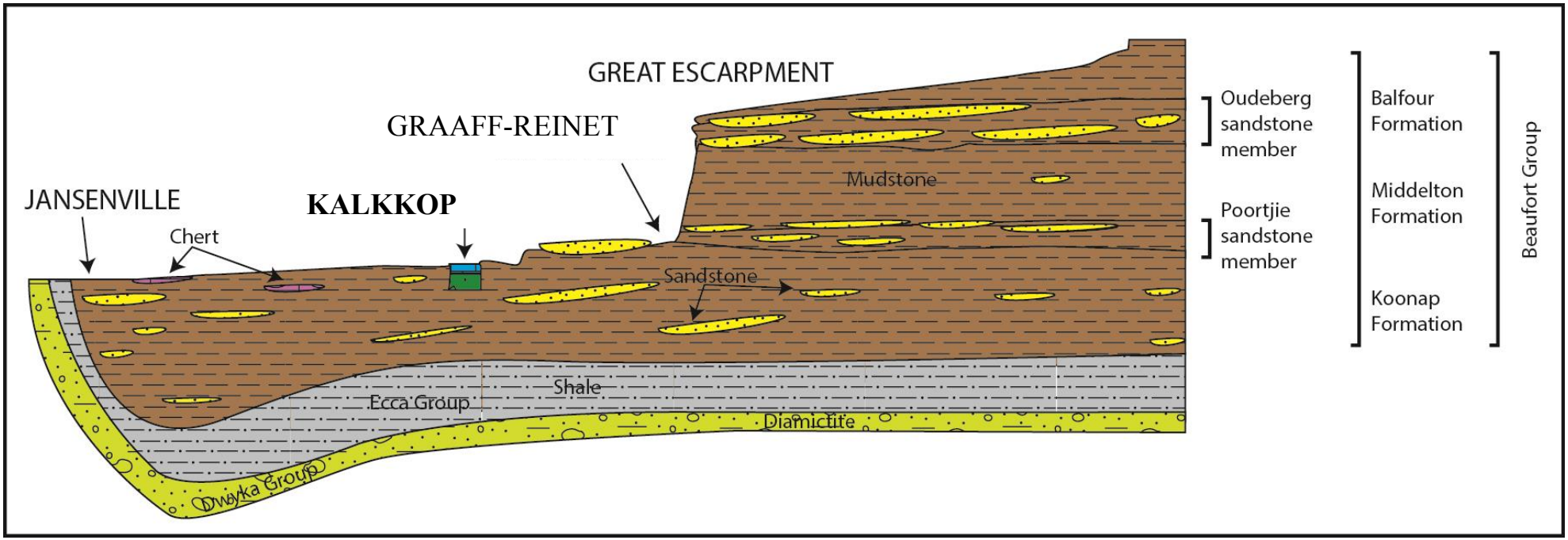

Figure 4: Schematic stratigraphy of the region around the Kalkkop Crater (Reimold et al., 1998).

1.4.2 Regional climate patterns

The southern region of South Africa can be subdivided into three major climate zones. In the southwest, a Mediterranean climate prevails where (winter) cyclonic polar frontal systems imbedded in the westerlies account for most of the rainfall (South African Weather Bureau, 1986; Tyson, 1999). The humid southern coastal region (south of Kalkkop) receives year-round rainfall, influenced by both the cyclonic and anticyclonic regional rain producing systems (Fig. 5). Kalkkop falls within the third climatic zone, namely the summer rainfall region of southern South Africa, more specifically in the (semi-arid) southern Karoo biome. The nearby town of Graaff-Reinet receives an average of 236 mm of rain per year, with the wettest months in the earlier and later summer. The lowest rainfall occurs in midwinter (6 mm) in July. The average midday temperatures for Graaff- Reinet range from 17.4°C in June to 30.4°C in January and the region is the coldest during July when average nightly temperatures drop to 2.5°C (South African Weather Bureau, 1986).

The relative aridity of the southern Karoo can partly be traced to the lofty Cape Fold Belt Mountains (up to 2300m), which form a rain shadow to both the cyclonic and anticyclonic regional systems that bring rain to the more humid coastal regions to the south and southwest. Precipitation in the summer rainfall region of southern South Africa is strongly influenced by the position of the northwest trending tropical-temperate trough that forms in response to the interaction between westerly and easterly waves (South African Weather Bureau, 1986; Taljaard, 1996; Tyson, 1999); moist air enters the trough from the continental tropics in the north and by onshore advection via the Indian Ocean Anticyclone (the warm Agulhas current plays a major role in this regard). The sector of the Karoo occupied by Kalkkop is located well southwest of the average position of the cloud bands associated with this trough, thus receiving relatively little rain from this feature (South African Weather Bureau, 1986; Taljaard, 1996; Tyson 1999). Cutoff lows, with a more random distribution over southern South Africa, are another major source of precipitation and develop mainly in spring (September/October) and autumn (March/April) (South African Weather Bureau, 1986; Taljaard, 1996; Tyson, 1999).

The nature and mutual boundaries of the major climate systems of southern South Africa as outlined above are thought to have fluctuated through time, in response to global events such as shifting landmasses and orbital forcing, as well as evolving regional atmospheric and oceanographic systems (Siesser, 1980; Tyson, 1999; Marean, 2010; Roberts *et al.,* 2011).

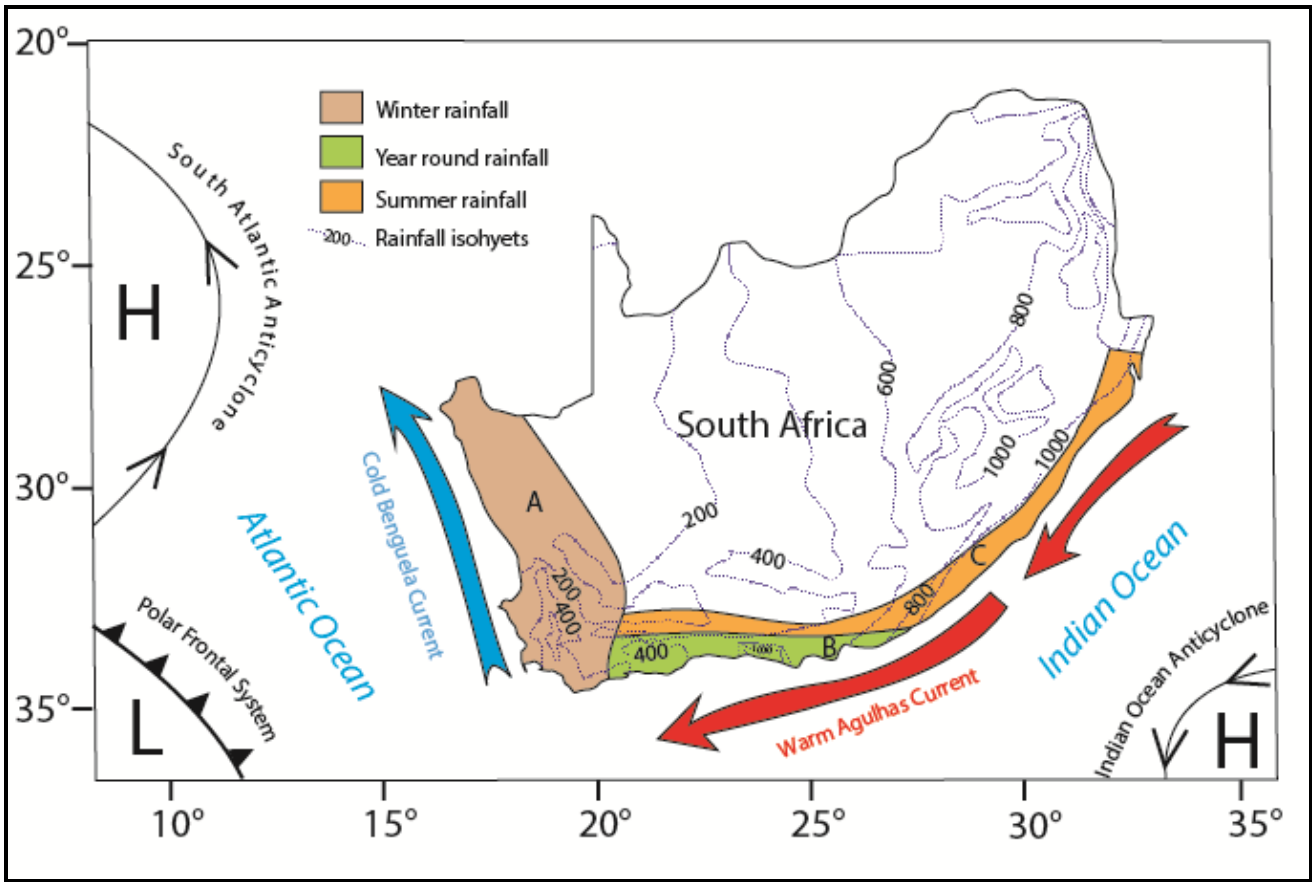

Figure 5: Climatic and oceanic conditions around the Southern African coastline. The Kalkkop Crater falls within a semi-arid, summer rainfall region (Roberts *et al.*, 2011).

2. ORIGIN AND CHARACTERISTICS OF THE KALKKOP CRATER

2.1 IMPACT CRATERS IN GENERAL

Impact cratering is one of the fundamental surface forming and modifying processes on all solid bodies in the solar system (Melosh, 1989, Koeberl 1994, Kumar 2005). Since the accretion stage of planets, impact cratering has played a major role in the geological and biological evolution of our planet (Koeberl, 1994). The population of impact craters must have once been much larger than what is preserved, due to modifying effects of geologic processes (Grieve, 1997). Smaller impact structures are prone to rapid erosion (Reimold, 2006), which is why only a handful of structures older than c.360 Ma are known. The presence of terrestrial impact structures or evidence of their existence is their circular outlines and the occurrence of shock metamorphic effects (Grieve, 1997); most of them can be recognized by geophysical anomalies (Reimold, 2006). According to (Schmieder, 2008), there are 175 impact structures (some shown in Fig.6) that have been recorded on Earth, and most of these structures have not been accurately dated as yet, with some notable exceptions. Eighteen (Fig.7) of these are found on the African continent, (Koeberl 1994). The target rocks provide the maximum age and some craters have been dated using radiometric methods such as the U-Pb method in zircon, and Crowley *et al.,* (2007) showed that improved analytical methods have led to their application with very good precisions.

Other methods like biostratigraphic dating (target rocks) or palynostratigraphic (infill) methods can yield good results but the problem is that they are often not very precise. Some of the identified craters include the Amguid (Algeria), Aomunga (Chad), Aouelloul (Mauritania), B.P. (Libya), Bosumtwi (Ghana), Highbury (Zimbabwe), Oasis (Libya), Ouarkziz (Algeria), Roter Kamm (Namibia), Talemzane (Algeria), Tenoumer (Mauritania), Tin Bider (Algeria), and in South Africa crater lake deposits of various ages occur and they include the Palaeoproterozoic Vredefort, Early Cretaceous Morokweng crater, and Middle Pleistocene Tswaing and Kalkkop craters , (Koeberl, 1994).

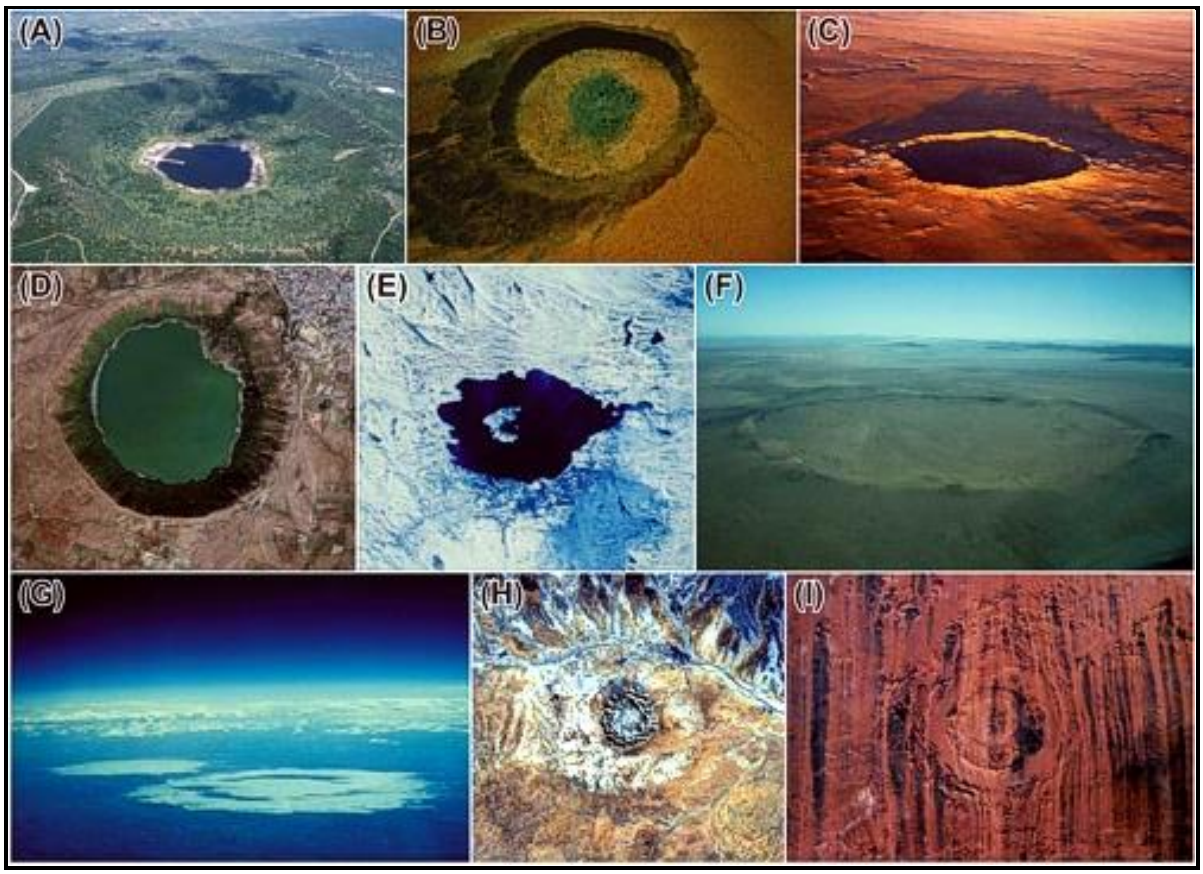

Figure 6: Examples of impact craters on Earth. From left to right; top row: (A) Tswaing, South Africa (1.2 km diameter, age 250,000 years); (B) Wolfe Creek, Australia (1 km diameter, age 1 million years); (C) Meteor Crater, Arizona, USA (1.2 km diameter, age 50,000 years); middle row: (D) Lonar, India (1.8 km, age ca. 50,000 years); (E) Mistastin, Canada (28 km diameter, age ca. 38 million years); (F) Roter Kamm, Namibia (2.5 km, age 3.7 million years); bottom row: (G) Clearwater double crater, Canada (24+32 km diameter, age ca. 250 million years); (H) Gosses Bluff, Australia (24 km diameter, age 143 million years); and (I) Aorounga, Chad (18 km diameter, age <300 million years, (http://lithosphere.univie.ac.at/impactresearch/elgygytgyn-crater/).

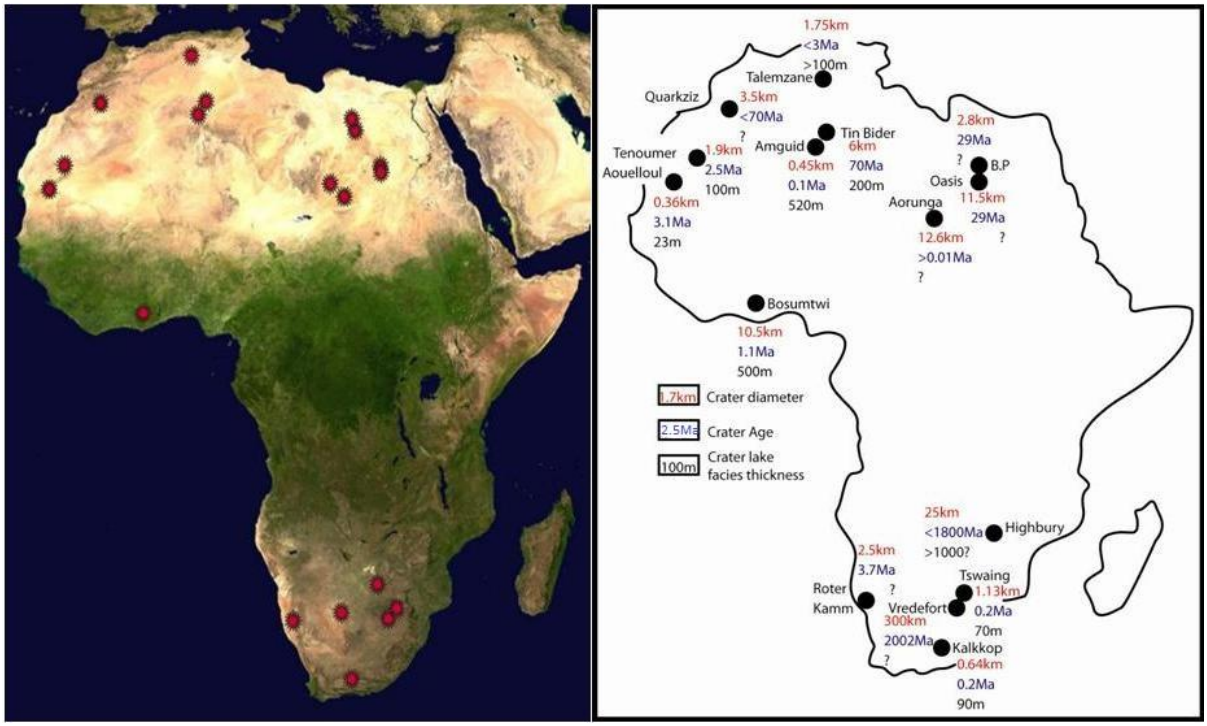

Figure 7: African Meteorite craters and their size and ages. The absence of craters from the tropics is probably due to poor exposure (modified from Reimold, 1998).

2.2 KALKKOP CRATER PREVIOUS STUDIES

The Kalkkop Crater Lake was first investigated by Haughton *et al.,* (1953). Their interest arose from its conspicuous shape (Fig. 8A), seen on aerial photographs and also the consideration of the surface geology, gravimetric data, the inflammable gas that occurs frequently in the springs and in boreholes in the area, as well as reports of presence of pseudocoal nearby. The presence of the unusual circular white circular feature seen on aerial photographs provoked immediate interest (Haughton *et al.,* 1953). Their study revealed that the rocks on the surface were gently deformed Beaufort sandstones and mudstones. The white circular feature proved to be white limestone, with a capping of a hard, massive limestone. Five pits were excavated and one of them showed wrinkled limestone in places with layers of chert and gravel at intervals. Silicified rush-like plants and fragments of bone occurred in the limestone, and in the gravels-beds small shells of the gastropod *Melanoides* were found.

The Haughton *et al.,* (1953), borehole reached a depth of 304.8 m and passed through limestone, breccia and lower Beaufort sandstone and shale.

At the top of the core a few meters of limestone and clay was found. As the borehole was sunk further the following rock types were observed: bands of hard brown chert, few centimeters of bands of fairly hard, spongy, porous limestone and bands of hard compact limestone, as well as argillaceous limestone. Between 19 m-86 m, there was a succession of gray, greenish-gray and dull white soft, well-bedded limestone. Occasional thin chert bands and hard porous limestone was observed down to 52 m, and below this depth there was no chert observed. At depth between 27 m and 47 m, there were two apparent concretionary structures in the limestone. At 66.5 m, the first recognizable gravel-bed is evident though, it is probable that others existed higher in the succession. The gravel bed consists of small angular pebbles of shale embedded in limestone. At 84.4 m there is another gravel bed that yielded small ostracod shells. Breccia alternating with limestone starts at 88 m, and that is where the limestones gradually change in colour to gray and gray-blue and become hard and shaly. The findings from this core showed that there was no indication of oil, igneous material or former existence of a salt dome. It was only later in the 90's when the crater was drilled again that its mode of formation was uncovered.

2.3 PRESENT STUDY

The most conspicuous feature of the site in aerial/satellite images is the whitish, calcareous palaeo-lake fill, a roughly circular feature ~650 m in diameter with a slight bulge on the eastern aspect (Fig. 8A). The Kalkkop crater represents one of the three confirmed impact craters in South Africa (Koeberl, 1994; Reimold *et al.,* 1998). The discovery of features such as extensive breccias, shocked quartz, suevite (impact breccia composed of angular fragments and glass inclusions) and geochemical signatures characteristic of meteorites in cores from the last drilling operations completed in 1992, showed conclusively that the Kalkkop crater was formed by a meteorite impact. Because the Kalkkop impact crater is <2 km in diameter, it comprises a simple bowl shaped feature, rather than the more complex structures of larger craters (Koeberl, 1994; Reimold et al 1998). Although the lake fill has weathered positively relative to the country rock, the topography of these surficially calcretised carbonate deposits is subdued.

The deposits are generally more elevated in the east (coinciding with the 'bulge'), but overall the topographic gradient is less than less than 10 m (Fig.8B).Surface pits and trenches were excavated at various times and according to Reimold *et al.,* (1998), showed that the bedding of the calcareous lake fill deposits dip inwards towards the center of the crater at angles of up to 40-60^0. A whitish halo around the limestone crater fill is widest in the east and was possibly caused by deflation of the carbonate.

In the 1990's, three boreholes were sunk; the most important of which (completed in 1992) was located in the center of the crater (Fig. 8B). This hole reached a depth of 151.8 m and revealed 89.3 m of lacustrine sediments (mainly limestone) underlain by breccias and finally undisturbed Karoo sediments (Koeberl, 1994; Reimold *et al.,* 1998). As noted by Reimold *et al.,* (1998) the crater rim has been almost entirely removed by erosion, with only ~2 m high remnants in the south and northeast (Fig. 9A), which are fractured and faulted with locally developed, small scale gentle folds. No ejecta blanket was reported and this feature too has presumably been eroded since the impact. The presence of debris flow deposits comprising angular clasts of country rock near the top of the lacustrine succession (Fig. 9B) indicates that the rim had still been largely intact towards the end of the lacustrine depositional phase.

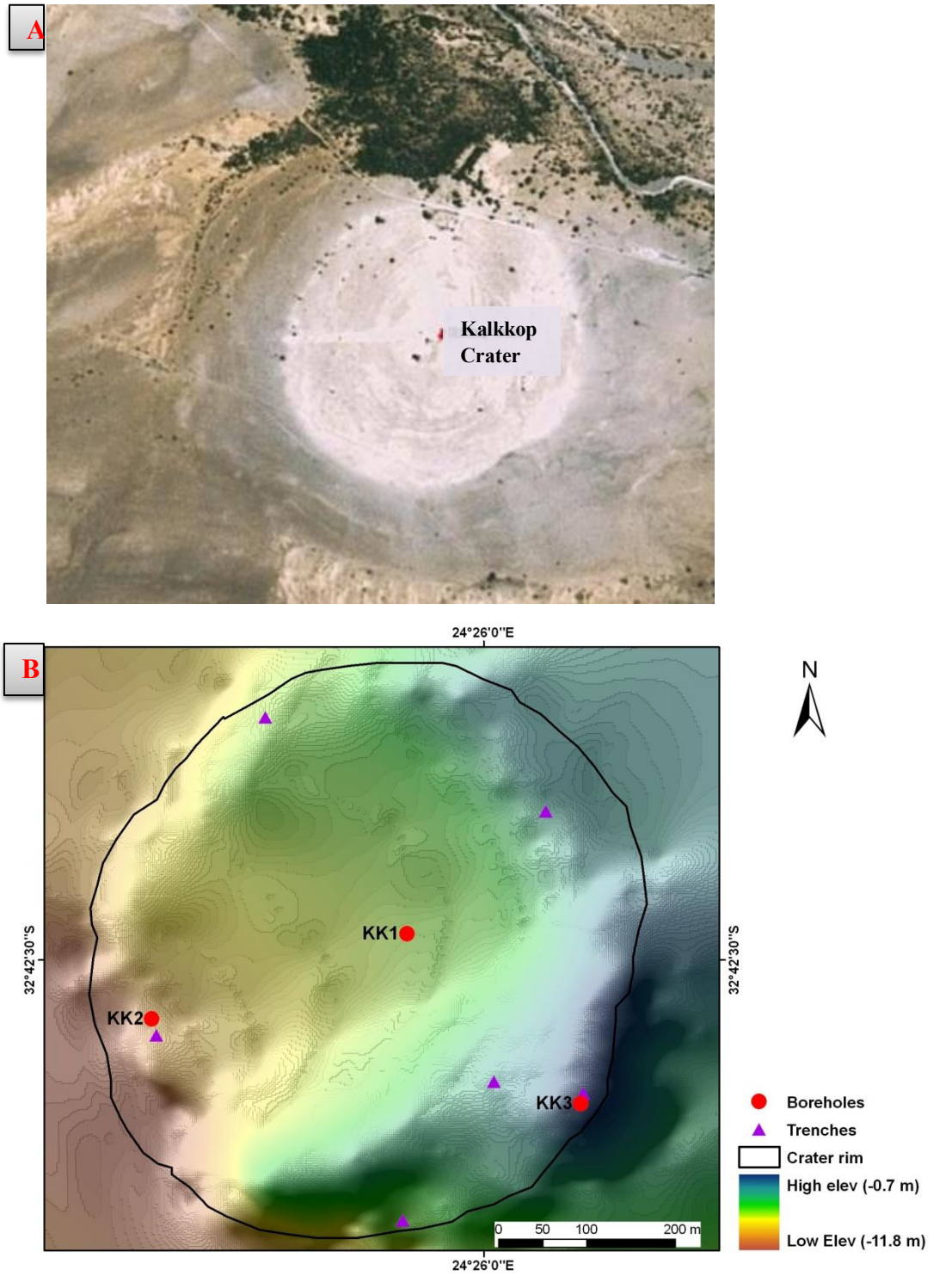

Figure 8: A) Google Earth image of Kalkkop showing the calcareous palaeo-lake fill, a roughly circular feature with a slight bulge on the eastern aspect; B) a digital elevation model (DEM) of the palaeo-lake fill. Location of exploration trenches and the various borehole locations are also shown (modified data from Reimold 1998).

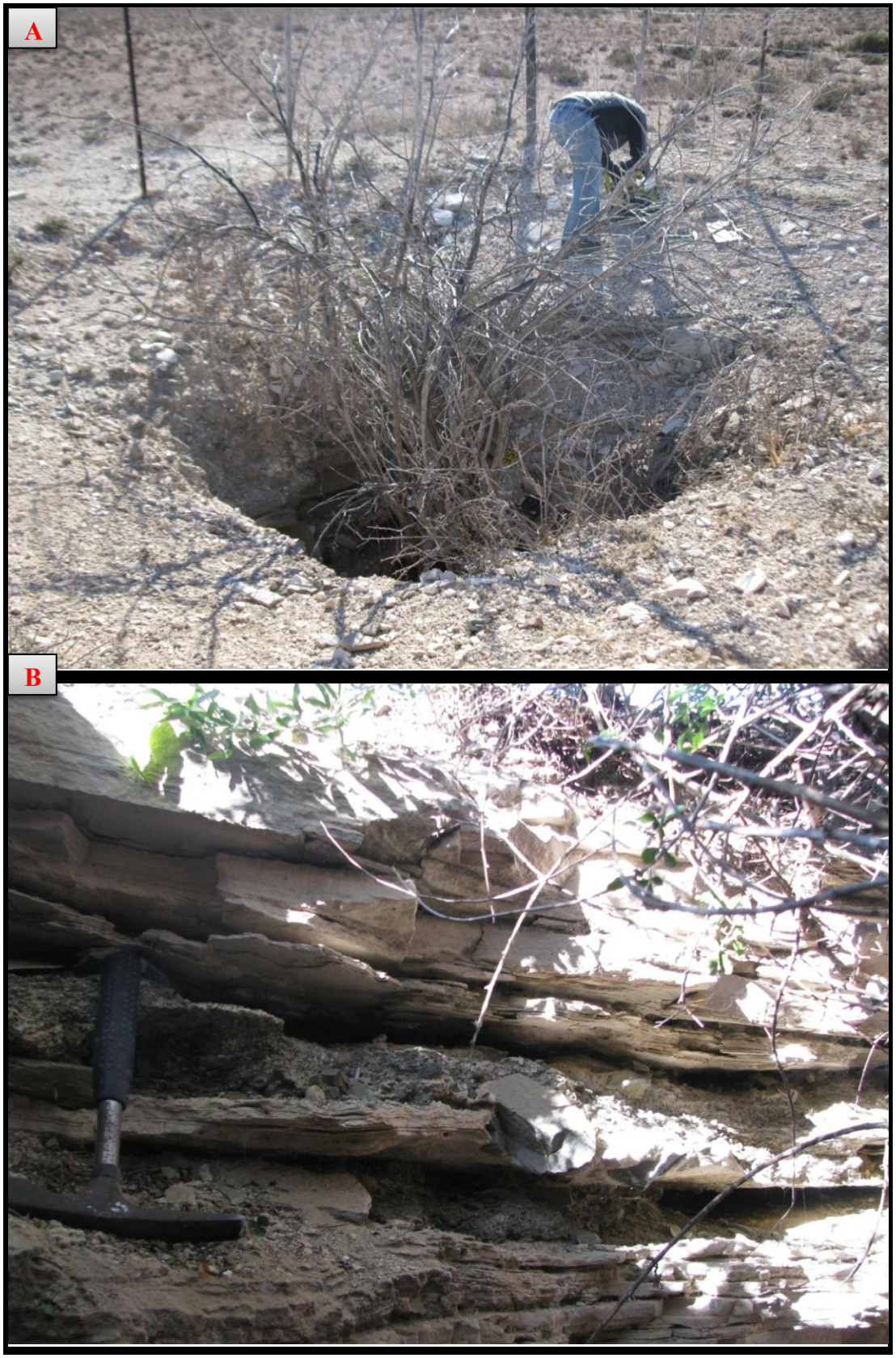

Figure 9: A) Pit excavated into the crater fill; B) Debris flow comprising angular fragments of country rock in laminated carbonates.

2.4 POLLEN ANALYSIS

Pollen comprises the microgametophytes of seed plants, which produce the male gametes (sperm cells). Pollen is microscopic and it can be easily transported by the wind and redeposited and preserved in sedimentary strata such as in lakes. The different types of pollen can reveal the type of vegetation that was close to the lake. Climate and vegetation are related because; plants are adapted to particular climate regimes (Bunbury, 2003). According to Scott (2000), the first publication on palynology of the Cenozoic of Southern Africa was by Kirchheimer (1932), which was based on the pollen of the Cretaceous/Cenozoic crater sediments at Banke (Arnot) in Namaqualand.

2.4.1 KK1 pollen

The core in KK1 most suitable for pollen recovery had already been removed by Mazus (1999) prior to this study. Several samples from the KK1 core which appeared to be more carbonaceous were sent to be analysed by Louis Scott, University of Free State (UFS). The pollen from these samples is very sparse. At the time of writing, a pollen diagram from this work had not yet been completed. However several pollen photomicrographs are available and are shown below (Fig 43). For this study, therefore most of the data is taken from Mazus (1999) who sampled the lacustrine part of borehole KK1 core at regular intervals and prepared the material for fossil palynomorphs using standard methods. Mazus (1999) used a Zeiss transmitted light microscope for identifying and counting pollen and spores. Due to scarcity of pollen grains in the crater sediment the results regarding past vegetation were based on the presence or absence of certain pollen types and their relative abundance in the pollen spectrum, rather than on percentages.

In her report on pollen from the KK1 borehole, Mazus (1999) identified various pollen assemblages in the lacustrine succession (Fig. 45) and divided it into four pollen zones, starting from the bottom (zone1) to the top (zone 4). The pollen concentration yielded was poor with only a few samples containing abundant pollen grains i.e. at horizons 17.0, 19.0, 26-36.0, 41.0, 46.0, 58-59.0 and 65.0 m. From a perspective of palaeo-environmental analysis, the diagram showing the relative proportions of the pollen groupings ‘trees’ (moist) and ‘Karoo-type shrubs + grasses’ (arid) was considered most useful and reproduced in Figures 43 and 44 represent for comparison with the $\delta^{13}C$ and $\delta^{18}O$ plots. The pollen types from various depths and their significance are considered in more detail in Chapter 7.

2.4.2 KK2 and KK3 pollen

Just like the KK1 borehole, the KK2 and KK3 borehole pollen analysis was divided into 4 pollen zones but the pollen was only seen or described until pollen zone 3.

Pollen zone 4 had poor pollen especially KK3, only at 2.5 m KK2 showed the only dominating pollen Compositae and this pollen indicates Karoo vegetation.

Pollen zone 3- KK2 at 18.0 m showed grassland with herbs and forest patches. Some important pollen such as the *Syzygium, Podocarpus, Olea, Myrica, Rhus* and others were among the woodland taxa. KK3 had very poor pollen record and consisted mostly of Graminaceae, Compositae and a few pollen grains of trees such as *Podocarpus* and *Olea* to a depth of up to 3.0 m.

Pollen zone 2 and 1 were not observed on these boreholes because the pollen spectra were too poor to reconstruct past vegetation.

.

3. METHODOLOGY

The methodology used in this project can be divided into three sections: field methods and sampling, core description and sampling, and the analytical methods.

3.1 FIELD MAPPING AND SAMPLING

Field work was conducted in August 2010, mainly to investigate the study area and collect samples. Before going to the field, ArcGIS was used to create a geological map of the area (Fig.3.), using existing CGS data. Five samples were collected in the trenches and on the surface and these are shown in Figure 9B, which also shows the location of the sampled borehole.

3.2 CORE LOGGING, SAMPLING AND THIN SECTIONS

The 1992 KK1 drill core was first logged in detail and then sampled for analysis (stable isotope, Sr-isotope analysis and XRD and pollen). The borehole was sampled using a drill (2 mm in diameter) at intervals ranging from 1.8-3 m and the drill bit was cleaned with compressed air after each sample was taken to avoid cross-contamination. The drill powder was placed into sample bottles and sealed. Some parts of the core are missing due to previous sampling or core loss during drilling, and the missing gaps are represented on the core logs (see 5.1).

The Munsell color system was used to identify the soil colour during logging (Fig. 10). At 70-88 m most of the core is missing, hence the lack of data. A second set of samples was collected from 47.4-47.76 m (B1-B19) and at 66.83-67.47 m (A1-A24) at close (few 2 mm) intervals to provide high resolution data.

The same intervals of the core that were used for the samples collected from 47.4-47.76 m (B1-B19), and at 66.83-67.47 m (A1-A24), were made into thin sections. The thin sections were produced from material that had been impregnated with araldite and they were studied under a petrographic microscope.

3.3 STABLE ISOTOPES

The five samples collected at the surface were analysed using the classical method of McRae (1950) in the Department of Geological Sciences (UCT).

The C and O isotope analyses of the core samples were made by using standard gas bench methods in the Department of Archaeology at UCT, with the gas bench interfaced to a Finnigan MAT 252 mass spectrometer. Samples were weighed into 12 ml borosilicate tubes and screw top lids containing a septum were used to close the tubes. The tubes were placed in a temperature controlled sampler tray set to 72^{o}C. The tubes were flushed with helium to remove the atmospheric air present in them. Five drops of warm (72^{o}C) acid (100% phosphoric acid with a density of 1.92 g/cc) were then manually added to each sample tube through the septum using a 1ml syringe. The samples were left to react for three hours before starting the run. The gas evolved from each reaction was sampled by the auto sampler and passed to a Thermo Finnigan (Germany) model II Gasbench, where the sample gas was passed through a Nafion water removal unit. It then passed through the "Poraplot Q" GC column to separate the gas compounds released by the reaction, and then through a second Nafion water trap. The gas was then passed from the gasbench to a Finnigan MAT 252 isotope ratio mass spectrometer (IRMS) computer controlled by Isodat software. The gasflow was controlled to give 10 sample peaks and 5 reference peaks. The CO_2 reference gas was also introduced into the mass spec via the gasbench and was also controlled by the Isodat software. C and O isotope ratios expressed as delta (δ) values relative to PDB and SMOW respectively. The standards that were used in each run are Lincoln Limestone, NBS18 and NBS20, which have a range of $\delta^{13}C$ and $\delta^{18}O$ values. The measured and accepted values were used to construct a calibration curve and this was used to correct the raw data, and to determine the precision of the method.

3.4 ICP-MS FOR TRACE ELEMENTS

Concentration data for Rb and Sr were obtained using solution inductively coupled plasma mass spectrometry (ICP - MS) at UCT using a ThermoFisher Xseries2 instrument (procedure updated from that used by Le Roex *et al.,* (2003)). Approximately 50 mg of sample powder were dissolved in a HNO_3 in sealed Savilex beakers on a hotplate for 48 hours, followed by evaporation to incipient dryness and two treatments of 2 ml concentrated HNO_3. The final dried product was then taken up in 5 % HNO_3 solution containing 10 ppb Re, Rh, In and Bi as internal standards. The Standardization was against artificial multi-element standards (Clemens *et al.,* 2010). The average relative errors for Rb and Sr were 0.26 ± 0.16 % and 1.96 ± 2.40%.

3.5 Sr ISOTOPES

The Sr-isotope data were obtained using a Nu instruments NuPlasma HR mass spectrometer, following the chemical separation procedure described by Miková & Denková, (2007). The average value obtained for the NIST SRM987 standard was 0.710302 ± 0.000021 (2σ, n = 5) A value of 0.710225 was used to normalize the $^{87}Sr/^{86}Sr$ data. All Sr isotope data were corrected for Rb interference and instrumental mass fractionation using the exponential law and $^{86}Sr/^{88}Sr$ value of 0.1194. Seventeen samples were analysed for the chemical compositions in the lacustrine sediments. The samples were analysed for Al_2O_3, MgO, SrO and CaO by using ICP-OES, in the Department of Chemical Engineering at UCT.

4. AGE OF THE KALKKOP CRATER

4.1. U-Th SERIES DATING

In the absence of datable impact melts for fission track or K-Ar methods, U-Th series dating on two samples of the lake carbonate deposits was attempted by Reimold *et al.,* (1998). A 5 m (close to the top) and 87.5 m (close to the bottom) samples from the KK1 core were used. The sample from 87.5 m had a date of 258 ±25 ka, whereas the shallow sample (at ~5 m depth) yielded a > 256 ka age. The 5 m sample was apparently rejected by Reimold *et al.,* (1998) and the deeper was accepted as the true age of the early part of lake deposition (and by inference the approximate age of the impact), and this date is close to the Tswaing Crater Lake age of 220 ±52 ka. In general U-Th series dates for carbonate deposits are only valid in a closed system and where the sample is 100% carbonate. Impurities like clay minerals may invalidate the underlying assumption that there is zero ^{230}Th present at the outset (Faure, 1986, Reimold *et al.,* 1998). In the shallow sample at 5 m depth 56% of the material dissolved, compared with 92% for the 87.5 m sample. This suggests that in both cases impurities were present, but more so in the shallower sample. Also, the top sample would have been subjected to a more dynamic weathering regime after the crater lake had dried up than the lower sample.

4.2. AGES FROM CRATER RIM EROSION RATES

4.2.1. Original rim height of Kalkkop

The relatively pristine character of the ~200 ka old Tswaing crater rim is in striking contrast to the highly degraded remnants seen at Kalkkop; in addition, the crater lake at Tswaing is still present, whereas at Kalkkop the lake, unconstrained by the (eroded) crater walls, has long since dried up and the carbonate fill has weathered positively relative to the surrounds. The difference in annual rainfall in the two areas is considerable, with Kalkkop crater and its surroundings having an average of 236 mm of rain per year, with the wettest months in the earlier and later summer, while the Tswaing crater and its surroundings varies from 535 mm to 900 mm a year (Partridge and Scott 2000). In view of these observations and given the unreliability of the U-series dating as observed above (indicating a similar age for the two craters), the age of Kalkkop appears to be much greater than Tswaing.

To further constrain the age of Kalkkop, an approach based on the erosion rate of its former crater rim was adopted, which requires the reconstruction of the original crater. However, a complication in this regard is the quoted 650 m diameter of the crater (Koeberl, 1994; Reimold *et al.,* 1998), which is based on the present surface diameter of the crater lake deposits -in the absence of the (eroded) crater rim. It is probable that this represents a major underestimate of the original rim- to -rim crater diameter (the normal crater size metric), as compared for example with the well preserved Tswaing impact crater. In a cross section of Tswaing, the diameter of the (extant) lake is shown as ~600 m (Koeberl 1994); slightly smaller than the diameter of the Kalkkop calcareous lake fill deposits. However, the rim- to -rim diameter of Tswaing is 1,130 m (Koeberl, 1994) and by inference the original rim- to -rim diameter of Kalkkop should have been similar (but possibly slightly larger) to Tswaing. The distance from the apparent rim remnants in the west to the center of the crater lake deposits is 0.53 km, which approximates the radius of the rim-to-rim diameter. Multiplying by 2 yields a similar estimate (1060 m) for the diameter of the original crater rim as deduced from the lake dimensions. The 50, 000 year old Meteor Crater in Arizona is only slightly larger (1.2 km) than Kalkkop/Tswaing and its rim height is ~50 m above the surrounds. Moreover, the target rocks are similar in age and lithology to Kalkkop (Roddy and Shoemaker, 1995). Allowing for minor erosion during the 50, 000 year history of Meteor crater, roughly compensated for by the slightly larger size we suggest the original rim height of Kalkkop was also ~50 m. This is broadly consistent with the present rim height of Tswaing (60 m).

Several methods were used to constrain the rate of crater rim erosion and one of them was adopted from Pike (1981). The present height of crater rims of impact craters in the broader size range of Kalkkop was considered, relative to their (independently) estimated age and regional climatic conditions. Their original height at time of impact was recalculated from the empirical relationship of Pike (1981), derived from the morphometry of fresh simple lunar craters, where erosion rates are very low. The height of a crater rim above the exterior topographic datum (h) differs with the crater diameter (D) according to the relationship $h=0.035D^{1.04}$. Because the target rocks of cosmic impacts are always extensively shattered and brecciated (Koeberl *et al.,* 1994b; Reimold *et al.,* 1998), their lithology should not play a significant role in determining the rim erosion rate.

The erosion rates of three craters were calculated:

1. Erosion rate of Aouelloul (Mauritanea)

   This Aouelloul is situated in the Sahara desert and has a diameter of 390 m . The target rocks mainly comprise Ordovician sandstone and the present crater rim rises from 15-25 m above the surrounds. The age of the crater was determined by apatite fission track and K-Ar dating (Fudali and Cressy, 1976; Storzer and Wagner, 1977; Koeberl, 1994), and it was found to be 3.1 ±0.3 Ma. The empirical original rim height (RHo) is given by (Pike, 1981):

   $RHo=0.035D^{1.04}$

   $RHo=0.035.0.39^{1.04}$

   $=0.01314$ km

   RHo=13.14m.

   Therefore the rim erosion rate (Re) is:

   Re= RHo-RH/Ma

   =13.14-20/3.1

   = 6.69 m/ Ma

2. Erosion rate of Tenoumer (Mauritanea)

   This crater Tenoumer is also situated in the Sahara desert and has a diameter of 1.90 km, ~400 km west of Aouelloul. The target rocks comprise Precambrian granitoid rocks and the present crater rim is ~68 m above the surrounds. The age of the crater was determined by apatite fission track and K-Ar dating to be 0.0214 ± 0.0097 Ma (French, 1970; Koeberl, 1996).

   $RHo=0.035D^{1.04}$

   $RHo=0.035.1.90^{1.04}$

   =0.0682 km

   RHo=68.2 m. Therefore the rim erosion rate (Re) is:

   Re= RHo-RH/Ma

   =68.2-68/0.0214

   =9.34 m/ Ma

3. Roter Kamm, Namibia

   The crater is 2.5 km diameter and 130 m deep. It is a meteorite crater and located within the Namibian section of the Namib desert in the Kars region. The age of the crater is estimated to be 3.7 ± 0.3 Ma, Pliocene. (2.5 km, age 3.7 million years)

   $RHo=0.035D^{1.04}$

   $RHo=0.035.2.5^{1.04}$

   $=0.0907$ km

   RHo=90.7 m. Therefore the rim erosion rate (m/Ma) is:

   Re= RHo-RH/3.7

   =90.7-91.2/3.7

   =- 0.135 m/ Ma

This method however produced erratic results as seen above, suggesting that the relationship determined from moon craters cannot readily be applied to terrestrial craters and the palaeo-erosion rate was then adopted from Erlanger (2011), see 4.2.2. The erosion rates of some of the craters according to the original rim height calculations were doubtful. It was anticipated that the erosion rate of Tswaing should be higher due to the fact that its regional climate is more humid than Kalkkop (Taljaard, 1996).

4.2.2. Age of Kalkkop

Erlanger (2011) conducted a study of the Pliocene and Pleistocene Sundays River terraces (located on the coastal plain ~300 km southeast of Kalkkop Crater), using cosmogenic ^{10}Be and ^{26}Al burial dating (Roberts *et al.,* 2011). An average palaeo-erosion rate of 6.63 m/Ma over the last ~4 Ma was calculated. The crater rim would have been sharply elevated above the surrounds and gravity would have played an important role in erosion (as opposed for instance to slow down wearing of a low relief area). The rocks comprising the rim (mainly weakly resistant mudrocks) would have been completely shattered. An erosion rate notably higher than the regional rate could be anticipated, it is suggested that an erosion rate of 8 ±2 m/Ma is reasonable for the Kalkkop Crater rim. Given that the rim is for practical purposes completely eroded, and was originally ~50 m high, this suggests an age of ~6.3 ±1.6 Ma, i.e. latest Miocene. The age is debateable, but is preferred to the initially estimated 250ka old age. The chemical data will also be used to try and distinguish between the young (250ka) and old (6 Ma) ages.

4.3. TIME SPAN OF LACUSTRINE DEPOSITION AT KALKKOP

It is important to estimate the deposition rate at Kalkkop, since this places constraints on the time span of lacustrine deposition, from the inception of the lake to the time that it dried up. Laminites similar to those at Kalkkop have been interpreted as annual layers in other lacustrine successions, such as the Holocene Derby Lake deposits, Michigan, USA. Here lamination counts were found to be consistent with radiocarbon age models throughout the deposits represented in the core (Wittkop *et al.,* 2009). Precipitation of $CaCO_3$ is favoured by high biological productivity and warm water conditions (Ohlendorf and Sturm, 2001; Nuhfer *et al.,* 1993; Wittkop *et al.,* 2009), and likewise we presume that carbonate precipitation occurred principally in the summer months at Kalkkop. In theory, it is possible to estimate the time span of lacustrine deposition from the total number of laminations in the core. Taking a mean lamina thickness of 0.5 mm and assuming each lamina represents an annual event and given the sediment thickness of 90 m at Kalkkop, this yields a time span of ~180 ka i.e. a sedimentation rate of ~0.5 m/ka. However, some core sections are more massive in nature and lacking laminations, whereas other sections are missing, creating uncertainty in this calculation. The calculated sedimentation rates at Kalkkop were therefore compared with other similar carbonate dominated crater lake deposits. For the Holocene Lake Derby, the sedimentation rate was estimated from the assumption of the annual nature of the laminae. This assumption was underpinned by radiocarbon dating at intervals in the core and gave a deposition rate of 0.56 m/ka (Wittkop *et al.,* 2009). The deposition rate at Tswaing was calculated from the present lake deposit thickness divided by the time elapsed since the impact event (Partridge, 1987), yielding a rate of 0.43 m/ka. Thus both Tswaing and Derby crater lakes have deposition rates comparable to the calculated value at Kalkkop.

.

5. RESULTS

5.1 SEDIMENTOLOGY OF THE KALKKOP CRATER LAKE SUCCESSION

Most of the data reported in this thesis comes from KK1 borehole and it is one of the three boreholes that were logged, the others being KK2 and KK3 drilled at approximately the same time as KK1. No detailed analyses were done on KK2 and KK3 because of clear indications of diagenetic alteration (recrystallization), but their situation close to the margin of the crater serves to illuminate lateral facies changes in the Kalkkop succession. The log of another borehole (KK1b, drilled in the 1970's) was compiled by De Beers is also provided (Fig.15). The description of a still earlier borehole also called KK1 that was previously studied by Haughton *et al.,* (1953) was also available for the present study. The KK1 (Fig. 10) core was logged by the author at the Council for Geoscience, Bellville office after it was transported from the Donkerhoek core shed in Pretoria. Some of the photographs (Figs.11-13) that were taken during the logging process are also described here. The 1992 KK1 core log is shown below in (Figs. 10).

The sedimentological observations made in the surface excavations provide a spatial perspective not available from the cores and these data, although depth limited, are nonetheless valuable. The KK1 core was previously sampled (Mazuz, 1999) resulting in much of the core being missing. Description and sampling is thus restricted to the remaining core. However, the De Beers core log provides data on the complete Kalkkop Crater succession, albeit slightly condensed (~60 m) relative to KK1 (90 m). Overall the thick Kalkkop succession is dominated by whitish limestone which rests with a diffuse contact on brecciated Karoo sandstone and mudrocks and is capped by a pedogenic calcrete (the calcrete only occurs at the top of the succession and is in places associated with plant roots). Closer examination of the core revealed considerable variation on this basic theme. Some sections of core are finely laminated, sometimes on a sub-millimetre scale, whereas others appear more massive in character. Fragments of Karoo rocks ranging from centimetre to sub-millimetre scale are present throughout the succession. Over some intervals the fragments are concentrated to form angular conglomerates. The core may also be darker and more clayey in places. Such lithological variability forms the basis for defining a range of sedimentary facies.

5.1.1 Facies A: Laminated arenaceous carbonate

The dominant sedimentary facies in the Kalkkop succession comprises of centimetre to sub-millimetre scale laminae of carbonate with a variable quartz and lithic grain component (Figs. 10). Scattered grains, platelets discontinuous laminae and small specks of carbonaceous material are common in the fabric of this facies, but are locally more concentrated. Small (up to 1 cm) carbonised plant fragments occur along partings and in a hand specimen alignment of the long axis of the fragments was observed. These detrital plant remains are also visible in thin section (Fig.16) as wavy, dark reddish brown bedding plane-parallel material. Soft sediment deformation structures, including water escape and small-scale folding are relatively rare (Fig.12G).

Examination of magnified, scanned polished sections and thin sections allowed facies A to be sub-divided into several sub-facies (Fig. 14):

5.1.1.1 Sub-facies Ai: micro-laminated coarser and finer grained micrite

Some core intervals comprise thin (0.1-0.5 mm), very regular alternations of whitish, coarser and pale brown, finer micrite. The brown laminae contain finely disseminated carbonaceous and clayey material, whereas the white laminae are almost pure micrite. The laminae are laterally persistent and from to 2-15 laminae in a single sequence were counted. The thickness of individual laminae within sequences of laminae is variable and in general the brownish examples are thicker

5.1.1.2 Sub-facies Aii: micro-laminated, clayey, fine grained micrite

Sub-facies Aii comprises darker coloured (greenish brown) fine grained, clayey micrite, typically containing dispersed black carbonaceous material. This sub-facies ranges up to ~1 cm in thickness and displays more or less distinct internal finer laminations. In thin section it is seen to comprise fine micrite with a minor proportion of very fine grained detrital quartz, with occasional larger grains. These laminae are also richer in finely disseminated organics and clay; biotite and chlorite were identified in thin section, the latter possibly accounting for the greenish tinge (Fig.14). The lighter coloured laminations mainly comprise coarser micrite with individual grains up to 1 mm.

5.1.1.3 Sub-facies Aiii: upward coarsening laminae

Some thicker laminae (up to ~1 cm) display an upward coarsening, in some instances with upward increase in the number and size of fragments of black carbonaceous material. Sub-facies A*iii* terminates abruptly upwards and the upper surface is flat and topped by carbonaceous and or clayey material or brownish, wavy micro-flaser laminations (sub-facies Aiv, see below).

5.1.1.4 Sub-facies Aiv

Thin (0.1-0.3 mm) dark grey to black, laterally persistent, slightly wavy carbonaceous laminae occur at irregular intervals in facies A. The laminae tend to occur at the interface of the other sub-facies of facies A.

5.1.2 Facies B: Chert

White chert bands are sparsely distributed within the KK1 core succession and were also seen in the surficial excavations where they have a lenticular geometry. The white cherts are typically a few centimetres in thickness and in some instances have been brecciated. Other core segments show greyish zones of incipient silicification; in which case a texture similar to the normal micrite dominated core is retained. This pure white chert was/ chalcedony was identified by its conchoidal fracture and lack of reaction with acid. These are prominent over the interval 15-10 m, (Fig.11 C-D). Another cherty layer occurs at 34-32 m, and contains carbonate rich micro-laminae of wavy bedding with a spongy texture (Fig.12 C-D). Chert is also prominent from 54-49.5 m (Fig.13 A-B) interbedded with carbonate. In this interval a fine- grained, finely laminated original carbonate has been replaced by cherty material.

5.1.3 Facies C: Greenish calcareous mudrock

Massive, greenish-grey, slightly calcareous mudrock intervals up to several centimetres in thickness occur within the Kalkkop core. It breaks easily, has rhizocretions (a process whereby plant roots are encased in mineral matter) at 18.7 m (Fig.11 E) and bioturbation on bedding planes (Fig.11 F).

5.1.4 Facies D: Massive arenaceous carbonate

Facies D comprises massive, slightly arenaceous carbonate ranging in thickness from a few cms to >1.5 m (absent core makes estimates difficult) although some contain rare internal laminae. The contact of this facies with the laminated facies was seen to be steep and erosive in places. A few thinner intervals consist of coarser –grained material.

5.1.5 Facies E: Allogenic gravels

Coarser grained intervals in the Kalkkop succession, marked by angular, allogenic clasts of Karoo sandstones and mudrocks ranging from ~6 m to a few mm in thickness are dispersed throughout the cores. In some instances the clasts are sufficiently concentrated to form a conglomerate, whereas in other examples the allogenic clasts 'float' in an authigenic carbonate matrix. As seen in the surficial excavations, the form of the gravelly units appeared lensoid and the base is typically erosive. The maximum clast size is ~20 cm and sorting is generally very poor. The thickest gravels occur between 12-6.5 m in the De Beers log (Fig.15) and comprise a series of mainly reversed graded units.

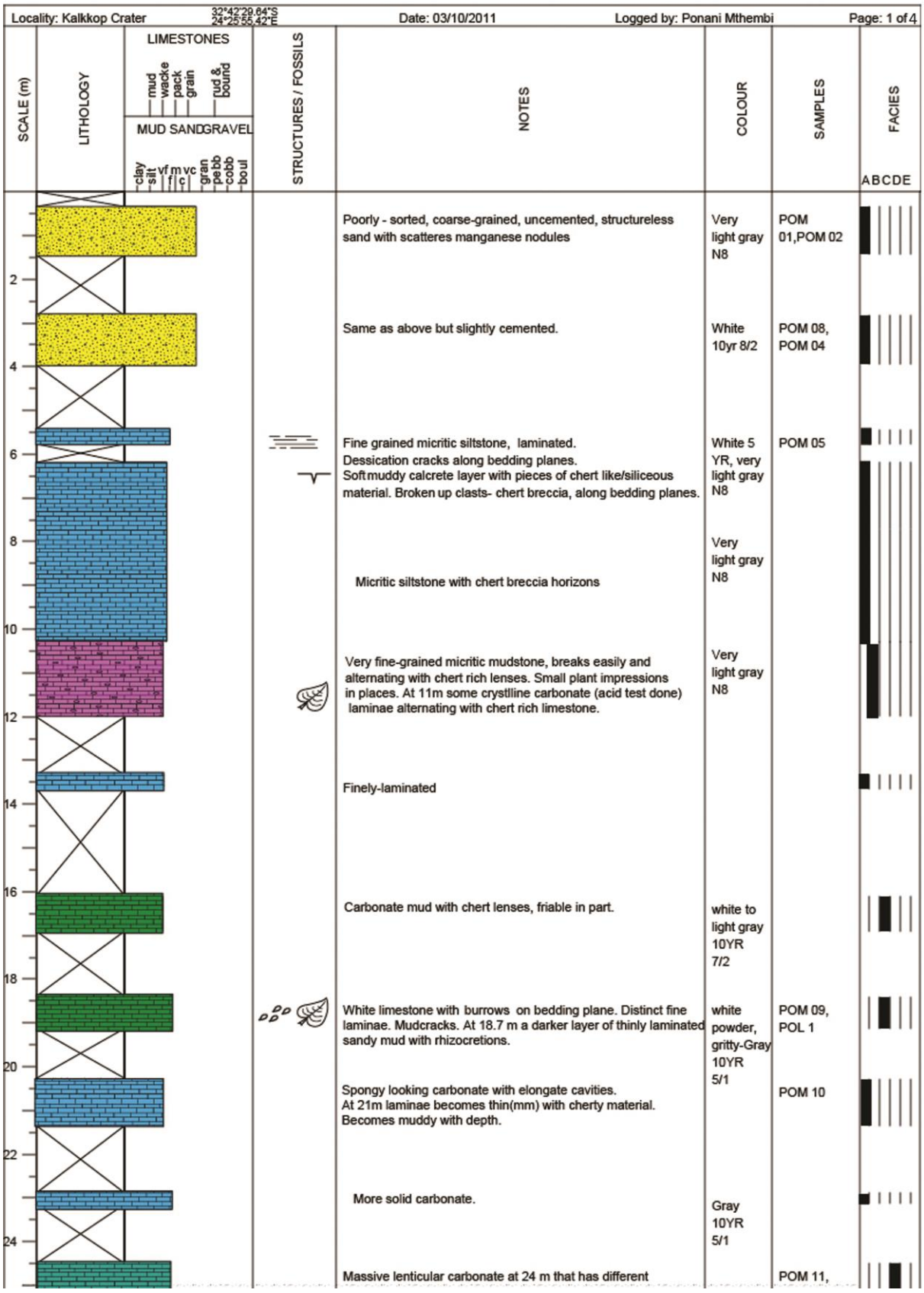
Locality: Kalkkop Crater
32°42'29.64"S
24°25'55.42"E
Date: 03/10/2011
Logged by: Ponani Mthembi
Page: 1 of 4
SCALE (m)
LITHOLOGY
LIMESTONES
mud
wacke
pack
grain
rud &
bound
MUD SAND GRAVEL
clay
silt
vf
f
m
c
vc
gran
pebb
cobb
boul
STRUCTURES / FOSSILS
NOTES
COLOUR
SAMPLES
FACIES
ABCDE
Poorly - sorted, coarse-grained, uncemented, structureless sand with scatteres manganese nodules
Very light gray N8
POM 01,POM 02
Same as above but slightly cemented.
White 10yr 8/2
POM 08, POM 04
Fine grained micritic siltstone, laminated.
Dessication cracks along bedding planes.
Soft muddy calcrete layer with pieces of chert like/siliceous material. Broken up clasts- chert breccia, along bedding planes.
White 5 YR, very light gray N8
POM 05
Micritic siltstone with chert breccia horizons
Very light gray N8
Very fine-grained micritic mudstone, breaks easily and alternating with chert rich lenses. Small plant impressions in places. At 11m some crystlline carbonate (acid test done) laminae alternating with chert rich limestone.
Very light gray N8
Finely-laminated
Carbonate mud with chert lenses, friable in part.
white to light gray 10YR 7/2
White limestone with burrows on bedding plane. Distinct fine laminae. Mudcracks. At 18.7 m a darker layer of thinly laminated sandy mud with rhizocretions.
white powder, gritty-Gray 10YR 5/1
POM 09, POL 1
Spongy looking carbonate with elongate cavities.
At 21m laminae becomes thin(mm) with cherty material.
Becomes muddy with depth.
POM 10
More solid carbonate.
Gray 10YR 5/1
Massive lenticular carbonate at 24 m that has different
POM 11,
2
4
6
8
10
12
14
16
18
20
22
24

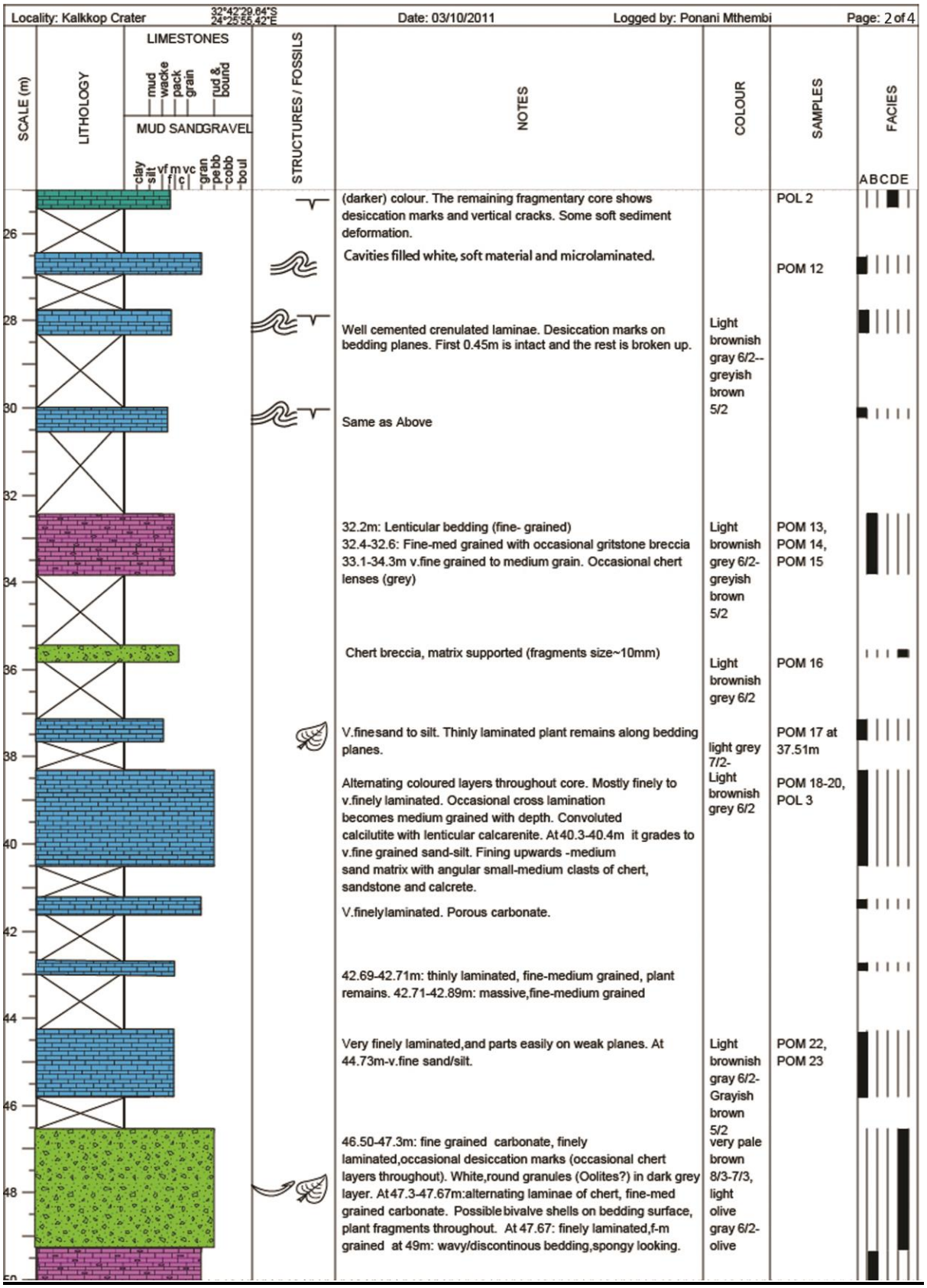
Locality: Kalkkop Crater
32°42'29.64"S
24°25'55.42"E
Date: 03/10/2011
Logged by: Ponani Mthembi
Page: 2 of 4
SCALE (m)
LITHOLOGY
LIMESTONES
mud
wacke
pack
grain
rud &
bound
MUD SAND GRAVEL
clay
silt
vf
f
m
c
vc
gran
pebb
cobb
boul
STRUCTURES / FOSSILS
NOTES
COLOUR
SAMPLES
FACIES
A B C D E
26
28
30
32
34
36
38
40
42
44
46
48
50
(darker) colour. The remaining fragmentary core shows desiccation marks and vertical cracks. Some soft sediment deformation.
POL 2
Cavities filled white, soft material and microlaminated.
POM 12
Well cemented crenulated laminae. Desiccation marks on bedding planes. First 0.45m is intact and the rest is broken up.
Light brownish gray 6/2--greyish brown 5/2
Same as Above
32.2m: Lenticular bedding (fine- grained)
32.4-32.6: Fine-med grained with occasional gritstone breccia
33.1-34.3m v.fine grained to medium grain. Occasional chert lenses (grey)
Light brownish grey 6/2-greyish brown 5/2
POM 13, POM 14, POM 15
Chert breccia, matrix supported (fragments size~10mm)
Light brownish grey 6/2
POM 16
V.fine sand to silt. Thinly laminated plant remains along bedding planes.
light grey 7/2-
POM 17 at 37.51m
Alternating coloured layers throughout core. Mostly finely to v.finely laminated. Occasional cross lamination becomes medium grained with depth. Convoluted calcilutite with lenticular calcarenite. At 40.3-40.4m it grades to v.fine grained sand-silt. Fining upwards -medium sand matrix with angular small-medium clasts of chert, sandstone and calcrete.
Light brownish grey 6/2
POM 18-20, POL 3
V.finely laminated. Porous carbonate.
42.69-42.71m: thinly laminated, fine-medium grained, plant remains. 42.71-42.89m: massive,fine-medium grained
Very finely laminated,and parts easily on weak planes. At 44.73m-v.fine sand/silt.
Light brownish gray 6/2-Grayish brown 5/2
POM 22, POM 23
46.50-47.3m: fine grained carbonate, finely laminated,occasional desiccation marks (occasional chert layers throughout). White,round granules (Oolites?) in dark grey layer. At 47.3-47.67m:alternating laminae of chert, fine-med grained carbonate. Possible bivalve shells on bedding surface, plant fragments throughout. At 47.67: finely laminated,f-m grained at 49m: wavy/discontinous bedding,spongy looking.
very pale brown 8/3-7/3, light olive gray 6/2-olive

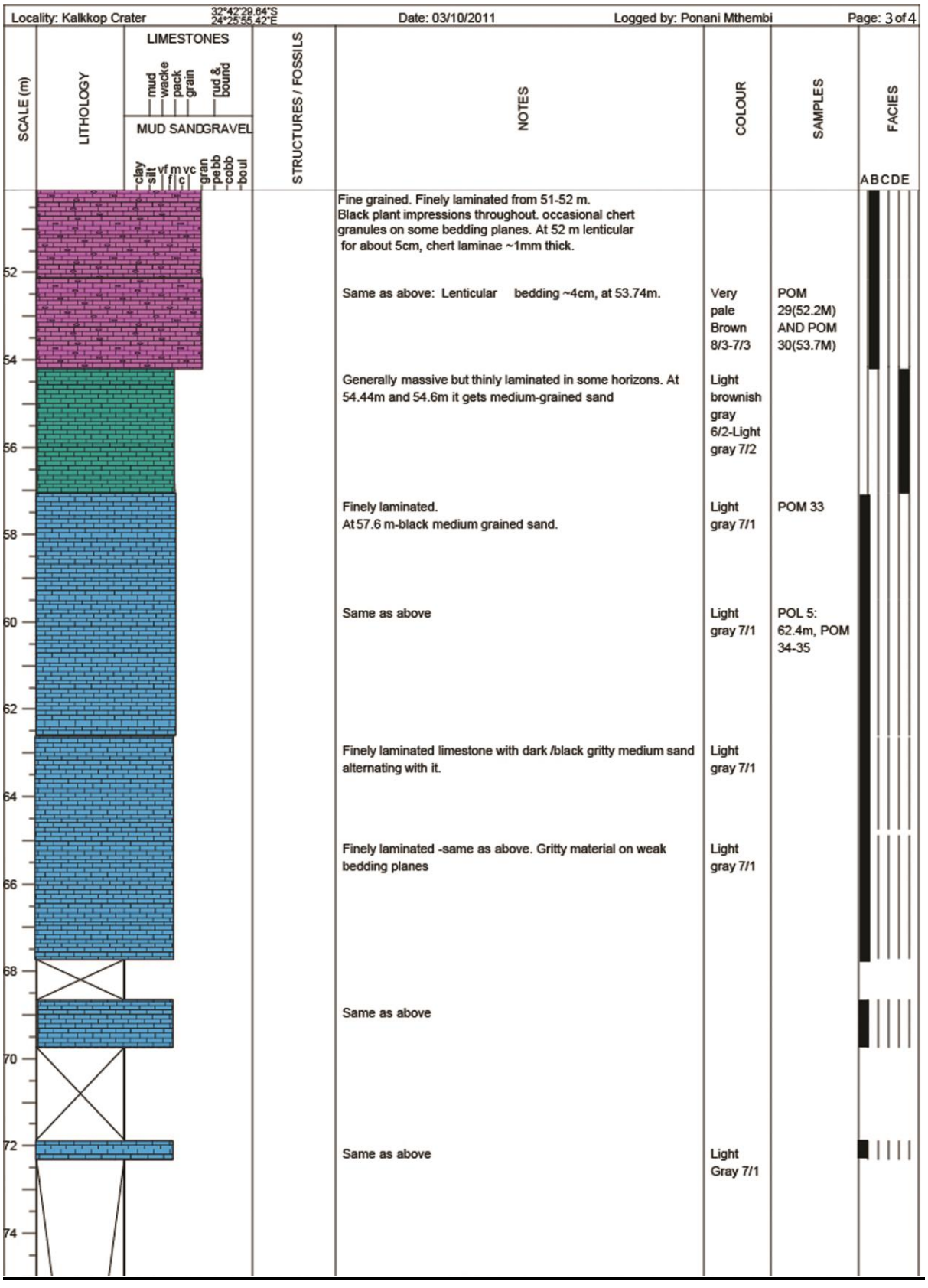
Locality: Kalkkop Crater
32°42'29.64"S
24°25'55.42"E
Date: 03/10/2011
Logged by: Ponani Mthembi
Page: 3 of 4
SCALE (m)
LITHOLOGY
LIMESTONES
mud
wacke
pack
grain
rud &
bound
MUD SAND GRAVEL
clay
silt
vf
f
m
c
vc
gran
pebb
cobb
boul
STRUCTURES / FOSSILS
NOTES
COLOUR
SAMPLES
FACIES
A B C D E
52
54
56
58
60
62
64
66
68
70
72
74
Fine grained. Finely laminated from 51-52 m.
Black plant impressions throughout. occasional chert granules on some bedding planes. At 52 m lenticular for about 5cm, chert laminae ~1mm thick.
Same as above: Lenticular bedding ~4cm, at 53.74m.
Very pale Brown 8/3-7/3
POM 29(52.2M) AND POM 30(53.7M)
Generally massive but thinly laminated in some horizons. At 54.44m and 54.6m it gets medium-grained sand
Light brownish gray 6/2-Light gray 7/2
Finely laminated.
At 57.6 m-black medium grained sand.
Light gray 7/1
POM 33
Same as above
Light gray 7/1
POL 5: 62.4m, POM 34-35
Finely laminated limestone with dark /black gritty medium sand alternating with it.
Light gray 7/1
Finely laminated -same as above. Gritty material on weak bedding planes
Light gray 7/1
Same as above
Same as above
Light Gray 7/1

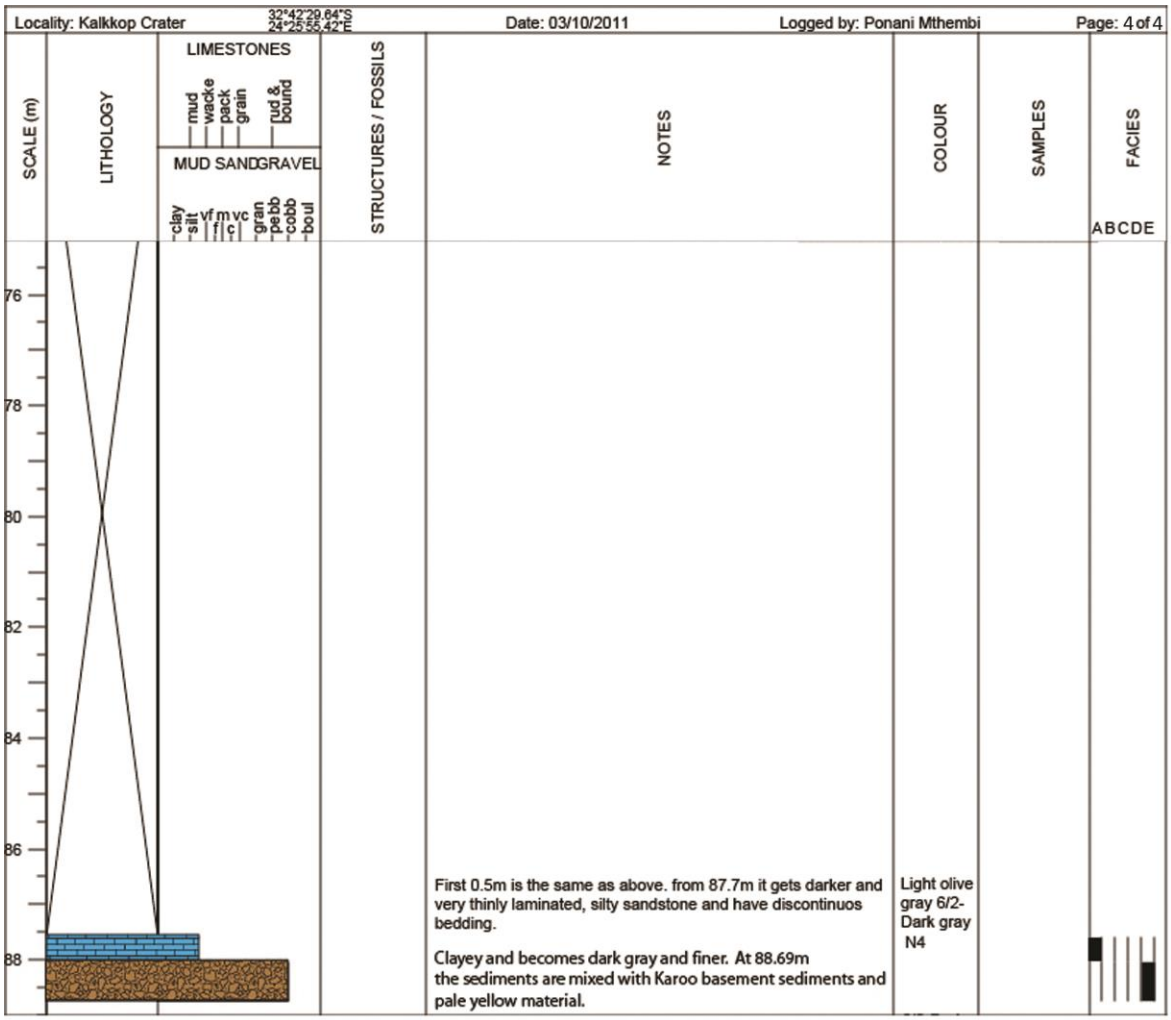

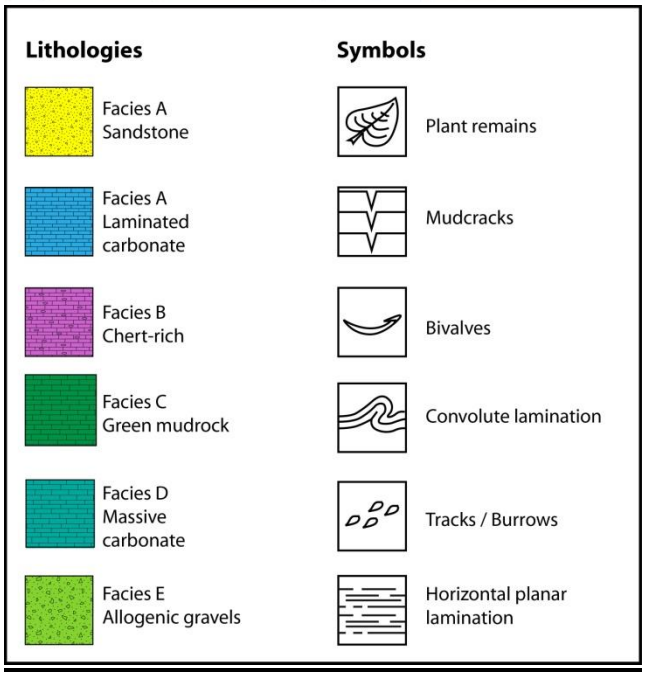

Figure 10: KK1 core log.

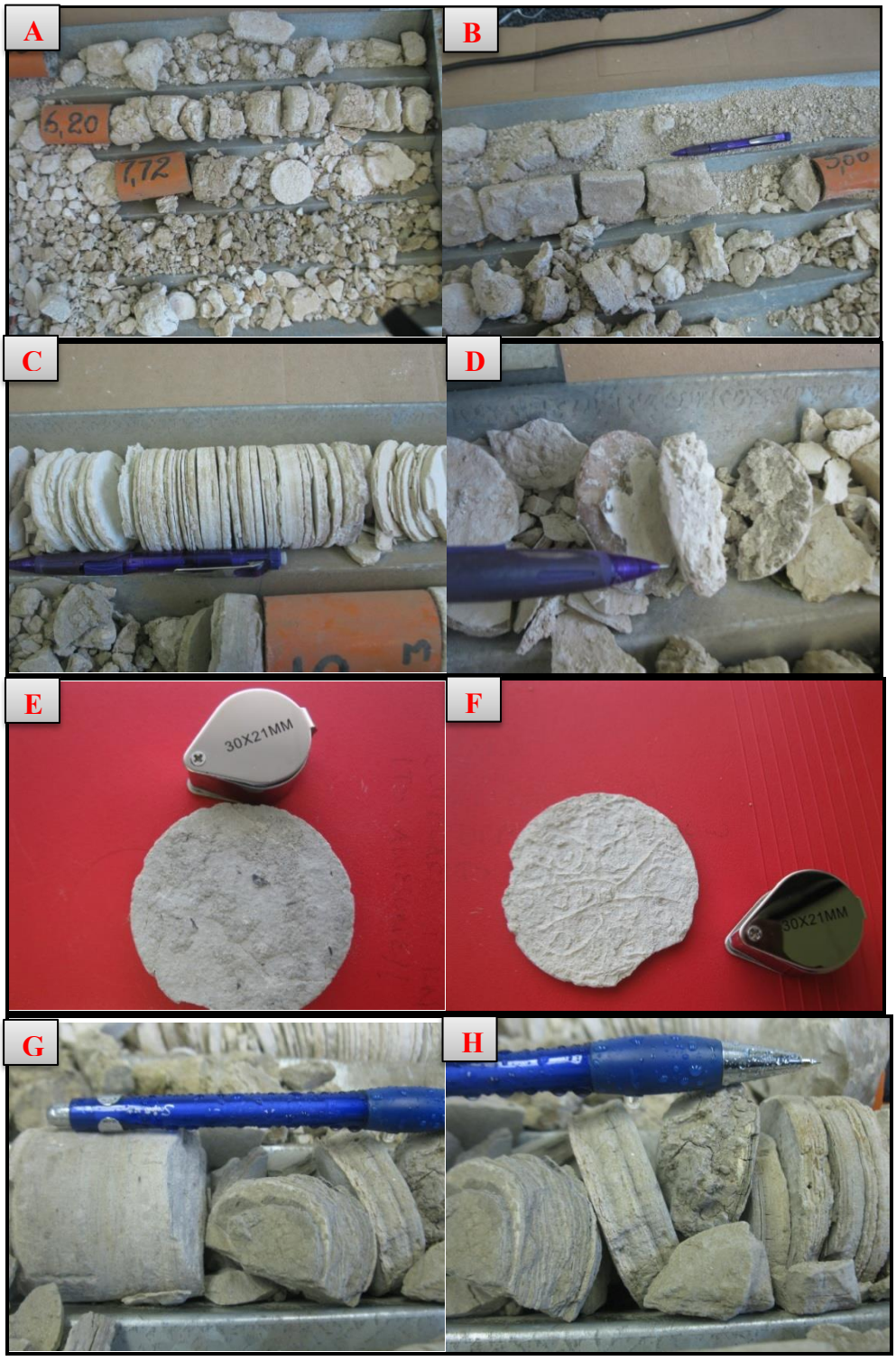

Figure 11: KK1 core A-H. A&B: Massive arenaceous carbonate from uppermost part of the succession; C: Friable laminated carbonate; D: intraformational clasts; E & F: biogenic structures on bedding planes; G & H: weakly laminated carbonate.

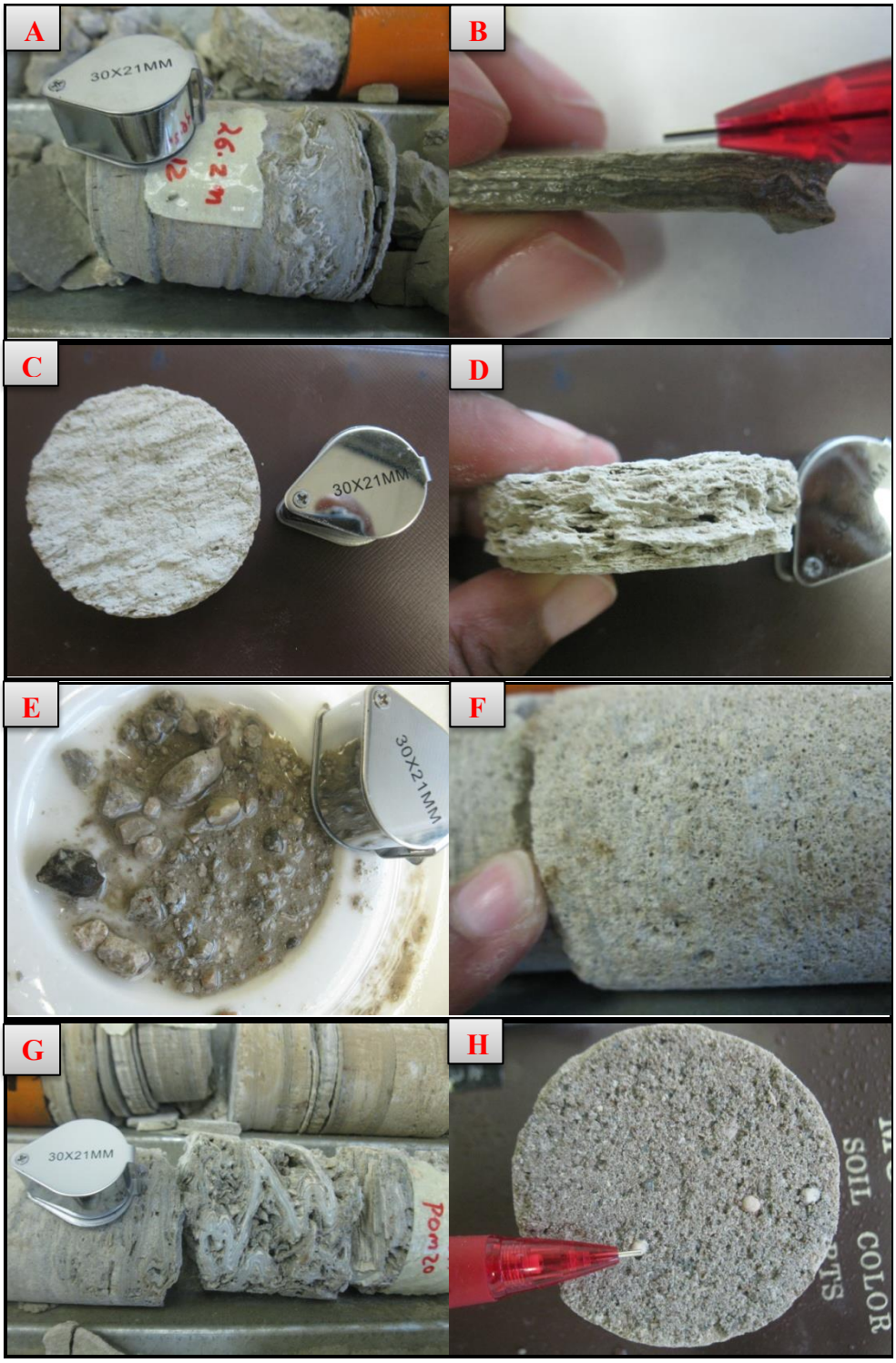

Figure 12:KK1 core A-H. A: Erosive base of debris flow deposit; B: possibly seasonal lamina C&D wavy lamination; E: Residue of exotic Karoo (Stratigraphic location) clasts. F: Massive core G: Brecciated siliceous horizon H: Small fresh water bivalves along a core parting.

Figure 13: KK1 core (A-E) A: Fine lamination; B Vertical view of lamina; C &D: Micro-debris flow; E: draped ripple surface, F: Chert found at Kalkkop site.

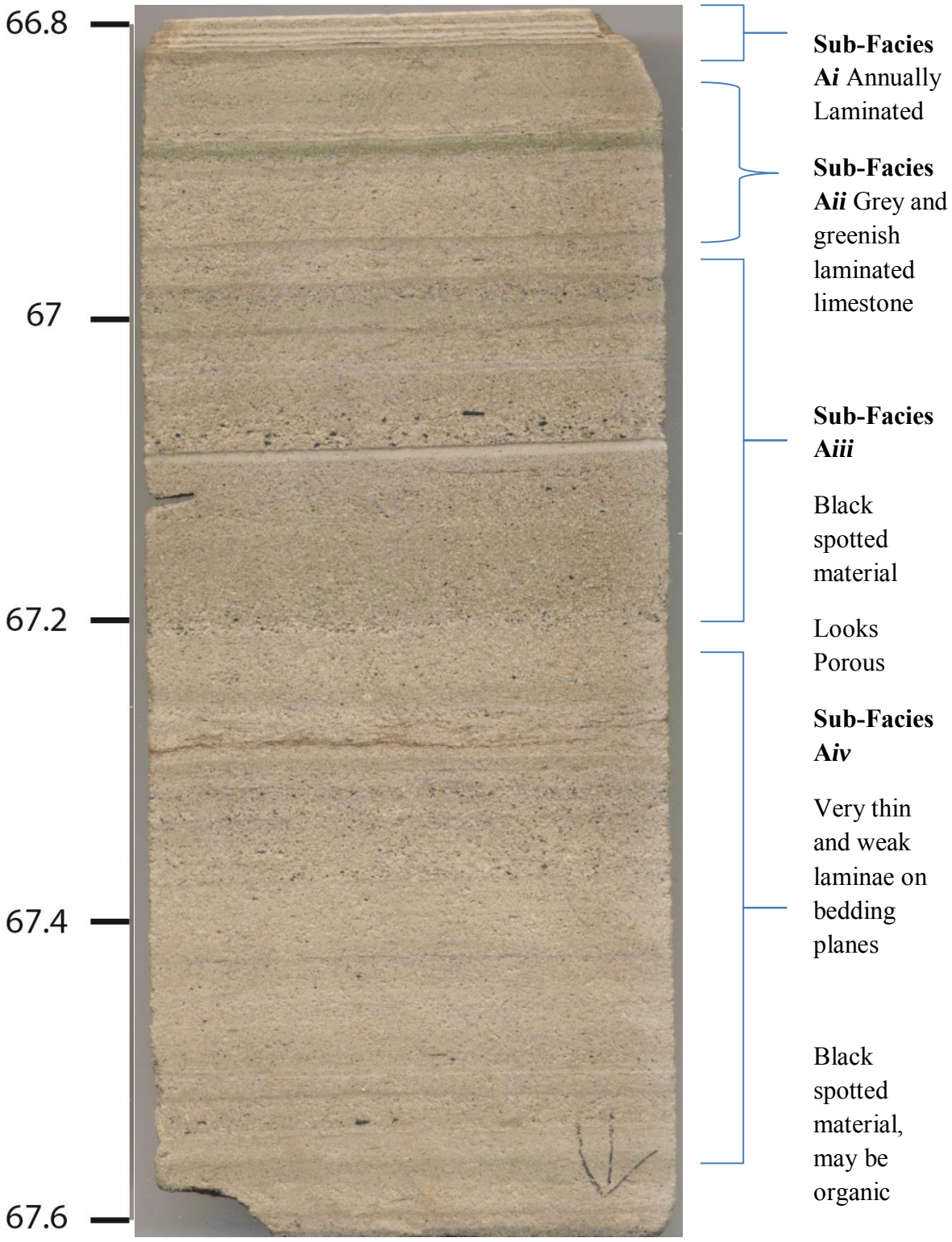

Figure 14: Detailed log at 66.8 m, showing very fine laminae with carbonaceous specks.

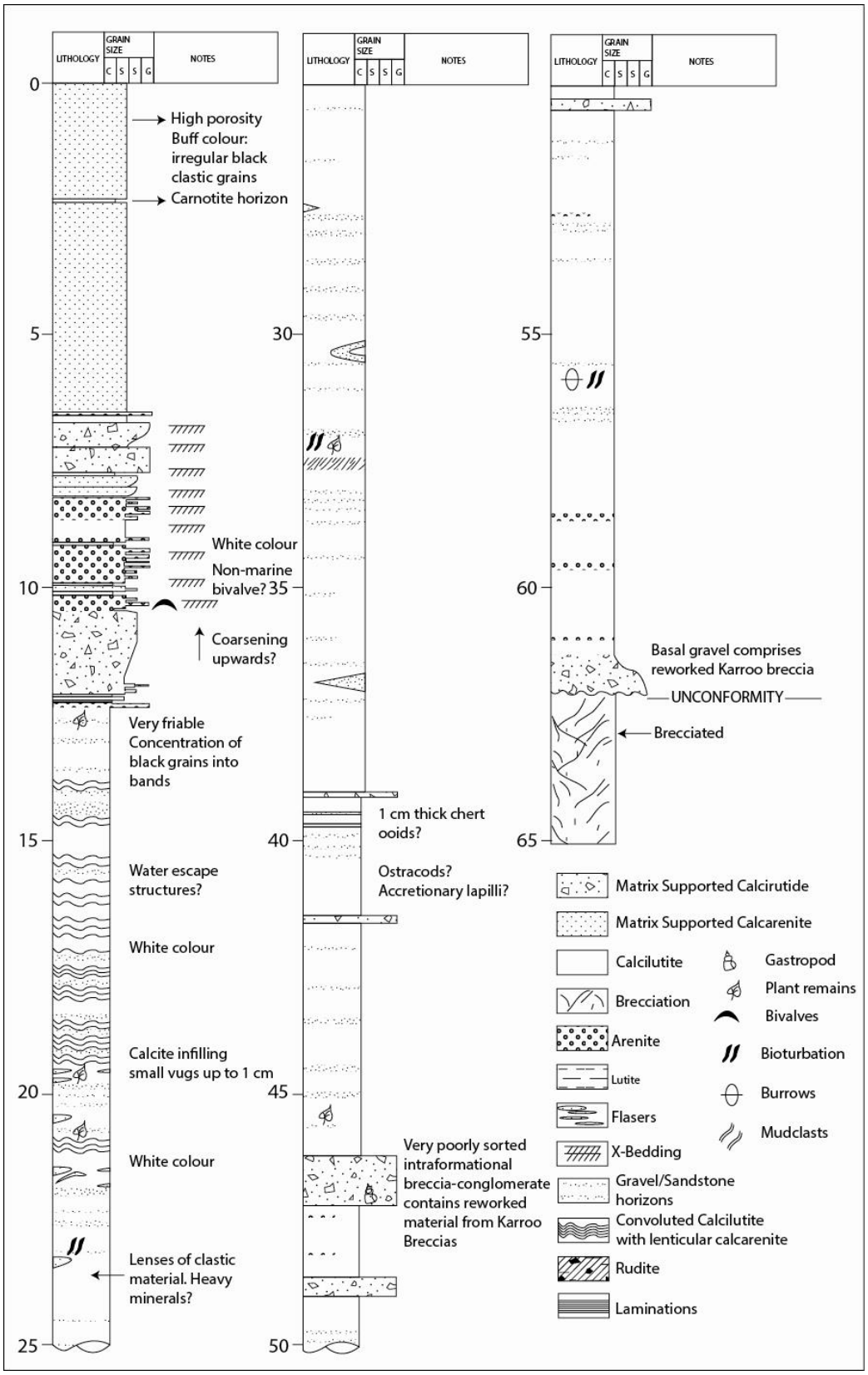

Figure 15: KK1b borehole situated 150 m west of the KK1 hole (logged by De Beers personnel). The complete although condensed Kalkkop lacustrine succession is shown.

5.2 PETROGRAPHIC STUDY

Reimold *et al.,* (1993); Koeberl *et al.,* (1994a) were the first to study the petrography of Kalkkop Crater rocks with the aim of determining the origin of the crater. The study was however focused on the breccia that was found under the 89.3 m crater sediments. Reimold *et al.,* (1998) examined the 1992 drilled core and in their study they recognised that the post-impact crater fill was extremely fine-grained and laminated on a sub-mm to several mm scale. The few clasts that were recognised were microcline-sericite, quartz, plagioclase and quartzite and shale.

In this study, the pieces of core that were used for the samples collected from 47.4-47.76 m (B1-B19), and at 66.83-67.47 m (A1-A24), were made into thin sections. The thin sections were cut perpendicular to the length of the core. The thin sections revealed very fine grained material and did not show much variation. The section contain small (<<1 mm) detrital grains of quartz. A representative thin section from 66.8 m shown in Fig.16 shows plant fragments and diatoms.

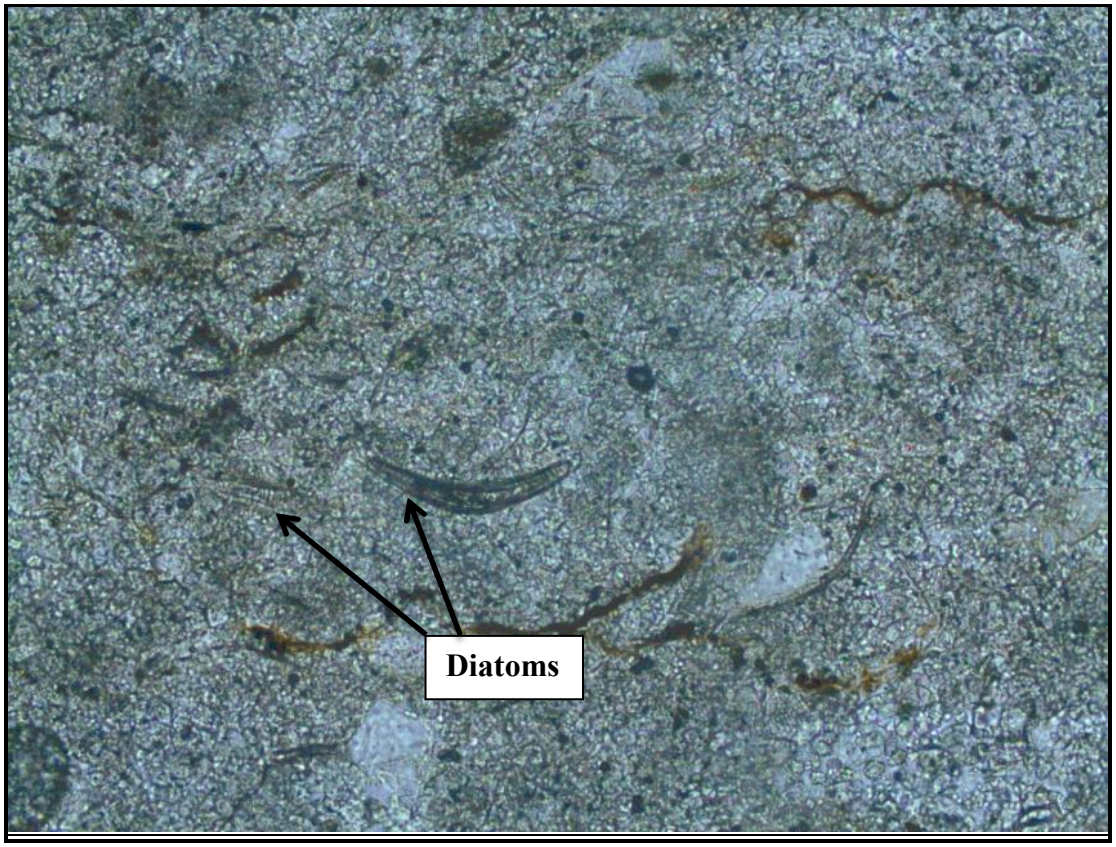

Figure 16: Photomicrograph (plane polarized light) at 66.8 m. Carbonaceous plant fragments, diatoms (left centre). Field= 1 mm.

5.3 CORES KK2 AND KK3

KK2 and KK3 are the additional boreholes that were located on the west and on the south east rim of the Kalkkop structure. Both borehole cores were logged at the Council for Geoscience Donkerhoek core shed in Pretoria. They were not studied in detail but used as comparison with the KK1 core to determine the morphology of the lake (Chapter 6.2).

5.3.1 KK2

KK2 core (Fig.17) is highly broken up and has softer material, compared to the other cores (KK1 and KK3). The upper part of the core fragments is powdered and contains about 30% (by visual estimation) of Karoo rock fragments which ranged from 1 mm to about 20 mm in size (Fig.21) in it. At 5.08 m it starts showing heavy debris flows, especially at 10 m (Fig.18 and 19) and the core starts dipping slightly. The debris flows continues to ~19.8 m and at 21.10 m the core is broken up into very soft material with occasional pieces of limestone. After 21 m, there is very little core preserved but only very soft material (palaeosoil). The core (KK2) that was examined for this study at ended at 51 m.

5.3.2 KK3

At the top of KK3 (Figs. 20 and 21), there are some shiny and translucent pieces of calcite crystals. The KK3 core is also highly broken up like KK2 and white in colour. At 2.90 m, there is crystalline laminated (Fig.22) layer, and some of it is visible from 1.60-16.6 m with thicker laminae at around 7 m as well as slumping in parts, especially at 5 m. The rock has a lot of cavities about 1-3 mm in size, which looks like tufa but harder and has a milky appearance. The vugs (cavities) end at 11.3 m. There is 1 m core loss from 11.63-13.10 m and there is slumping in some parts of the core. From 17.10 m-28.5 m there is more basement rock and the rock has a green looking colour that looks like impact breccia (sharp angled fragments) at 16.60 m.

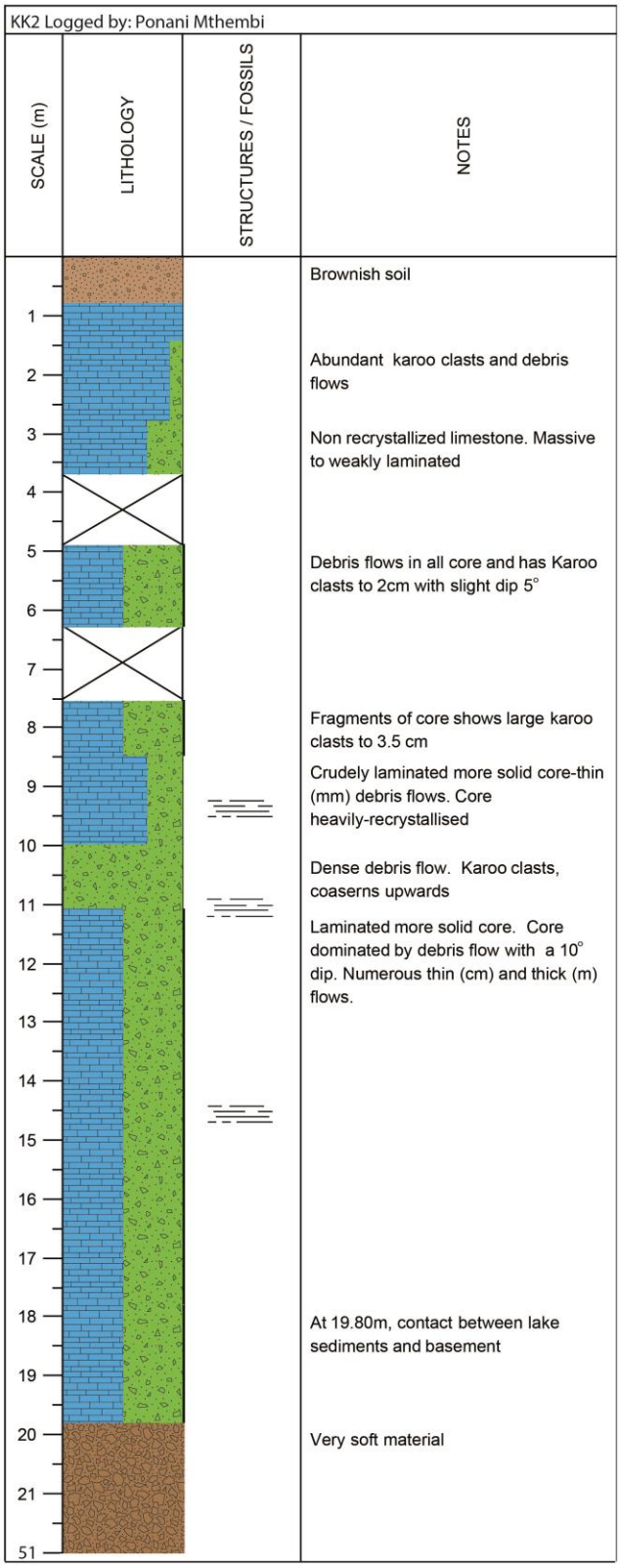

Figure 17: KK2 borehole log.

Figure 18: KK2 Borehole showing poor state of preservation of material.

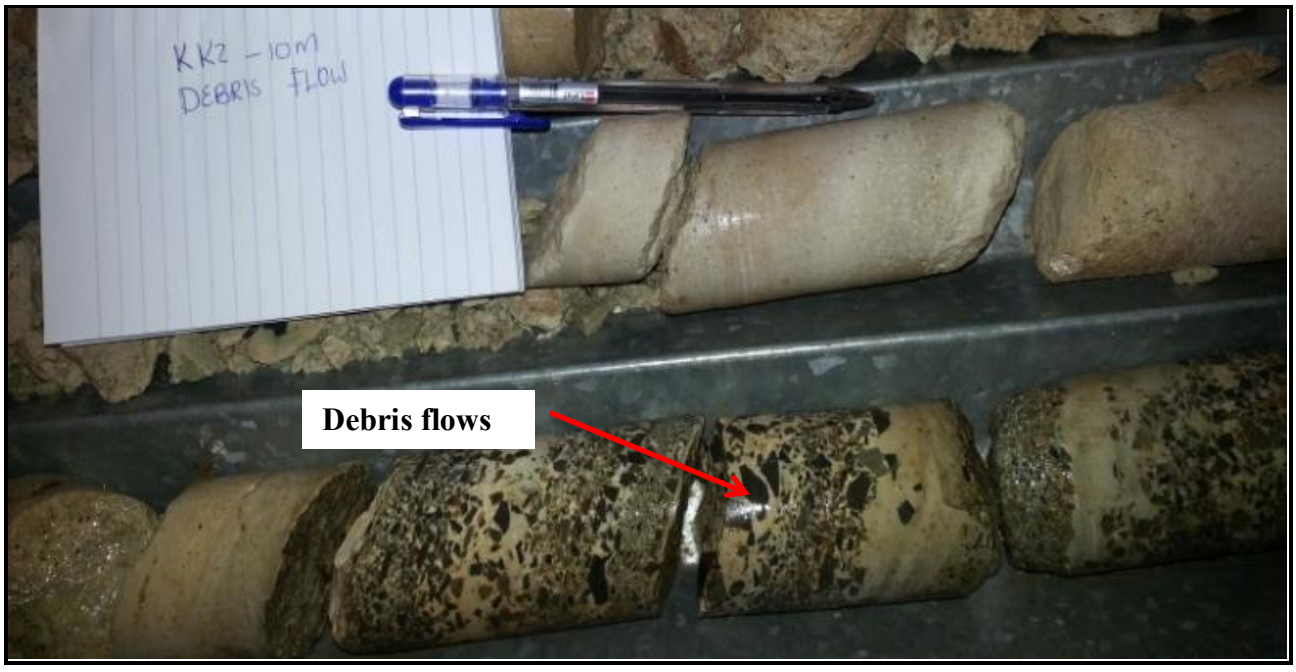

Figure 19: Debris flows in KK2.

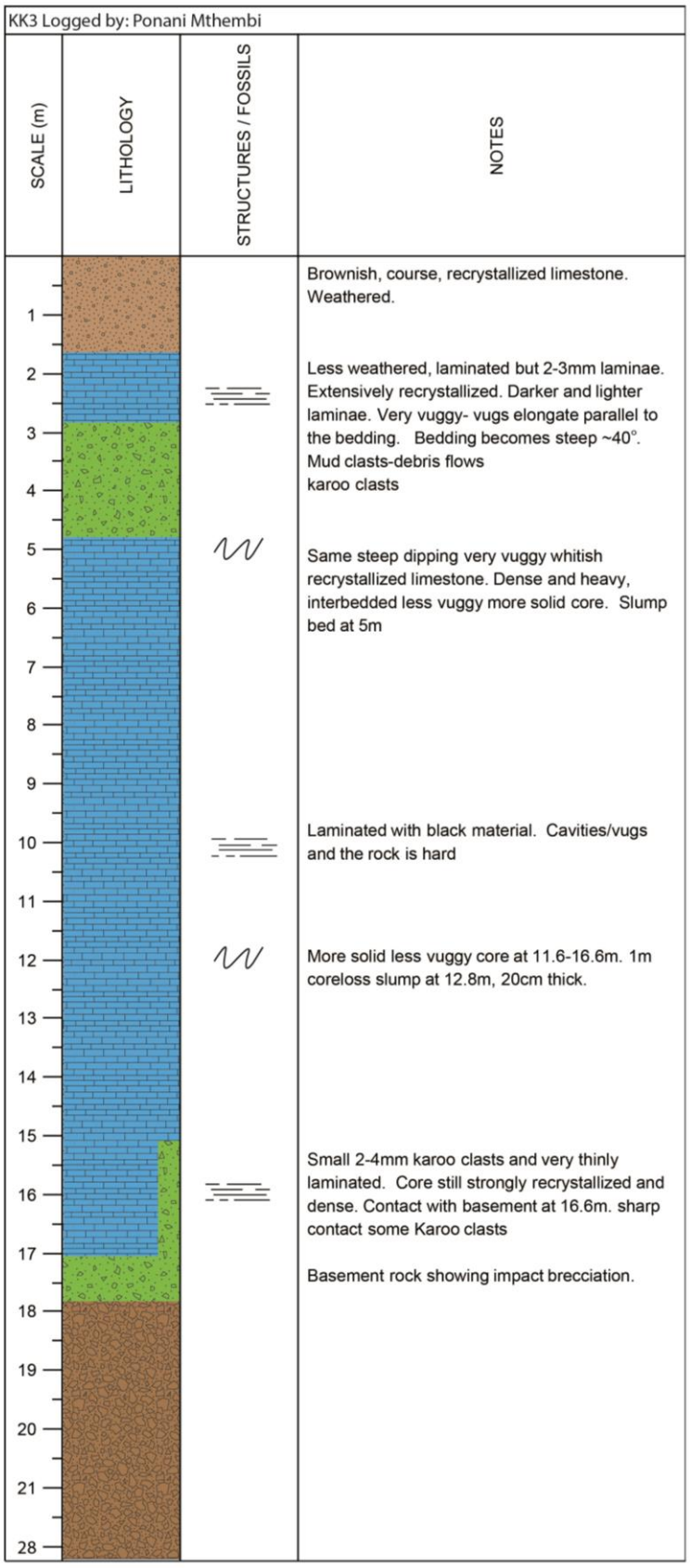

Figure 20: KK3 borehole log.

Figure 21: KK3 Borehole.

Figure 22: Extensively crystallized darker and lighter laminae.

5.5 GEOCHEMICAL DATA

5.5 .1 Chemical composition

Seventeen samples were analysed by ICP-OES, in the Department of Chemical Engineering at UCT, for chemical compositions in the lacustrine sediments (Table 1). The samples were analysed for Al_2O_3, MgO, SrO and CaO. The results showed $Al_2O_3 < 3.2$ wt.%, except for one sample (POM60) with 0.99 wt.%. This sample must have significant quantities of clay minerals in it. In some cases, the atomic Mg/Ca ratio is > 1. This ought not to be possible given that dolomite has Mg/Ca = 1 and the core samples are unlikely to contain minerals with Mg/Ca > 1 (e.g. magnesite). The best explanation for this is that the error on the Mg determination is quite high. It should be noted that this analytical work was undertaken primarily to determine the Sr content of the samples, because this was too high to determine by ICP-MS. The Al_2O_3 (as a proxy for feldspar or clay content) and SrO contents are considered to be relatively precise, whereas the CaO and MgO. The MgO content is the highest in samples at top of core (Fig. 23) and reaches 25 wt.%. This corresponds to about 50% dolomite (but there is not enough CaO for there to be this much dolomite), assuming the sample is pure carbonate. The only other element present in significant proportions is Sr. Samples contain between 0.21 and 1.12 wt.% SrO except sample POM68 which has 0.05 wt.% SrO. This sample is carbonate-poor (on basis of high Al content, therefore high clay).

Table 1
Chemical compositions

	Molec	Wt.% oxide			
Sample	Mg/Ca	CaO	MgO	Al_2O_3	SrO
PM04	1.58	18.29	20.70	2.13	0.39
PM05	1.65	21.35	25.30	1.46	0.51
PM08	2.04	18.95	27.82	0.98	0.55
PM11	0.92	27.49	18.12	1.15	0.22
PM12	0.72	34.81	18.07	0.71	0.21
PM20	0.03	51.24	1.14	0.47	0.88
PM29	0.10	42.38	2.97	0.70	0.78
PM37	0.03	48.06	1.01	0.34	0.61
PM45	1.35	26.57	25.84	0.74	0.33
PM46	1.10	28.10	22.28	0.84	0.24
PM49	1.07	29.13	22.47	0.48	0.23
PM51	1.21	28.51	24.83	0.62	0.41
PM52	0.49	29.81	10.52	1.05	0.38
PM54	0.95	22.28	15.16	1.77	0.38
PM59	0.11	45.39	3.43	0.75	0.82
PM60	0.25	39.38	6.95	0.99	0.76
PM64	0.03	46.55	0.87	1.52	0.26
PM68	2.24	1.37	2.20	4.52	0.05

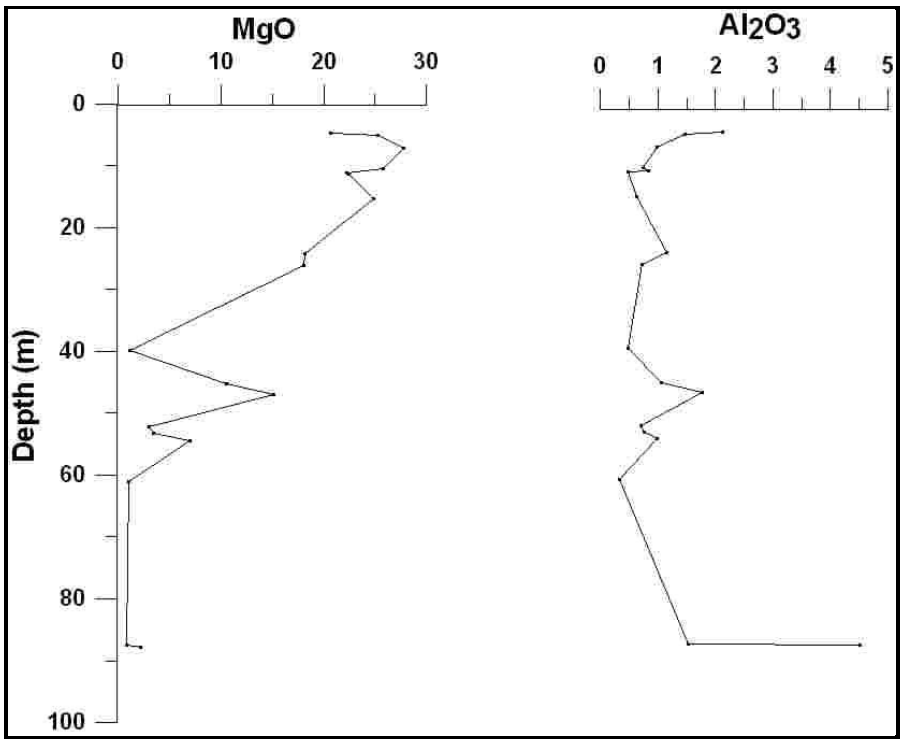

Figure 23: MgO and Al_2O_3 vs depth in KK1 core.

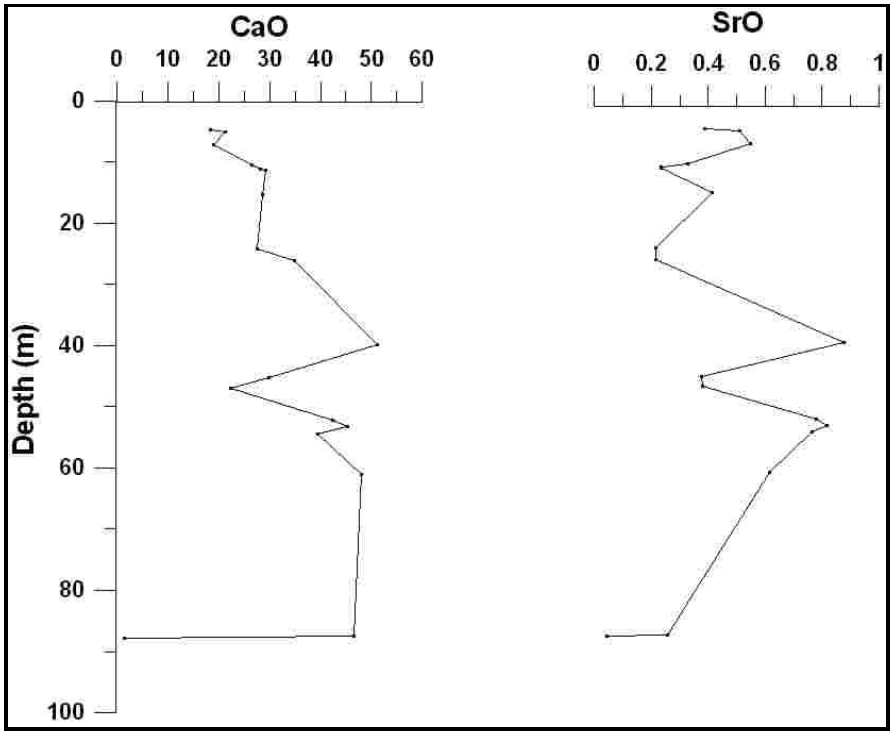

Figure 24: CaO and SrO vs Depth in KK1 core.

Table 2
Trace elements concentration and Sr isotopes.

sample	pom 04	pom 05	pom 07	pom 08	pom 45	pom 46	pom 49	pom 51	pom 09	pom 11	pom 12	pom 20	pom 52	pom 54	pom 29	pom 59	pom 60	pom37	pom 39	pom 63	pom 64	pom 68
87Sr/86Sr	0.71057	0.71053	0.71051	0.71051	0.7105	0.71051	0.71048	0.71039	0.71064	0.71046	0.71054	0.71032	0.710329	0.71039	0.71037	0.71023	0.710262	0.71027	0.71026	0.709999	0.7099	0.71074
ppm																						
Li	551.7	547.4	576.7	859.7		107.4		81.2		101.5		18.3	51.6	151.8			47.2					97.3
Sc	2.5	1.6	0.6	1.2		1.3		1.6		1.4		1.0	1.2	2.0			1.6					10.8
V	88.3	59.6	40.0	59.4		11.0		11.8		12.4		7.9	8.3	16.8			13.0					75.8
Cr	18.7	7.2	4.5	10.1		4.8		6.8		5.4		4.3	4.4	7.6			6.0					73.8
Cu	13.9	5.4	8.6	5.7		4.9		4.6		8.6		7.7	4.2	8.3			5.8					22.7
Zn	77.8	61.9	29.5	63.5		27.4		19.2		87.4		39.9	56.1	34.6			30.7					96.6
Rb	26.8	25.4	8.3	15.8		15.9		14.6		20.3		10.8	13.2	25.9			19.4					106.8
Y	5.1	3.4	1.9	2.5		3.6		3.2		3.9		2.6	3.0	4.6			3.8					22.1
Zr	24.1	14.1	6.4	11.2		11.3		14.8		18.3		10.1	12.6	24.5			14.9					117.4
Nb	2.5	1.6	0.9	1.4		1.3		1.2		1.9		1.0	1.3	2.4			1.6					12.1
Ba	178.4	177.7	127.3	118.4		150.4		112.6		147.7		169.2	197.4	179.0			168.8					456.2
La	6.8	4.6	2.8	3.5		4.3		7.2		5.7		3.0	4.0	5.0			5.0					21.4
Ce	13.6	9.3	5.7	7.1		9.3		13.3		11.7		6.4	8.3	10.7			10.8					50.2
Pr	1.7	1.1	0.7	0.8		1.0		1.4		1.4		0.7	1.0	1.2			1.2					5.9
Nd	6.3	4.4	2.7	3.1		4.1		4.9		5.1		2.8	3.7	4.8			4.7					23.9
Sm	1.3	0.9	0.6	0.6		0.9		0.9		1.0		0.6	0.7	1.0			0.9					4.9
Eu	0.2	0.2	0.1	0.1		0.2		0.2		0.2		0.1	0.2	0.2			0.2					0.9
Tb	0.1	0.1	0.1	0.1		0.1		0.1		0.1		0.1	0.1	0.1			0.1					0.6
Gd	1.0	0.7	0.4	0.5		0.8		0.7		0.8		0.5	0.6	0.9			0.7					4.1
Dy	0.9	0.6	0.3	0.4		0.6		0.6		0.7		0.4	0.5	0.8			0.6					3.9
Ho	0.2	0.1	0.1	0.1		0.1		0.1		0.1		0.1	0.1	0.2			0.1					0.7
Er	0.5	0.4	0.2	0.2		0.4		0.3		0.4		0.2	0.3	0.5			0.4					2.3
Tm	0.1	0.1	0.0	0.0		0.1		0.0		0.1		0.0	0.0	0.1			0.1					0.3
Yb	0.5	0.3	0.2	0.2		0.4		0.3		0.4		0.2	0.3	0.4			0.3					2.2
Lu	0.1	0.0	0.0	0.0		0.1		0.0		0.1		0.0	0.0	0.1			0.1					0.3
Hf	0.7	0.4	0.2	0.4		0.4		0.4		0.5		0.3	0.4	0.7			0.4					3.7
Ta	0.3	0.2	0.1	0.1		0.2		0.2		0.2		0.1	0.2	0.2			0.2					0.9
Pb	6.5	3.4	3.1	2.2		7.2		4.1		5.0		4.4	3.1	6.5			4.4					23.3
Th	2.3	1.1	0.9	0.7		2.7		0.9		2.3		1.7	1.4	1.8			1.9					14.8
U	25.8	7.8	7.0	6.0		24.3		8.1		21.2		30.8	25.6	21.2			16.9					3.6

***Sr concentration was too high to analyze by this method.**

Trace element concentrations are presented in Table 2, and the concentration of most elements is highly variable. For example, Li varies between 18.3 and 860 ppm, V varies between 8 and 88ppm, and U varies between 3.6 and 30.8 ppm. Figure 25 is a plot of Zr vs Y and Zr vs Nb. They are present in relatively small concentrations (Zr < 30 ppm; Nb < 3ppm; Y < 5 ppm) except for sample POM68. The samples have the same Zr/Y (~5.3) and Zr/Nb (~10) ratios. There is a strong correlation between Zr and Nb. This suggests that the source of Zr and Nb has a very similar Zr/Nb ratio which is either a single source of that multiple sources contribute in constant proportions. The same effect was seen by Midgeley *et al.,* (2013) for Heuweltjies calcrete in the Western Cape.

The REE (Fig. 26) are incompatible in carbonates and all of the samples analysed have approximately parallel REE patterns. The REE is most likely to be hosted in the non-silicate component of the samples. POM68 has significantly higher total REE in keeping with its much higher Zr, Nb and Y. All samples have a negative Eu anomaly but none of the samples have a Ce anomaly which might indicate a marine origin. Also shown are the REE profiles for calcrete from Heuweltjies in the Western Cape (Midgeley *et al.,* 2013). These patterns are parallel to the Kalkkop patterns but with higher total REE. Note that the REE-rich sample POM68 has a REE pattern that is not parallel to the others, being more HREE-enriched. The parallel patterns can be interpreted as that the 'dust' in various parts of southern South Africa is of fairly similar in composition at least as far as its REE are concerned.

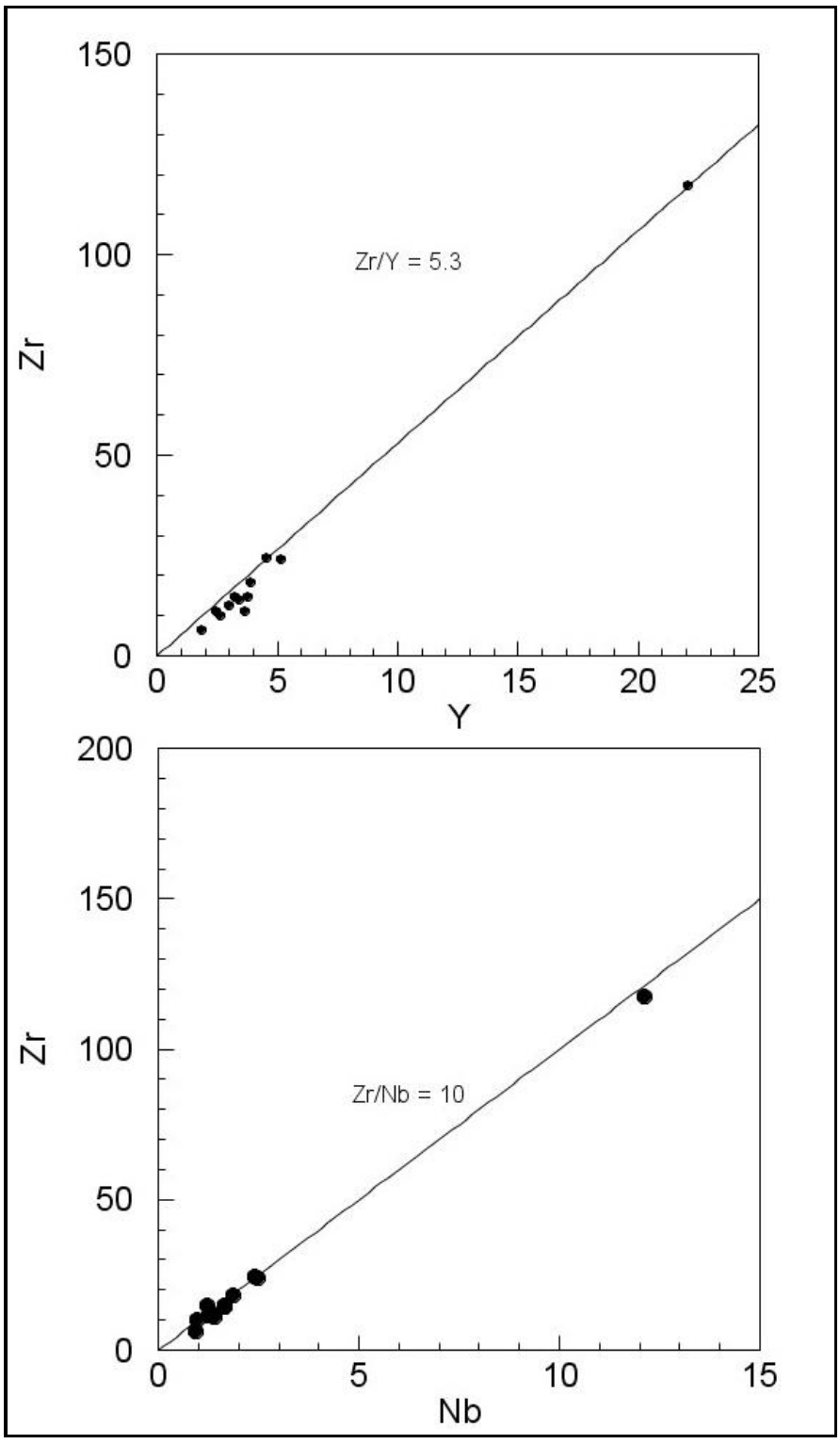

Figure 25: Plots of Zr vs Y and Nb in core samples, Midgley et al (2013) also found a ratio of about 10 in heuweltjie calcrete.

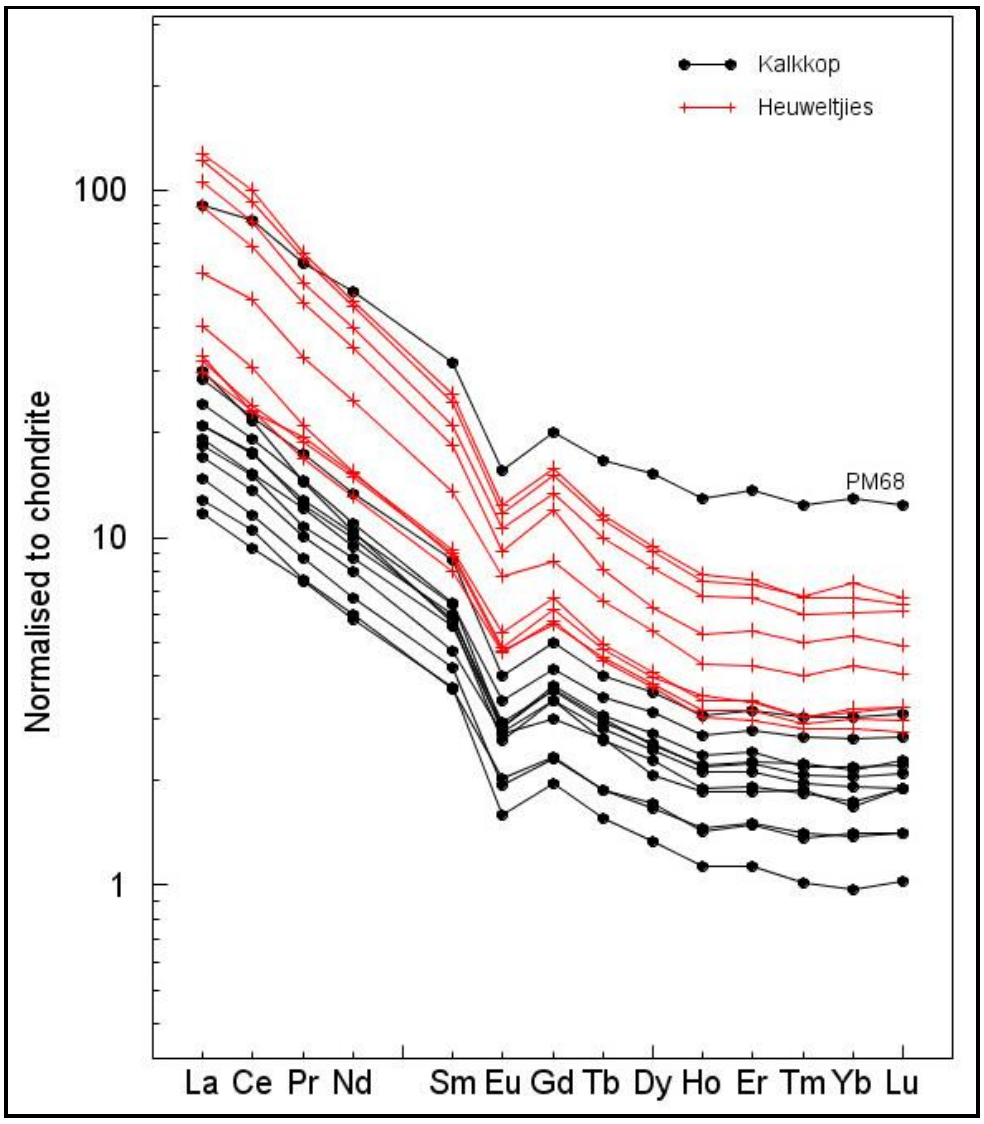

Figure 26: Chondrite-normalized REE profiles for KK1 core samples. Chondrite-normalized REE, (Sun and McDonough 1989) profiles for calcretes associated with Western Cape heuweltjies in red (Midgley *et a.,l* 2013).

5.5.2 C and O stable isotope

Table 3: Stable isotope data (POM=Core samples, BH-KK=surface samples)

Sample	δ13C (‰) PDB	δ18O (‰) PDB	Depth (m)	Sample	δ13C (‰) PDB	δ18O (‰) PDB	Depth (m)
BH-KK1	-6.99	-4.27	0.0				
BH-KK2	-5.68	-4.33	0.0	POM 54	2.81	6.37	46.9
BH-KK3	-5.27	-4.39	0.0	POM 55	3.09	6.40	47.0
BH-KK5	-5.57	-3.35	0.0	POM24	1.36	3.27	47.2
BH-KK7	-5.19	-0.67	0.0	POM 56	1.64	3.70	47.3
POM01	0.05	7.93	0.4	POM25	2.52	5.10	48.0
POM02	-0.35	7.37	0.9	POM 57	0.46	2.78	48.4
POM03	-0.08	7.81	2.2	POM26	0.88	2.62	49.0
POM04	0.16	8.11	4.8	POM27	1.39	4.09	50.0
POM05	0.01	6.57	5.1	POM28	0.20	2.88	51.0
POM07	0.15	6.53	6.4	POM29	0.33	3.15	52.2
POM08	0.54	6.90	7.2	POM 58	0.38	3.48	52.8
POM 45	-1.94	5.38	10.5	POM 59	0.53	3.87	53.3
POM 46	-0.28	7.40	11.1	POM30	0.19	3.07	53.7
POM 47	-0.18	6.80	11.2	POM31	1.57	4.63	54.4
POM 48	0.02	7.23	11.2	POM 60	1.22	4.64	54.4
POM 49	-0.17	6.56	11.3	POM 61	0.35	3.57	54.9
POM 50	-0.14	6.84	11.3	POM32	0.35	2.95	55.2
POM 51	0.06	7.45	15.3	POM33	-0.20	1.45	57.3
POM09	0.02	7.38	18.4	POM34	-0.49	1.67	58.5
POM10	-0.54	6.13	20.0	POM35	-0.34	2.26	59.3
POM11	0.25	6.19	24.3	POM36	-0.32	2.53	60.0
POM12	0.10	6.10	26.2	POM37	-0.80	1.71	61.0
POM13	-0.63	4.47	31.8	POM38	-1.33	1.18	62.5
POM14	-0.52	4.72	32.2	POM39	-1.65	1.27	63.2
POM15	0.45	5.96	32.5	POM40	-1.98	1.29	64.1
POM16	2.85	6.55	35.0	POM41	-2.27	1.41	65.4
POM17	-0.42	3.83	37.0	POM42	-2.87	0.09	67.0
POM18	0.21	3.86	38.1	POM43	-2.82	0.07	70.1
POM19	0.29	4.26	38.7	POM 62	-3.70	0.27	87.0
POM20	0.08	4.10	39.8	POM 63	-3.84	0.18	87.2
POM21	-0.18	3.84	42.0	POM 64	-3.70	-1.20	87.5
POM22	0.39	3.76	43.8	POM 65	-3.93	0.04	87.5
POM23	0.34	3.67	44.4	POM 66	-4.72	-2.93	87.6
POM 52	1.74	5.11	45.3	POM 67	-6.51	-3.25	87.7
POM 53	1.07	4.21	46.9	POM44	-6.08	-3.85	88.4

Stable isotope data for both core and surface samples (but not the detailed core data) are given in Table 3. The samples named POM (1-67) are the core samples and BH-KK represents all surface samples at 0 m. The $\delta^{13}C$ values vary between -6.99‰ and 3.09‰ and the $\delta^{18}O$ values vary between -4.39‰ and 8.11‰. In Figure.30 and 31, there is great variation between $\delta^{13}C$ and $\delta^{18}O$ both in PDB.

There is a good correlation between $\delta^{13}C$ and $\delta^{18}O$ for the data as a whole. Figure 27 shows two groups of samples, surface samples (BH-KK) and core samples (POM). Surface samples $\delta^{13}C$ range from -6.99 to -5.19 and $\delta^{18}O$ range between -4.27 and -0.67. Figure 27 and 28 also shows two groups of samples that show one group (A) $\delta^{13}C$ and $\delta^{18}O$ plotting at ~0 and group (B) plotting off the main trend at ~7. The $\delta^{13}C$ values show no systematic change with depth but a systematic decrease towards the base and the $\delta^{18}O$ values are showing the systematic decrease from the top to bottom of the core.

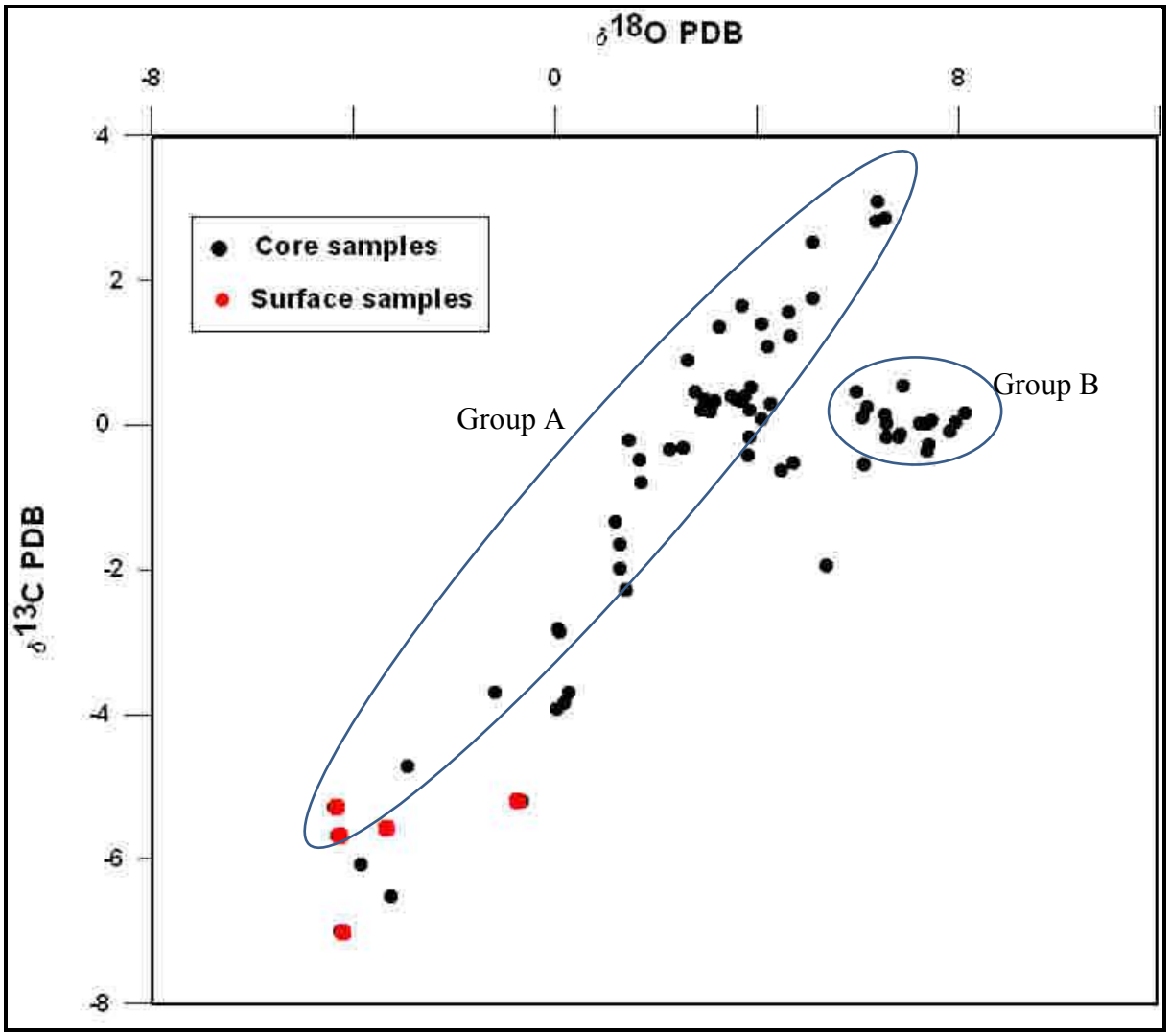

Figure 27: Plot of $\delta^{13}C$ vs $\delta^{18}O$ of core samples and surface samples.

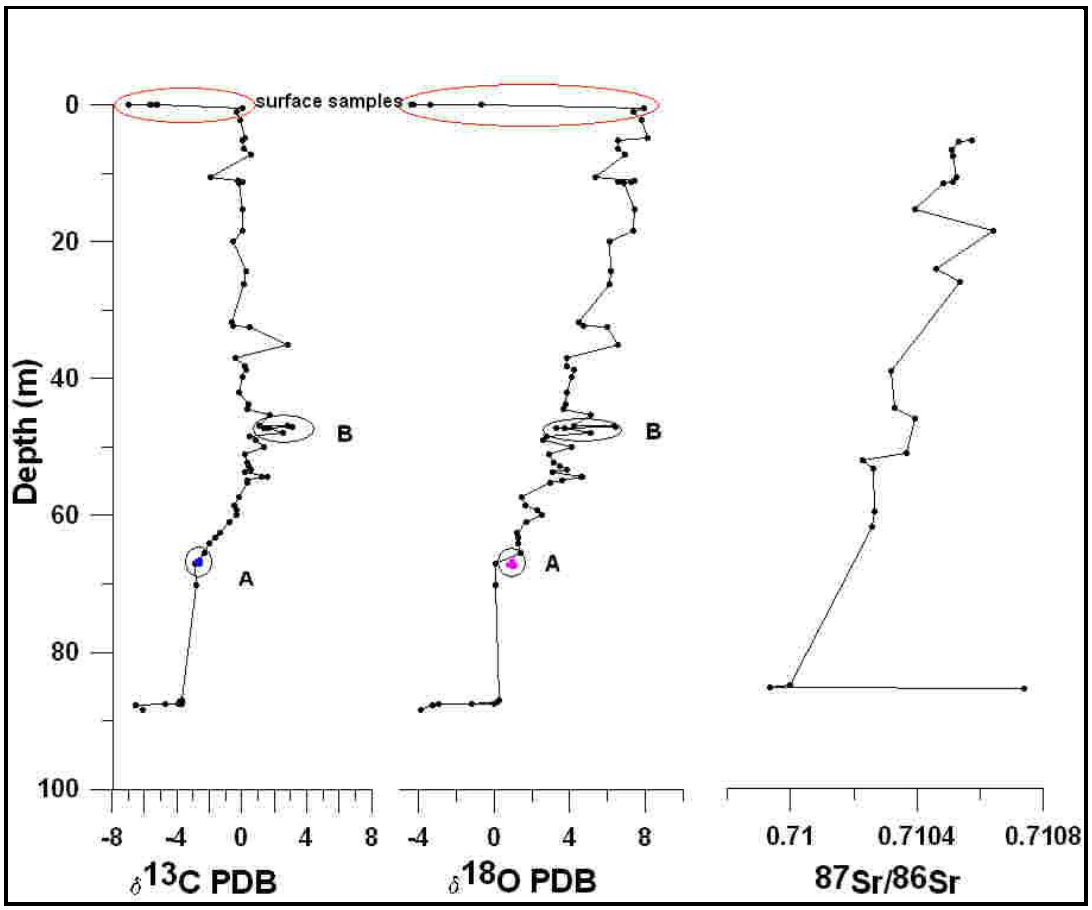

Figure 28: Variation of $\delta^{13}C$ and $\delta^{18}O$ with depth in core and surface samples (not collected in same place as cores were drilled) circled in red. Detailed Sections A and B also shown and $^{87}Sr/^{86}Sr$.

The variation of $\delta^{13}C$ and $\delta^{18}O$ for the whole data set is shown by figures 28 and 29. Above ~50 m the $\delta^{18}O$ continues to increase, whereas the $\delta^{13}C$ remains relatively constant over the upper core section. The $\delta^{13}C$ and $\delta^{18}O$ show a strong correlation ($r = 0.81$) in the lower part of the succession. There is a generally strong correlation between $\delta^{13}C$ and $\delta^{18}O$ except for samples with $\delta^{13}C \sim 0$. These correspond to the samples from 0-40 m in the core.

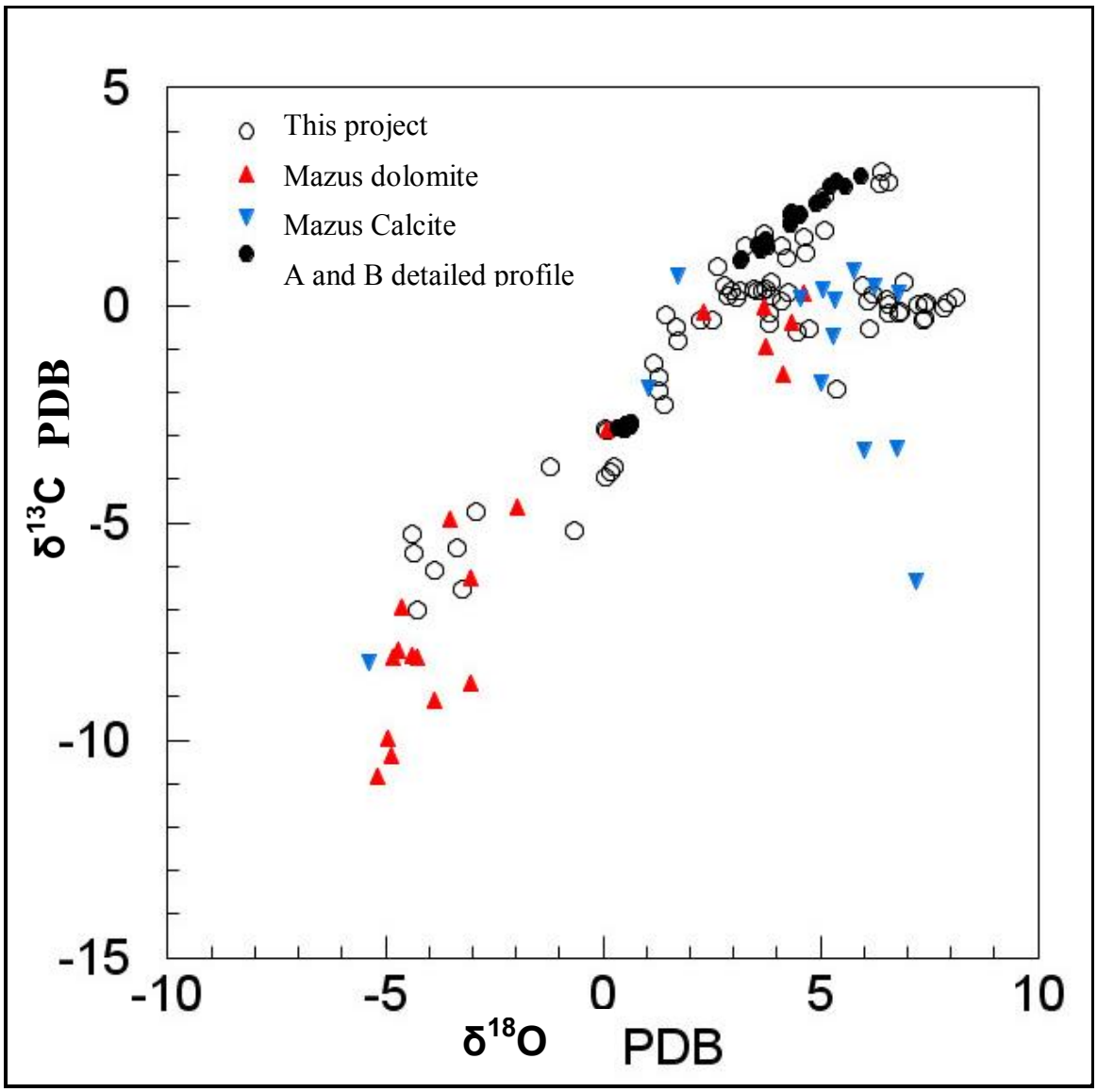

Figure 29: Plot of $\delta^{13}C$ and $\delta^{18}O$ for Core carbonates and detailed sections A and B. Data from previous study by Mazus, (1999) also shown.

Figure 29 shows mineralogy data from previous CGS reports (Mazus, 1999). Some of the calcite data (Mazus, 1999) extend to lower $\delta^{13}C$ than the samples from this project and some of the dolomites plot off the main trend, as does B group of our data.

Samples were collected at small intervals from 47.4-47.76 m (B1-B19), and at 66.83-67.47 m (A1-A24), to look for variation in smaller scale, represented in table 3 and (Fig.30). The detailed analysis was done on two sections of the core that showed large variation in isotope composition. Results of the detailed samples for high resolution, from 47.4-47.76 m (B1-B19, Fig. 31), and at 66.83-67.47 m (A1-A24, Fig.32), shows variation significantly greater than the analytical error. Section (A) shows very little significant variation in either $\delta^{13}C$ or $\delta^{18}O$.

In section A, $\delta^{13}C$ and $\delta^{18}O$ values are between -2.87‰ to -2.72‰ and 0.35‰ to 0.65‰ respectively (Fig.33). The difference in variation is < 0.2 per mil for $\delta^{13}C$ and < 0.3 per mil for $\delta^{18}O$ and this is close to the analytical error. The variation is probably is due to analytical error.

Section B is from a depth where both $\delta^{13}C$ and $\delta^{18}O$ values are highly variable, and where $\delta^{13}C$ values change from increasing with height to showing no systematic change with height in (Fig. 34). In section B, $\delta^{13}C$ values are between 1.03‰ to 2, 96‰ and the $\delta^{18}O$ values are between 3.16‰ to 5.92‰. Section B has variation up to 3 per mil in $\delta^{13}C$ and $\delta^{18}O$ at the cm scale.

Table 3: C and O Isotopes in sections A and B

Sample	δ13C (‰) PDB	δ18O (‰) PDB	Depth (m)
A1	-2.75	0.52	66.83
A2	-2.78	0.60	67.03
A3	-2.74	0.56	67.05
A4	-2.75	0.57	67.07
A5	-2.79	0.53	67.09
A6	-2.79	0.49	67.11
A7	-2.87	0.48	67.13
A8	-2.79	0.51	67.15
A9	-2.79	0.60	67.17
A10	-2.82	0.36	67.19
A11	-2.87	0.51	67.21
A13	-2.79	0.55	67.23
A14	-2.80	0.60	67.25
A15	-2.80	0.52	67.27
A16	-2.74	0.58	67.29
A17	-2.82	0.35	67.31
A18	-2.77	0.64	67.33
A19	-2.75	0.55	67.35
A20	-2.72	0.65	67.37
A21	-2.75	0.58	67.39
A22	-2.74	0.64	67.41
A23	-2.75	0.60	67.43
A24	-2.81	0.59	67.45
A25	-2.79	0.54	67.47
B1	1.05	3.18	47.40
B2	1.34	3.77	47.42
B3	1.26	3.61	47.44
B4	2.08	4.53	47.46
B5	2.04	4.50	47.48
B6	1.48	3.73	47.50
B7	1.03	3.16	47.52
B8	2.33	4.90	47.54
B9	2.71	5.21	47.56
B10	2.83	5.36	47.58
B11	2.39	5.04	47.60
B12	2.96	5.92	47.62
B13	2.71	5.57	47.64
B14	2.12	4.34	47.66
B15	1.83	4.31	47.68
B16	1.88	4.31	47.70
B17	2.10	4.29	47.72
B18	1.45	3.71	47.74
B19	1.37	3.55	47.76

Figure 30: Samples 47.4 m and 66.83 m before drilling for sampling, showing very fine possibly seasonal laminations, more visible on B than on A.

Figure 31: Sample at 47.4 m (pencil as scale) after sampling at <cm level.

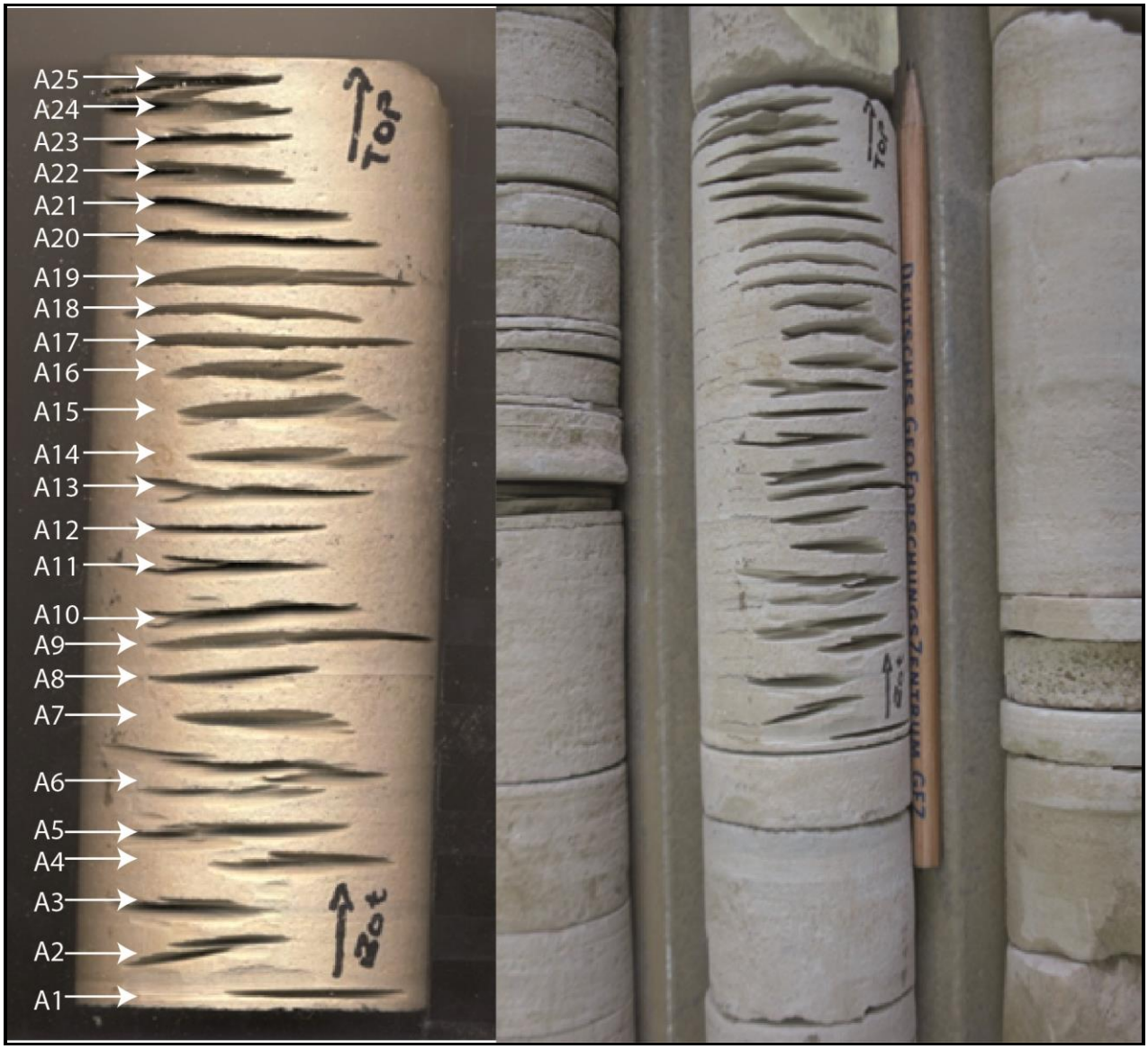

Figure 32: Sample at 66.83 m after sampling for detailed study of the core.

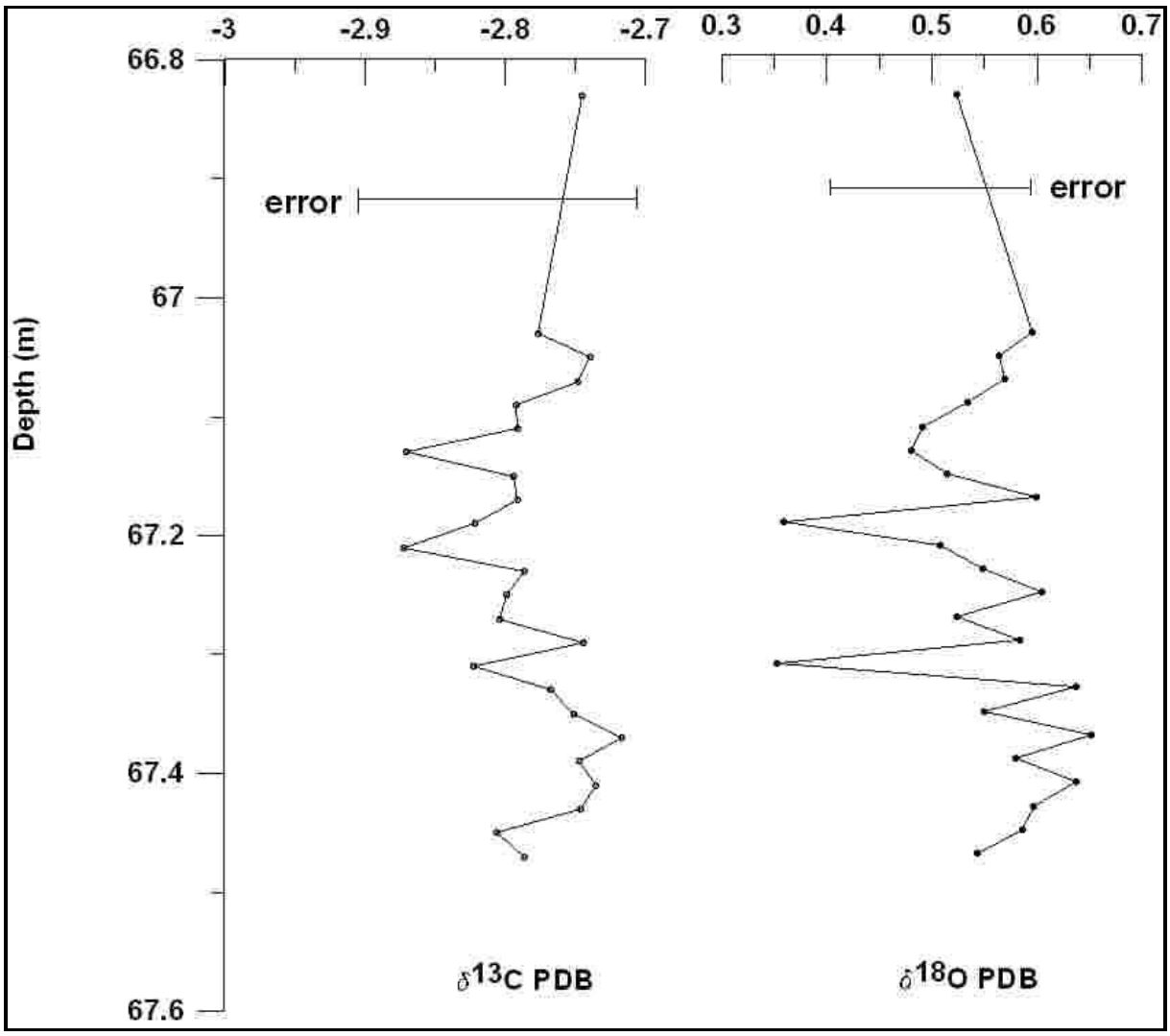

Figure 33: Variation of $\delta^{13}C$ and $\delta^{18}O$ with depth in detailed Section A.

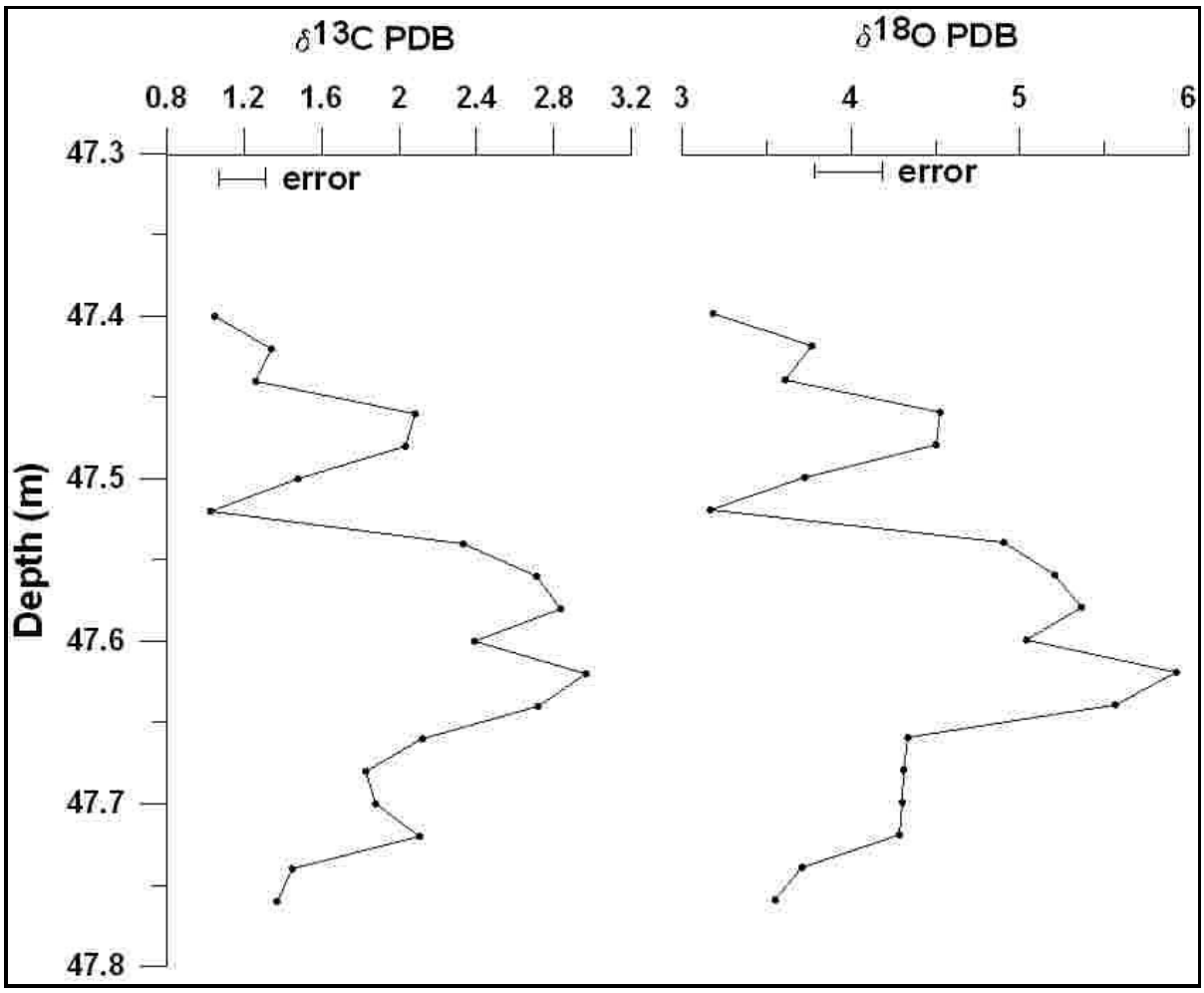

Figure 34: Variation of $\delta^{13}C$ and $\delta^{18}O$ with depth in detailed Section B.

Figure 35 shows plots of $\delta^{13}C$ and $\delta^{18}O$ for Sections A and B. Section A shows a reasonable correlation but not as good as section B ($r = 0.6$) which is to be expected given that the variation is little more than the analytical error. Section B however shows an extremely strong positive correlation between $\delta^{13}C$ and $\delta^{18}O$ ($r = 0.98$).

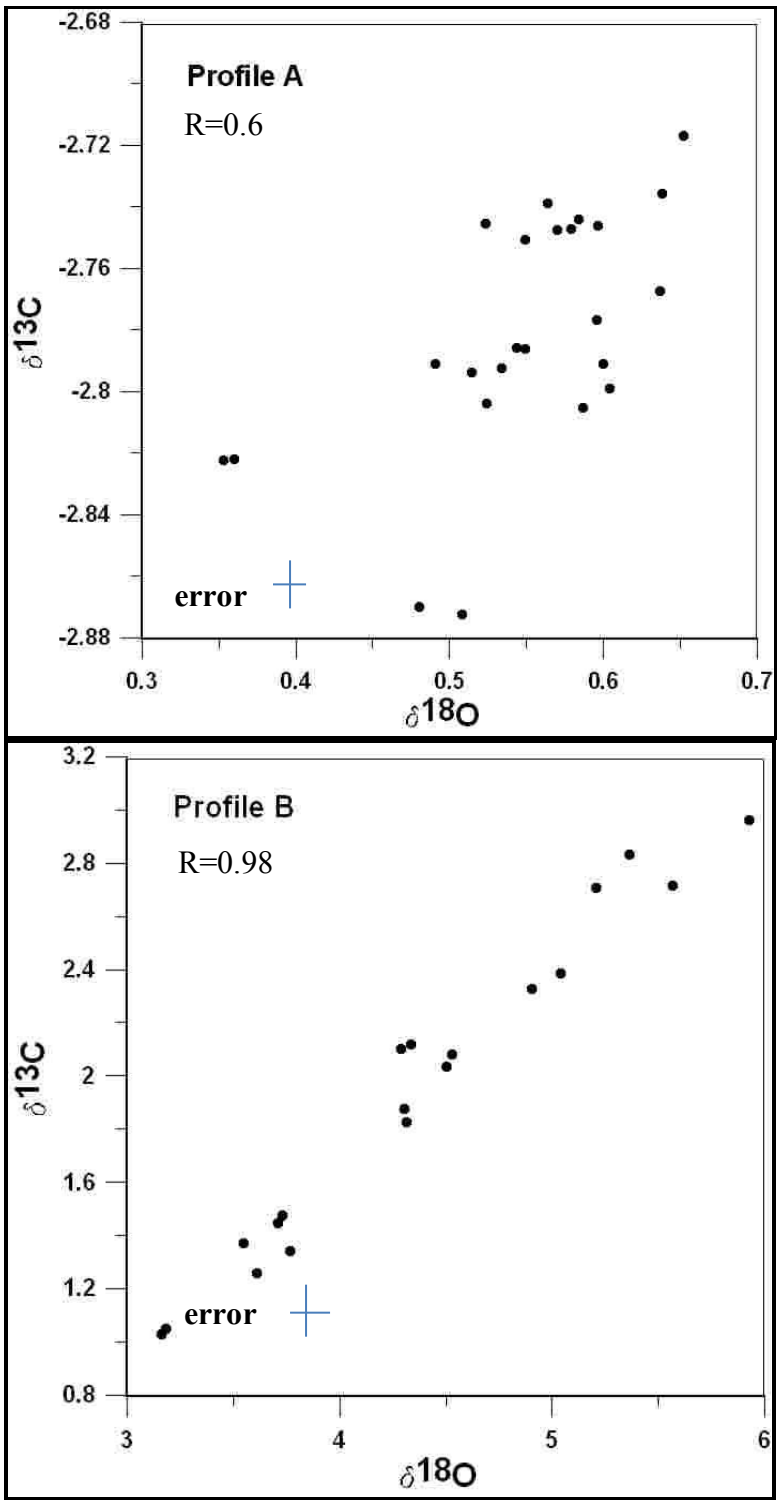

Figure 35: Plot of $\delta^{13}C$ and $\delta^{18}O$ for detailed sections A and B.

5.5 3 Sr Isotopes

The $^{87}Sr/^{86}Sr$ ratios of the Kalkkop Crater core are shown in Table 1 and figures 36 and 37. Only a smaller number of samples were analysed. The $^{87}Sr/^{86}Sr$ ratio values go higher up to 0.710740 and the lowest value is 0.709935. The results show a gradual decrease in Sr-isotope ratio with increasing depth (r = -0.92). The Sr content shows no systematic variation with depth (Fig. 36). The $\delta^{13}C$ values show no significant correlation with Sr-isotope ratio whereas $\delta^{18}O$ shows a good positive correlation (r = 0.90) with Sr-isotope ratio (Figs.36 and 37).

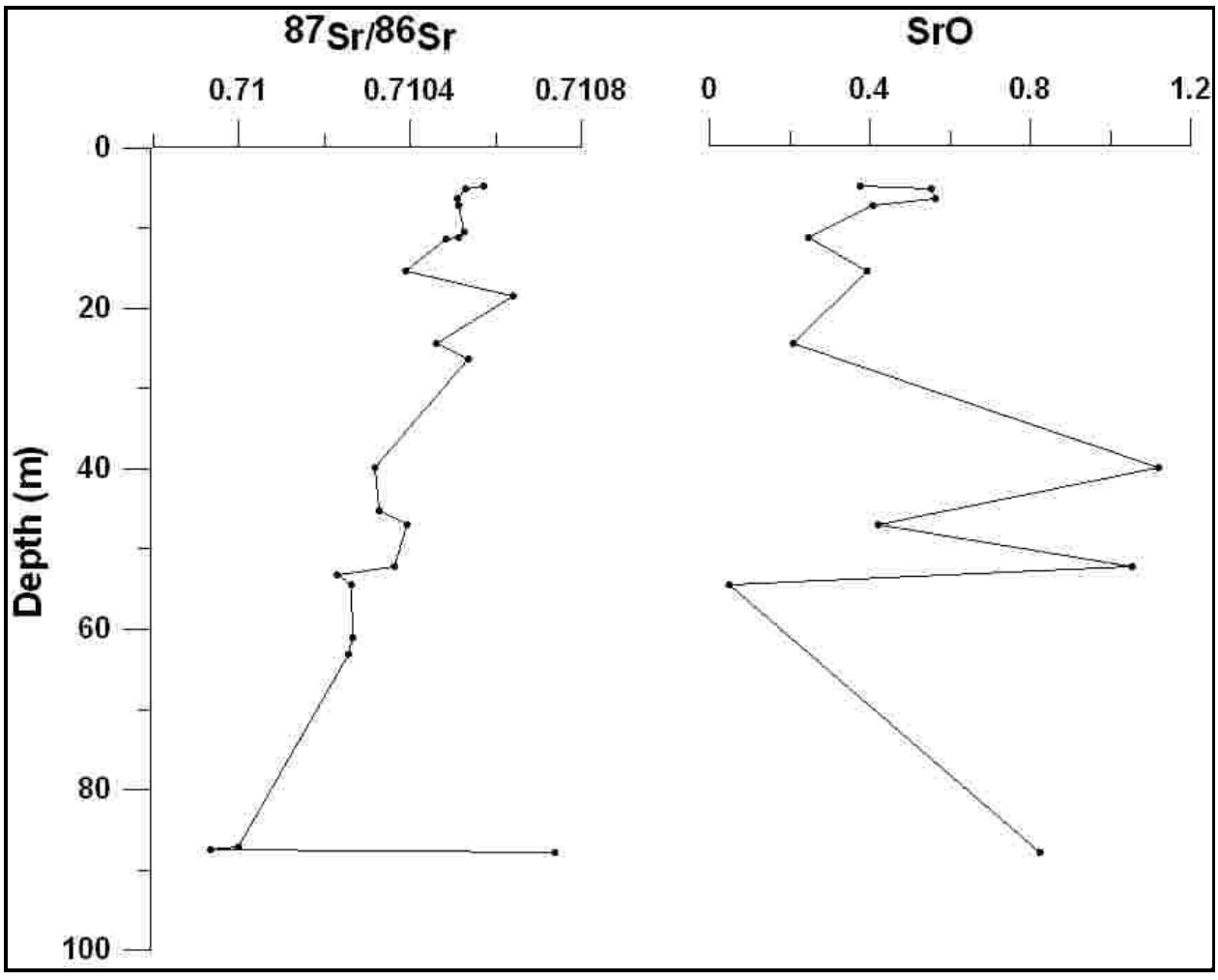

Figure 36: Plot of $^{87}Sr/^{86}Sr$ and SrO vs depth for the core samples.

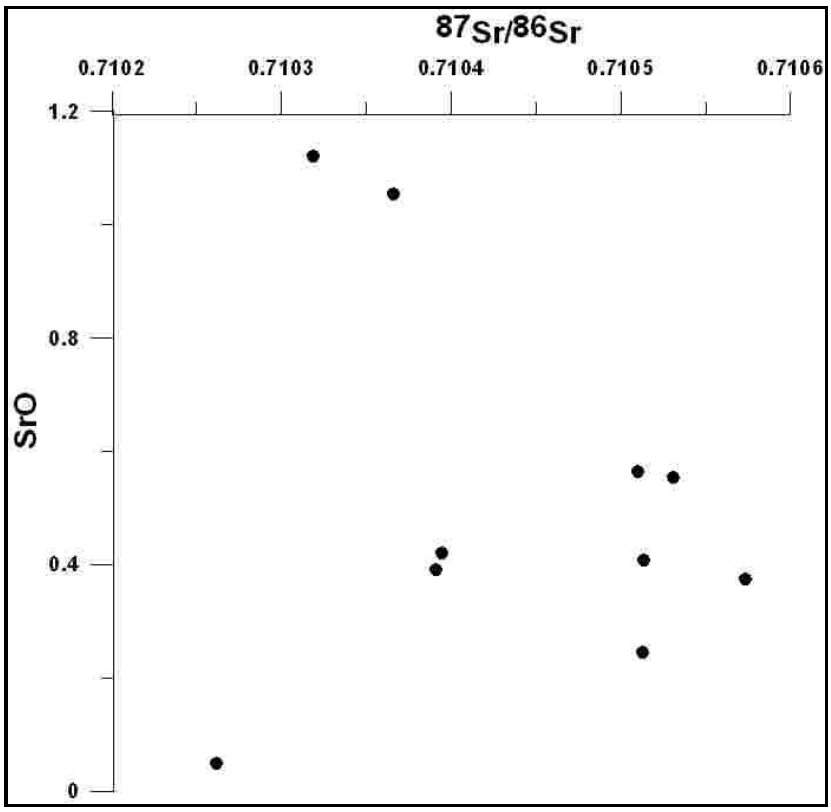

Figure 37: Plot of SrO vs $^{87}Sr/^{86}Sr$ for core samples.

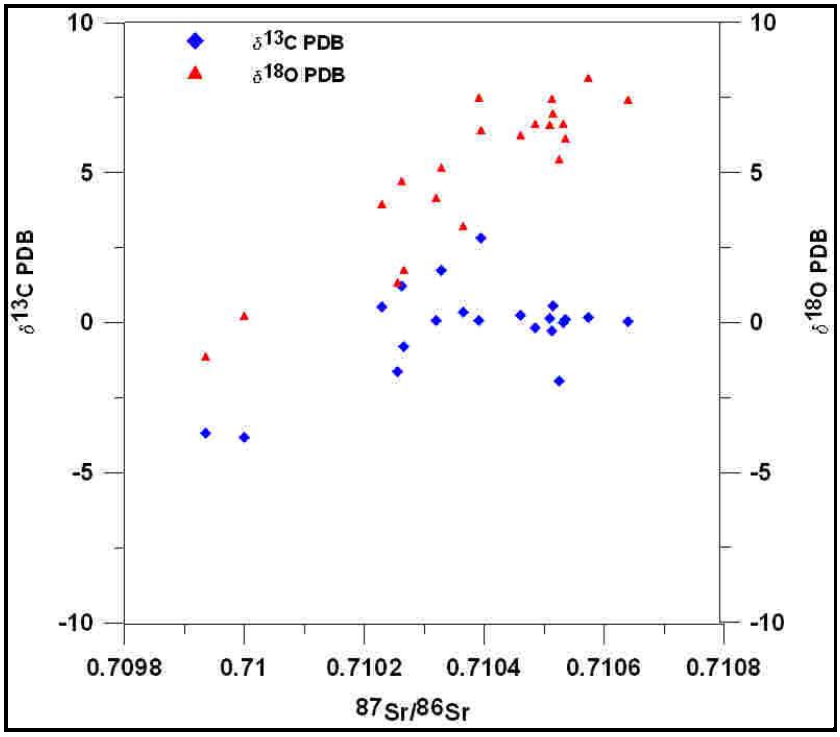

Figure 38: Plot of $\delta^{13}C$ and $\delta^{18}O$ vs $^{87}Sr/^{86}Sr$ for core samples.

6. DISCUSSION

This section will discuss and attempt to explain all the main points and observations that were covered in the results section to tie all the measured parameters from the Kalkkop Crater core.

6.1 KK1 FACIES INTERPRETATIONS

A 150 m deep crater would have been instantly excavated by the meteorite impact at Kalkkop, All faunas and floras in the immediate vicinity of the blast would have been destroyed, and would only through time have become re-established. The country rock is seen to have been extensively shattered in outcrop and cores, changing groundwater flow patterns. Groundwater would have immediately started flowing into the crater, supplemented by rainwater inflow, forming the initial lake and from this time the various sedimentary facies would have begun accumulating in the lake. The lowermost part of the core comprises upward fining reworked Karoo clasts and this is likely to represent aerial fallout following the impact explosion. The initial lacustrine sediments consist of weakly laminated, greyish and only slightly calcareous clayey and silty material, suggesting somewhat reducing conditions and deep water. Possibly the extensively shattered country rock would have given rise to rapid inflow of water during floods or high rainfall, thus explain this feature. The development of lake basin and lake margin facies is controlled by the depth of the lake and its morphology (Platt, 1991). In Lake Bosumtwi (Ghana), the lake compositional variation was partly constrained by the concentric shape of the basin, the depth and the distance from the lake margins were greatly linked (Shanahan *et al.,* 2013). The accumulation of carbonates in crater lakes occurs under all climates and in any tectonic setting (e.g. Gierlowski-Kodrdesch, 2010). The question arises concerning the cause and periodicity of the fine laminations (sub-millimetre scale in places) which is the predominant facies in all 3 borehole cores of the Kalkkop succession. As the partial pressure of CO_2 (PCO_2) in lacustrine waters increases, pH falls and $CaCO_3$ solubility increases; the reverse is also true. When the lake temperature increases, algae will proliferate and photosynthetically uptake more CO_2 thereby reducing PCO_2 which promotes carbonate precipitation (Wittkop *et al.,* 2009). These kinds of seasonal changes in the lake temperature can account for the finely laminated character of facies A, a mechanism commonly invoked to account for laminated carbonate sequences in lacustrine settings (e.g. Wittkop *et al.,* 2009).

The dispersed quartz and lithic fragments imbedded in the carbonate may be locally derived from surficially inflowing water or wind-blown. The core sections where argillaceous laminae are more prominent may record deepening of the lake, which would have led to cooler water and possibly reduced sunlight for photosynthesis, thereby inhibiting carbonate precipitation. This is supported by the observation that fine clastic sediments occur in the deeper parts of lakes, whereas carbonates are restricted to the lake margins (Wittkop *et al.,* 2009). In Lake Bosumtwi, the dominant control of silica precipitation is most likely the transport of silicate minerals to the lake via rivers and streams and the concentrations usually drop off steeply in the shallow margins of the lake, which indicates that the streams entering the lake lack enough energy to transport clastic minerals to the deep basin even in high rainy seasons (Shanahan *et al.,* 2013).

6.1.1 Facies A: Laminated arenaceous carbonate

6.1.1.1 Sub-facies Ai: micro-laminated coarser and finer grained micrite

The cleaner, coarse micrite is considered to represent periods of rapid carbonate precipitation (Bell, 1989), possibly as a result of increased algal photosynthetic CO_2 degassing; higher temperatures and/or increased sunlight would promote algal activity. The 'dirtier' fine grained laminae may record the opposite situation and thus a seasonal or other rhythmic control is indicated (Bell, 1989). The variation in lamina thickness may reflect inter-seasonal climate fluctuations.

6.1.1.2 Sub-facies Aii: micro-laminated, clayey, fine grained micrite

The internal fine (sub-millimetre) laminations of sub-facies Aii are less distinct than in sub-facies Ai and the facies is 'dirtier' (more clay and organic rich) throughout. This may indicate that seasonality is less pronounced with overall cooler waters leading to slow carbonate precipitation and therefore more time for impurities to accumulate.

6.1.1.3 Sub-facies Aiii: upward coarsening laminae

The interpretation of these small scale upward coarsening units should be considered in conjunction with their larger scale counterparts (Facies D, Chapter 6.1.4). Sub-facies Aiii is thus regarded as the distal expression of minor debris flows and the causes of the upward coarsening should be the same. The carbonaceous material may derive from rip up of algal mats by bottom currents (sub-facies A*iv*, below) and possibly other plant material.

6.1.1.4 Sub-facies Aiv

The algal mats mentioned above in sub-facies Aiii (e.g. Haar and Javor, 1982) usually contain authigenic nonskeletal calcium carbonate granules and traces of lensoid gypsum that range up to 2 or 3 cm thick.

6.1.2 Facies B: Chert

The Pleistocene cherts from alkaline Lake Makgadi in the Rift Valley in Kenya, are believed to have formed inorganically from the sodium silicate precursor magadiite [$NaSi_7\ O_{13}\ (OH)_3.3H_2O$], which transforms to the related sodium silicate, kenyaite. Percolating waters eventually convert kenyaite to chert (Eugster, 1967). These minerals are considered as modern analogs for cherts found in ancient lacustrine deposits and probably represent a chemical precipitate from alkaline brines (Eugster, 1967). Evidence that a similar process may have operated at Kalkkop is the identification of kenyaite in the core (Mazus, 1999). The whitish, rather pure and massive chert may have resulted from the geochemical pathway described by Eugster, (1967). The silicification of original carbonate probably records temporary changes in lake geochemistry; local concentrations of siliceous diatoms may also have played a role. The numerous non- diagnostic artefacts made on chert at the Kalkkop site (Fig. 16F), reflect the attractiveness of this hard, fine grained material to stone age people.

6.1.3 Facies C: Greenish calcareous mudrock

This facies is considered to represent suspension sedimentation in deeper waters of the lake. Carbonate sedimentation is prevalent more on the lake periphery, whereas clastic deposition dominates in the central areas of the lake (Wittkop *et al.,* 2009). The presence of this facies may therefore indicate more humid phases and a rise in lake levels.

6.1.4 Facies D: Massive arenaceous carbonate

In some instances, the core representing the longer intervals of facies D have the appearance of plastic deformation, conveying the impression that the strata (possibly weakly cemented) may have lost their structure during the drilling process. Thin (10-20 cm) intervals of facies D of more ‘normal’ core displayed erosive bases, possibly representing debris flows initiated by slumping of the crater floor sediments. Another possibility for the thicker structure less intervals was the loss of primary structure due to bioturbation, but no clear ichno-fossils could be seen. The non-laminated character of the sediments could also indicate lengthy periods of persistent high temperatures, so that carbonate precipitated rapidly year round.

6.1.5 Facies E: Allogenic gravels

The allogenic lithology of the clasts, poor sorting, sharp erosive base and lenticular form of the gravelly units suggest that they represent debris flows that originated on the slopes of the crater rim surrounding the lake Debris flows feature prominently on crater rims and on entry to the lake would transform into subaqueous flows. The highly brecciated character and steep slopes of impact crater rims (Reimold, 1998) would be conducive to debris flows. To account for reversed grading in subaqueous flows as seen in the multiple flows between 6.5 and 12 m, as well as the small (centimetre) scale distal flows seen in detailed section A, high dispersive pressure, kinetic sieving, fluid dynamic boundary effects, variable clast fall-out rate and inherited stratification are possible mechanisms (Naylor, 1980). More than one mechanism acting either consecutively as the flow evolves or simultaneously on different grain populations may be involved (Lowe, 1982). Inherited stratification should not have been operable at Kalkkop as the Beaufort rocks should have been uniformly shattered by the impactor. Other indications of debris flow activity seen at Kalkkop are tool marks and soft-sediment deformation structures, such as microfolding and water escape structures. Other indications of bottom flow are the micro-flasers reported here and the flaser bedding recorded on the De Beers log (Fig.18).

6.2 KK2 AND KK3 FACIES INTERPRETATIONS

Debris flows constitute the mass transport of clasts in a muddy matrix along a slope (Mazus, 1999, Tucker and Wright, 1990). Where the flows entered the lake from the crater margin, they became subaqueous in nature. The abundance of debris flows with slumping throughout the KK2 and KK3 cores may reflect their more marginal situation in the crater relative to KK1. Therefore, the thicker, coarser grained, more proximal component of debris flows would be represented in these boreholes. The steeper slopes along the crater margin, reflected in the relatively steeply inclined bedding, would have been conducive to slumping. Triggers for debris flow may have been heavy rainfall or possibly, seismicity. The recrystallization of the limestone seen in KK3 might have been caused by post-depositional groundwater percolation in the marginal lake facies. Mazus, (1999) also reported hard limestone with bubble-shaped pores in KK3, and mentioned that they could be formed by gas generation or as a result of air escaping during floods.

6.3 GEOCHEMISTRY

6.3.1. Chemical composition

MgO increases rapidly above ~60 m, with a concomitant decrease in CaO (Figs. 23 and 24), suggesting rising substitution of Mg for Ca in the carbonate lattice. Mazus (1999) reported increasing dolomite in the upper part of the succession. Since salinity is the major control of such a process it may be inferred that salinity increased with time. This proposition is further strengthened by the presence of halite in the upper 20 m of the KK1 core (Mazuz. 1999).The coincident rise in $\delta^{18}O$ also supports this interpretation and may indicate the climate became more arid in the later depositional phase, altering the balance between evaporation and water input. If so, with resultant decreasing vegetation cover more dust entering the lake could be expected-and this may explain the close correlation of $\delta^{18}O$ with Sr isotopes (terrigenous rocks have high $^{87}Sr/^{86}Sr$ ratios).

Trace elements Zr, Y, and Nb are present in small concentrations and these are highly incompatible in most common rock forming minerals and their concentrations would be expected to be highly variable in the common rock types in the area. Incompatible elements are not expected to be present in the groundwater, and the most likely source is wind-blown dust. The fact that all samples have the same Zr/Y (~5.3) and Zr/Nb (~10) ratios suggests that the composition of the dust component remained constant throughout deposition. The variation in concentration of incompatible elements is presumably controlled by the proportion of dust at a particular level; higher dust concentration is equal to higher incompatible element concentration. There is however no significant correlation between trace element concentration and depth and these ratios are similar to the calcrete in South Western Cape which is typical of the continental crust in the region (Midgley *et al.,* 2013).

Rare earth elements (REE) can provide information about sediment sources and they are not easily fractionated during deposition (Lee *et al.,* 2013). The fact that the samples have no Ce anomaly confirms that seawater cannot be the source of the REE because seawater has a negative Ce anomaly. The parallel REE patterns of Kalkkop and calcrete from heuweltjies, (Midgley *et al.,* 2013, Potts *et al.,* 2009) suggest that the source of the dust is similar (or at least of similar composition), which is the same as the trace elements (Zr, Y and Nb). The more Heavy Rare Earth Elements (HREE) enriched sample 68 might indicate a transient exotic component at this stratigraphic level.

6.3.2. $\delta^{13}C$ and $\delta^{18}O$ isotopes

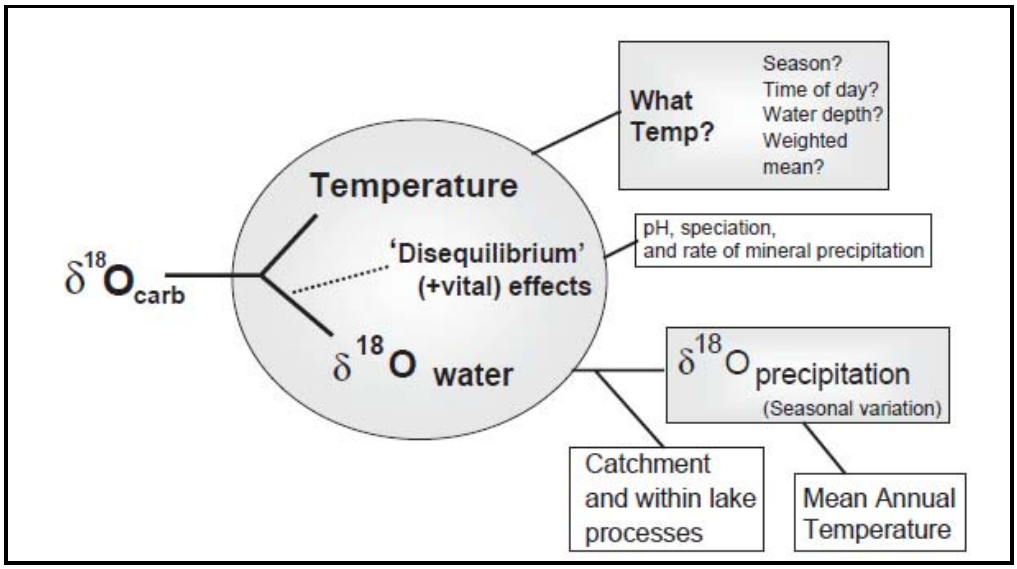

Figure 39: Controls on the oxygen isotope composition of lacustrine carbonates (Leng and Marshall, 2004).

A number of proxies such as stable isotopes, limnology and sedimentary study of crater lakes can be vital for providing valuable information on changes in weathering profiles and depositional environments and they are also crucial in understanding the complex interaction among the atmosphere, lithosphere, hydrosphere and biosphere of the Earth system in the timescale (Huntsman-Mapila *et al.,*2007; Colman, 2007). The lithology of the Kalkkop lake deposits and interpretation of stable isotopes, which show a general strong correlation between $\delta^{13}C$ and $\delta^{18}O$, may be used as proxy for changing climate through time. For example, according to Leng, (2004); Valero-Garcés *et al.,* (2000), the $\delta^{13}C$ and $\delta^{18}O$ isotope values in crater lakes in general might have been affected by factors (Fig.39) such as temperature of condensation of atmospheric moisture (increases with decreasing temperature), evaporation of lake water (increases with increasing evaporation) and biological factors with an increase in $\delta^{18}O$. The effects of vapour exchange between the lake and the atmosphere forces both $\delta^{13}C$ and $\delta^{18}O$ values to reach a steady-state values (Li and Ku, 1997). In most cases when the correlation of $\delta^{13}C$ and $\delta^{18}O$ is significant, is due to a kinetic effect and in some cases may indicate the hydrological closure of the lake (lack of input from rain, streams etc., but continued loss of water to evaporation) (Hodgson *et al.,* 2005). Hydrologically closed lakes like the Kalkkop Crater Lake will have waters with variable and elevated oxygen isotope ratios because of evaporation (e.g. Leng and Marshall, 2004).

It is not safe to assume that past lake water $\delta^{18}O$ value will reflect that of the weighted mean annual precipitation because the $\delta^{18}O$ value of any standing body of water changes significantly as a result of evaporation will affect the water composition. Figure 40 shows the major controls on the $\delta^{13}C$ and $\delta^{18}O$ of lake waters. The most important factor to consider is that $\delta^{18}O$ value of the lake water increase during arid conditions and conversely decreases during cool, wet periods, (Abell *et al.,* 1982). The Valle di Castiglione paleolake in Italy (Zanchetta, 1999), is a perfect example of how evaporative effects play a role of controlling oxygen isotope values. The paleaolake's water oxygen isotope composition of Valle di Castiglione is enriched in high $\delta^{18}O$ of biogenic carbonate (Zanchetta, 1999). The factor controlling the $\delta^{13}C$ value of lacustrine carbonate is the $\delta^{13}C$ value of the dissolved inorganic carbon (DIC) and it also depends on several sources each with their own isotope signature characteristics. Zanchetta, (1999) suggests that the carbonates with $\delta^{13}C$ with zero or positive values represent equilibrium of the DIC with atmospheric CO_2.

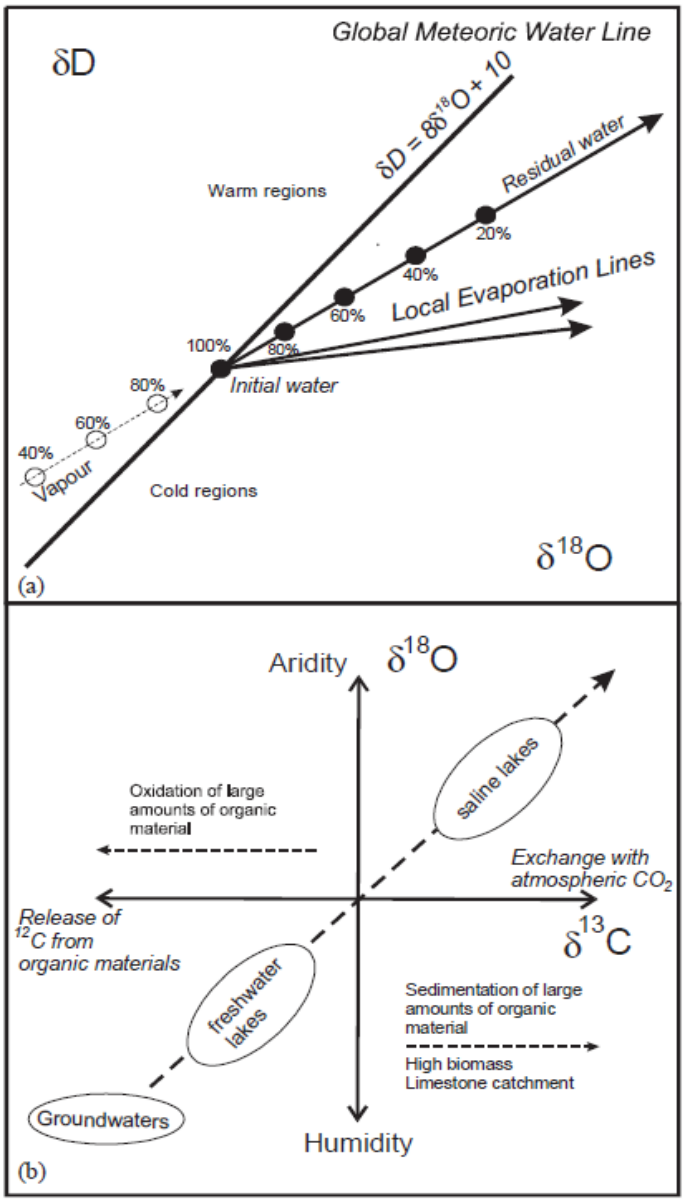

Figure 40: (a) major controls on the $\delta^{18}O$ vs δD of precipitation and lake waters (b) $\delta^{13}C$ vs $\delta^{18}O$ of lake waters (Leng and Marshall, 2004).

The carbon isotope ratios of lake carbonates are mostly controlled by the $\delta^{13}C$ values of dissolved inorganic carbon in the lake and the isotopic fractionation between dissolved inorganic carbon and the precipitated carbonate. Lake Qinghai has been investigated by Li *et al.,* (2012), to examine the carbon isotopic distribution of carbonates in the lake and to evaluate its response to environmental conditions. Another reason was to investigate the carbon isotopic differences between ostracods, fine grained carbonates and bulk carbonate as proxies for palaeoenvironmental reconstruction.

Lake Qinghai is a perfect study area because it is situated in the People's Republic of China, which is extremely sensitive to changes in climate because it lies in a critical transitional zone between the humid region controlled by the East Asian monsoon and the dry inland region affected by westerly winds. The results of this study by Li *et al.,* (2012) shows that the carbon isotopic composition of carbonates are mainly controlled by the isotopic composition of lake water dissolved inorganic carbon in the Qinghai area.

It is well known that in speleothems, strong positive correlations between $\delta^{13}C$ and $\delta^{18}O$ result from rapid loss of CO_2 from solution and a kinetic fractionation between the HCO_3- and CO_2 (aq) (Hendy,1971; Potts *et al.,* 2009). This would appear to be the case where the correlation is strong in the lower half of the core (>45 m depth) and in detailed results (Section B, Fig, 34). The isotope data cannot therefore be used to make direct inferences about the temperature of precipitation. Above 45 m depth, there is less correlation between $\delta^{13}C$ and $\delta^{18}O$, which means that it is possible to use these data as a climate proxy. The observed increase in $\delta^{13}C$ may be influenced by lake salinity, decomposition and respiration of plants/cyanobacteria, groundwater and runoff (isotopically heavier CO_2 under arid conditions), equilibration of atmospheric CO_2 with the lake and oxidation of lacustrine and terrestrial organic matter. Cyanobacterial mats preferentially extract CO_2 from the lake water (enriching them in ^{13}C), and are favoured by hypersaline conditions formed in arid settings. Poor soils under arid conditions and evaporative effects also lead to high $\delta^{13}C$ and $\delta^{18}O$ values in CO_2. It is also mentioned by Kaakinen *et al*., (2006) that usually the soil carbonates possess higher $\delta^{13}C$ values than the coexisting local biomass. Similar isotopic patterns to Kalkkop have been noted in Chinese lakes (Li, 2012), and have been attributed to complex interactions between biological and non-biological agencies. In particular, the algae prefer the light isotope ^{12}C, so biological activity would tend to increase $\delta^{13}C$, in which case the patterns of carbon fractionation seen in (Fig. 27 and 28) should reflect conditions favorable for biological activity. This implies warmer water with nutrient balance also playing a significant role. On this basis water temperature may have increased in the earlier phase of sedimentation and then remained relatively constant. The $\delta^{13}C$ and $\delta^{18}O$ are considered to indicate evaporative conditions in the lake. On this basis the continual rise in $\delta^{18}O$ may record water temperatures which are in general accord with the $\delta^{13}C$. Figure 41 shows the detailed variations of $\delta^{13}C$ and $\delta^{18}O$, probably on a seasonal basis in some instances.

The $\delta^{18}O$ values at the bottom level of the core are the lowest and it is at this level that appreciable forest elements are present. These observations indicate warmer and more humid conditions immediately after the impact. The low $\delta^{18}O$ values at the bottom of the core also suggest the less arid conditions probably due to reduced evaporation rate. In view of the evidence from pollen of a wet climate in the earlier phases of deposition this mechanism seems likely. Subsequently, up to a level of ~73 m the core becomes more calcareous with increasingly distinct lamination, suggesting that the lake had become shallower and possibly less stratified. The micro-lamination indicates that the seasonal pattern of algal blooms had become established at this time.

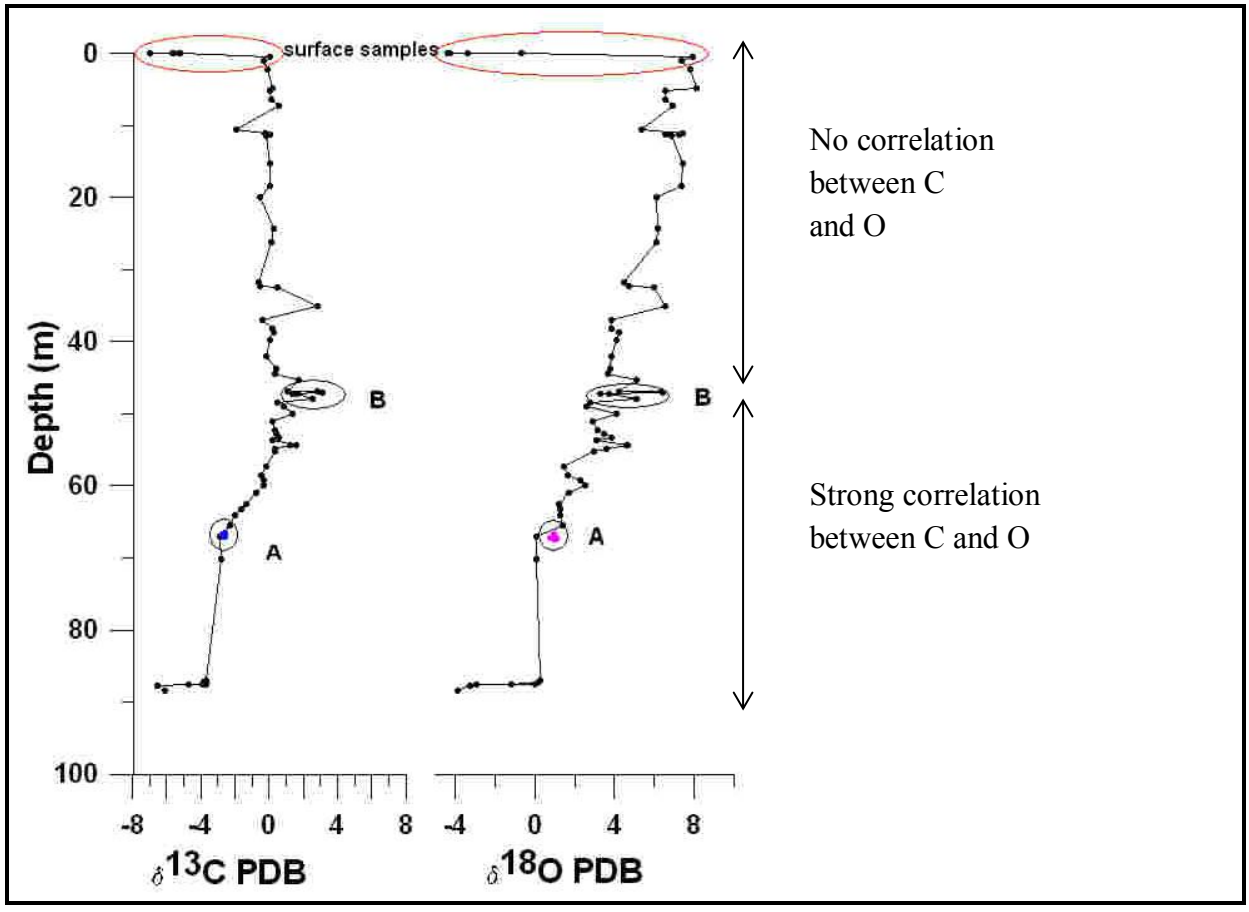

Figure 41: Controls of O and C isotopes.

6.3.3 Sr isotopes

The strontium isotope ratio ($^{87}Sr/^{86}Sr$) of the ocean is mostly determined by the continental runoff and groundwater runout which provides radiogenic ^{87}Sr to the ocean and also by seawater-oceanic crust interaction particularly at mid ocean ridges that depletes seawater in ^{87}Sr due to low $^{87}Sr/^{86}Sr$ ratio of fresh basalts (e.g. van Geldern *et al.,* 2006).

The Sr isotope data was produced by dissolving the carbonate fraction in HCl + nitric acid and that means that the large solid sand–sized feldspar grains were not dissolved, basically all of the Sr in the silicates was not dissolved. The $^{87}Sr/^{86}Sr$ ratio values range from 0.709935 to 0.710740 and the observed decrease in Sr content with depth may be due to one rainfall event and it evaporated afterwards.

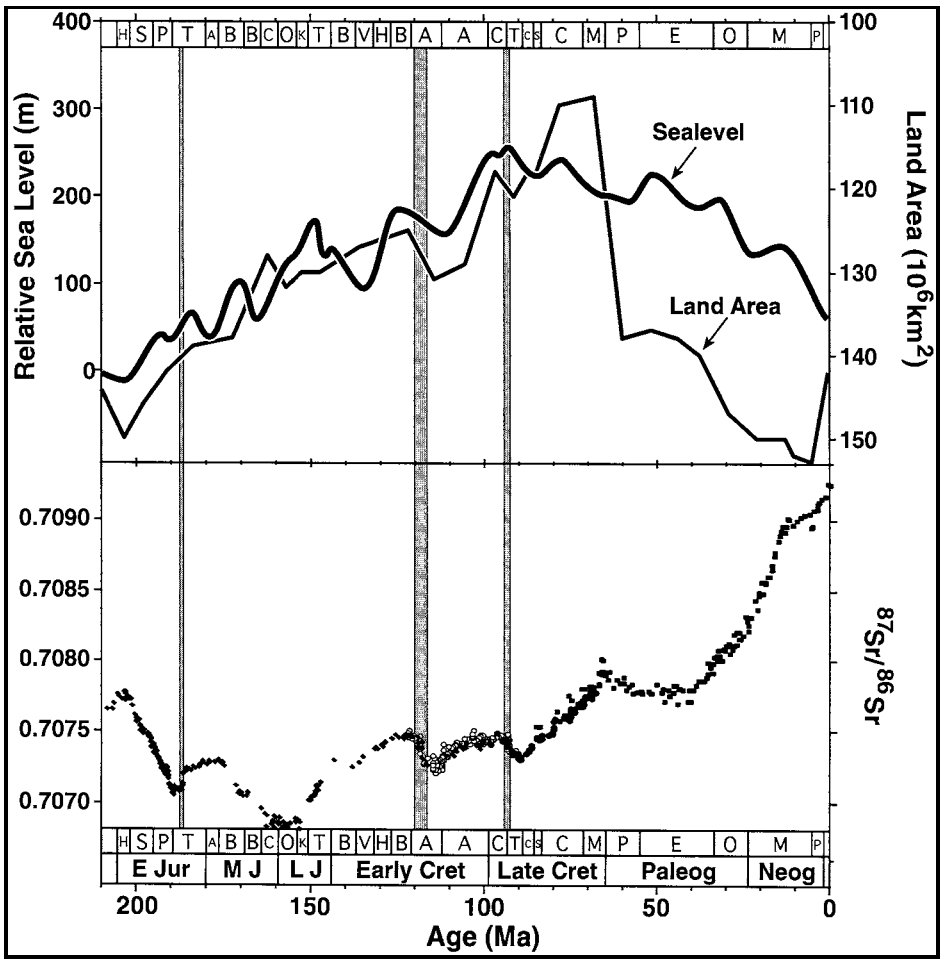

Figure 42: A plot to show the comparison between the eustatic sealevel curve, the land-area curve and the seawater Sr-isotope curve (Jones and Jenkyns, 2001).

The strong positive correlation between $^{87}Sr/^{86}Sr$ ratio and $\delta^{18}O$ is striking r=0.90. The $\delta^{18}O$ is increasing and this is most likely to be due to evaporation. This could be a single filling followed by evaporation, or continuous filling and evaporation where the loss of water to evaporation > input from rain/groundwater. It is presumably due to the continued input of dust and its dissolution into the water. The dust might have entered the lake rapidly and the increase in Sr ratios represents the effect of gradual dissolution of some component of the dust.

A study that was done in Santa Fe, New Mexico showed that 80% of the strontium that was in the biomass was derived from atmospherically transported dust while only 20% was from the bedrock (Graustein, 1989 and Goede *et al.,* 1998), and the study was done on the Tesuque watersheds to assess the contribution of atmospheric strontium relative to components that came from chemical weathering of the granitic rocks that overlie the watersheds. It would seem most likely that the correlation is high because $\delta^{18}O$ and $^{87}Sr/^{86}Sr$ ratio are both increased by the same process, but it is difficult to see what could be added to the lake that would increase both simultaneously. Given that evaporation is the most effective process that will increase $\delta^{18}O$, there has to be a relationship between evaporation and increase in Sr-isotopes i.e. the salinity of the lake may be increasing through time. Possibly the lake started off with a seawater $^{87}Sr/^{86}Sr$ ratio (around 0.709, e.g. Fig 42) and has gradually increased as the water strips more radiogenic Sr out of dust that settles in the crater (or both input into biomass and Sr is derived from that).

6.4 PALAEONTOLOGY

Crater lakes host a variety of organisms of both the plant and animal Kingdoms which may shed light not only on the immediate lacustrine environment, but also the broader landscape (Partridge, 1987). The Geological Survey of South Africa publication by Haughton *et al.,* (1953) reported some bone fragments that were found in the crater, but none were seen in the (later) KK1 core. Although, a freshwater snail of the genus *Melanoides* was recorded Haughton *et al.,* (1953) in one of the five pits found on the Kalkkop depression (mentioned in Chapter 2.2). Presently, this genus is confined to the warmer northeastern part of South Africa, and is excluded from the Kalkkop region (De Kock and Wolmarans, 2009), suggesting a climate warmer than the present during accumulation of the crater fill succession. Non–marine bivalves and a gastropod were observed in the De Beers (Fig. 15) core at 10 m and 46 m respectively. Both were associated with debris flow deposits.

Ostracods with their calcium carbonate shells are well preserved in core samples which are helpful for allowing extensive understanding of their long-term ecological responses in the lake basins they are found (Park, 2011). Ostracods were reported at 40 m in the De Beers core log. These small crustaceans are common in marine environments and saline lakes. Small horizontal burrows were observed in this study along partings in the KK1 core (Fig. 11F), and also in hand specimens from the excavations at the Kalkkop site, recording the presence of invertebrates in the lake. The KK1 core had poor diatom preservation but at a depth of 68 m (Chapter 5.2, Fig.16), diatoms and single (unidentified) benthic foraminifera was seen in thin section. As a result of increased turbulence and sediment mixing, diatom preservation can be poor (Valero-Garcés *et al.,* 1997). Foraminifera are rare in fresh water lakes and always reflect brackish conditions. Diatoms are most features of crater lakes and they are the major group of algae as well as the most common types of phytoplankton. Diatoms can exist as colonies in the shape of filaments or ribbons (e.g. *Fragilaria*), fans (e.g. *Meridion*), zigzags (e.g. *Tabellaria*), or stars (e.g. *Asterionella*), although they are unicellular. The diatom cells have a unique feature, and this feature is that they are encased within a cell wall made of silica (hydrated silicon dioxide) called a frustule, (Round and Crawford, 1990).

Both fauna and flora found in the lake will assist with tying the climate evidence (geochemical data and pollen) to the age of the sediments.

7. PALAEOENVIRONMENTAL SYNTHESIS

A multi-proxy approach to the palaeo-environmental evolution of the region around Kalkkop was employed during the course of this study, including sedimentology, palaeontology, geochemistry, stable isotopes and mineralogy. In Chapters 5 & 6, variation in individual parameters were examined for systematic variations, and interpreted as far as possible. The extent to which these parameters resonate or otherwise over the core depth (i.e. time) is investigated here to resolve possible conflicting lines of evidence (e.g. the age) and to highlight periods where congruence of the proxies inspires confidence in the inferences drawn. It is also apparent that some proxies like the pollen may reflect the geographically broader setting because of the considerable transport distances of wind dispersed types. Systematic variations in isotope ratio reflect more than changes in local environment and the extent to which conclusions drawn may be extrapolated is more limited. Thus, to an extent, the proxies complement one another in terms of the geographic extent over which inferences can be drawn.

The Kalkkop carbonate dominated succession indicates an alkaline/saline lake setting (Wittkop *et al.,* 2009), but does not necessarily mean an arid climate. For instance the Tswaing Crater experiences a rainfall range of 400-750 mm p.a. but is still carbonate dominated (Metwally, 2011). It appears that if the catchment is limited, as at Kalkkop, a saline carbonate lake may develop under a wide range of conditions. The current mean annual temperature is ~19^0 C with mean midday temperatures of ~30^o C in mid-summer. A freshwater snail of the genus *Melanoides* was recorded in a detailed log of a hole drilled by the Geological Survey (Haughton *et al.,* 1953). This genus is currently confined to the warmer northeastern part of South Africa, and does not occur in the Kalkkop region at all (De Kock and Wolmarans, 2009). This suggests that the climate was still warmer in the Neogene than at present, which would have favoured a saline lake. Climate is a very important parameter that strongly controls the characteristics of a lake (Reineck and Singh, 1975), including the balance between precipitation and evaporation, the nature of the soil, weathering in the catchment area, as well as the vegetation. The later Miocene (the period during which lake sedimentation occurred) following on the Monterey global cooling event at ~13 Ma was colder than the Middle Miocene, but nonetheless warmer than the present according to the marine record.

This record however, suggests shorter period stable oxygen isotope fluctuations, superimposed on broader trends. Spectral analysis of the isotope data reveals orbital (Milankovitch) forcing in high frequency precession (23 ka) and obliquity (41 ka) bands, as well as the lower frequency eccentricity (100 and 400 ka) beats (Roberts *et al.,* 2011). In a recent study of Miocene fluvial sediments in the coastal Western Cape, an overall more humid and warmer climate prevailed than at present, although strong evidence was found for significant shorter term fluctuations in climate. The extent to which Neogene climate may also have fluctuated in the region around Kalkkop is a question central to this study. The estimated time span of sediment accumulation at Kalkkop was ~180 ka (0.5 m per 1000 yrs.), sufficient time to record precession (23 ka) and obliquity (41 ka) bands, as well as the higher frequency eccentricity signal of ~100 ka. However, none of the geochemical proxies such as $\delta^{13}C$ and $\delta^{18}O$ showed any fluctuations that matched the orbital frequencies.

An example that is similar to the Kalkkop Crater is Tswaing Crater, located 40 km north-west of Pretoria in Gauteng province, South Africa. It is 1.13 km wide in diameter and was previous called the Pretoria Saltpan (Partridge and Maud, 1987). The crater also formed due to an impact event (Reimold *et al*., 1992), and the target rock (Fig. 2a-b) was the Nebo Granite of the Bushveld Complex. It was first investigated as a potential climate archive by Partridge *et al.,* (1993) and he initiated the first scientific coring campaign in 1988/1989 (Kristen *et al.,* 2010). The impact has been dated to 220 ± 52k years BP using fission-track dating (Scott, 1999; Kristen *et al.,* 2010). The lake is presently about 2-3 m deep (Fig. 2c-d) with a pH of 10 and hypersaline. Just like the Kalkkop Crater, Tswaing Crater also reveals a 90 m sequence of lake sediments, (Scott, 1999). Studies conducted on the 90 m sequence have shown that the sequence consists of carbonate-rich sediments, sands and muds (Fig.1). The sedimentation rates during the past 43 ka obtained from the algal debris in the upper sections of the crater conformed closely to that which prevailed since inception of the lake at around 200 ka (Partridge *et al.,* 1997, Partridge and Scott, 2000). The clastic components of the sediments were derived from the weathering and soil formation of the granitic rocks of the crater walls (Partridge and Scott 2000). Tswaing Crater's present climate is subtropical with hot, rainy summers (630mm/year) and cool, dry winters. The lake's hydrological balance is such that an annual evaporative loss of 175 000 m^3 is balanced by the 48000 m^3 rainfall and 100000 m^3 of crater-wall runoff (Partridge *et al.,* 1997).

Climate can, to a degree, be inferred from fossil plants found in palaeolake deposits, including pollen. The recovered pollen from the Kalkkop core is generally sparse both in terms of productive horizons and richness of the palynofloras, thus limiting the conclusions that can be drawn. Öberg *et al.,* (2013) mentioned the fact that pollen concentration in lake sediments is often associated with the moisture conditions at the site. The wet conditions will favour pollen preservation, which means high pollen concentration in the sediments, while low pollen concentration instead is associated with drier conditions (Öberg *et al.,* 2013, Faegri and Iversen, 1989) and these findings were from a study done in Tanzania (Lake Duluti). The climate as indicated by the palynology in Kalkkop was relatively dry with a dominance of grasses and *fynbos* taxa like the Ericaceae and Asteraceae featuring prominently.

Mazus (1999) recognised a series of pollen zones in the KK1 core, providing a commentary on the vegetation types and their palaeo-environmental implications. Other palaeo-environmental indicators such as geochemistry and sedimentology from the present study and earlier borehole descriptions are also considered. Pollen Zone 1b (88.75- 75 m) showed Asteraceae (daisies), Chenopodeaceae (usually is found in arid, hot areas and also margins of salt pans and along watercourses); grasses and Ericaceae (moister heathland) dominate the lower part of the core. A relatively dry grassland setting is inferred (Mazus, 1999). The lower most sediment, consisting of angular Karoo rock fragments in a finer matrix, represents aerial fallout following the impact (Koeberl, 1994). The succeeding more clayey, carbonate depleted sediments (Fig.17) i.e. facies A*iii* suggests a distal facies deposited in a water depth too great (maximum ~90 m) and stratified for biogenic carbonate to have precipitated in the central part of the basin. However, carbonate increases sharply above this level (90 m); suggesting that carbonate precipitation took hold early in the sedimentation history. No core remains above this basal zone and no detailed core log or photographs are given by Mazus (1999). This section of core is described by her as 'soft white massive limestone'. This appears to be facies D, interpreted as material that has lost its structure in the drilling process or by downslope slumping. The low $\delta^{18}O$ and $\delta^{13}C$ isotope values suggest low evaporation or biogenic influence respectively

From 75.0 m -36.0 m the pollen of grass and herbs (Umbelliferae, Gentianaceaea, Malvaceaea and Labiatae) is generally well represented, along with Ericaceae suggesting moist grassland with herbaceous plants and heathland. Aquatic plants and sedges indicate open lacustrine conditions (Mazus, 1999). The abundance of aquatics also suggests eutrophic conditions in the lake. This interval represents a long time span (~78 ka) and it is probable that the climate fluctuated considerably. Unidentified plant fragments are common in this interval and faunal remains such as molluscs and bioturbation were also observed, supporting the concept of a generally eutrophic lake system. Biogenic fine carbonate laminites are also well developed, indicating frequent algal blooms and probable seasonal laminites (Wittekop, 2009). The microscopically examined interval at ~66 m showed features such as carbonaceous laminae that may represent algal mats, flasers and micro-upward-coarsening laminae that may record distal debris-flows. The more proximal borehole KK1b shows numerous macro-debris flow deposits characterised by angular Karoo rock fragments and episodes of heavy rainfall may be inferred. Cherty horizons become common in this interval and probably represent a chemical precipitate from alkaline brines (see Chapter 6.1.4), possibly indicating drier, and more evaporative periods. A systematic change of $\delta^{18}O$ values for KK1 with time is consistent with the overall strong variation over this interval which may indicate an overall drying climate. However fluctuations in this parameter are common (such as the lower $\delta^{18}O$ interval from 46-36 m, a period of some 20 ka) and support the notion of notable climate fluctuations.

In Pollen zone 2 (36- 30 m), the pollen record from this interval is very poor, mostly represented by grass and Asteraceae, suggesting relatively dry conditions (Mazus, 1999). The sparse pollen preservation itself is supportive of this interpretation. Again, cherts are common in this interval and desiccation cracks appear near the top, suggesting a period when the lake dried out. The $\delta^{18}O$ value of KK1 is significantly higher supporting the idea of a drier period based on the sparse pollen data and presence of chert. MgO and CaO show a systematic increase/decrease with height (Figs 23 and 24), indicating dolomitisation of the limestone and, therefore higher salinity. Overall this interval is consistent with a drier climate at the site.

From 16.50-30 m (zone 3) the core contains good pollen in the lower part and the top. Grass in this interval generally dominates the pollen spectra.

Aquatic 'grass' of the *Juncus*-type is very common in the lower part of the zone, found also with abundant Cyperaceae, a group with a strong affinity for moisture (Mazus, 1999). There are various herbs, Ericaceae and Euphorbiaceae present in the zone. Forest elements like Podocarpus, Olea and Myrica are present. *Botryococcus* algae were noted in the lower parts of the zone. In general, the interval at ~30 m depth seems to be among the wetter phases of the Kalkkop succession with expansion of the sub-tropical forest. However, most of this interval produced poor pollen, suggesting only brief wetter periods at the beginning and end. The $\delta^{18}O$ for KK1 does show a negative variation at about 30 m lending some geochemical support for the pollen. Clay-rich sediments also appear in KK1 between ~22-19 m, suggesting deepening of the lake, again consistent with a moister climate regime (Deepthy and Balakrishnan, 2005; Asikainen *et al.,* 2006).

Pollen zone 4 represents the terminal phases of deposition at Kalkkop (Mazus, 1999). In this zone, different pollen spectra contain types of grass, the Asteraceae and Chenopodiaceae families. Artemisia and Stoebe are among the Asteraceae, and are typical *fynbos* types. Most pollen like *Acacia, Podocarpus, Euclea* and *Myrica* are present in very low abundances apart from *Pinus* and *Eucalyptus* which are contaminants. The Chenopodiaceae have an affinity for saline soils in a dry climate (Mazus, 1999), and the grasses and *Acacia* suggest a dry Karoo type of vegetation. The KK1b log (Fig 15) shows multiple debris flows near the top of the succession between 12.0 and 6.5 m, also observed in the surface exposures. The possible mechanisms for initiating such intense debris flows include: high rainfall; fire (which reduces substrate solidity, but no charcoal has been found to substantiate this factor), and seismic activity (Naylor, 1980; Lowe, 1982).

Kalkkop is situated near the Baviaanskloof-Coega fault which has been active in the Holocene (Parker *et al.,* 2011). The multiple large flows between 6.5 and 12 m are possibly best explained by seismicity as multiple seismic events over brief intervals (foreshocks/aftershocks) are a common feature of seismicity related to fault displacements. It could be anticipated that after ~200-250 ka the steepness of the crater rim should have declined and should have been less susceptible to failure, requiring a stronger trigger to initiate slumping. High rainfall is probably the main cause of the intermittent larger and smaller scale events below 12 m; similar upward coarsening micro-units are scarce in the upper part of the KK1 core, suggesting fewer high rainfall events.

In the central part of the Kalkkop succession, the strata are flat lying, but nearer the periphery are steeply dipping, reflecting the form of the original crater floor. These marginal deposits are dominated by debris flows and the carbonate is extensively recrystallized, probably due to groundwaters percolating around the margins of the lake. These considerations support the evidence from pollen for an arid climate. The presence of halite (Mazus, 1999) lends weight to this interpretation. Pedogenic calcrete illustrates termination of lake sedimentation and a lengthy period of surficial exposure. The causes of final lake desiccation are debatable. At the time the lake dried up, it had been in existence for some 180 ka on the basis of sedimentation rates (see Chapter 4.3). The two craters are a far apart but the erosion rate ought not to be that different and judging from the presently still well preserved state of the Tswaing Crater rim after some 200 ka (Figs 1 and 2.); the rim of the Kalkkop Crater should not have been sufficiently degraded to have caused the lake to drain. It would therefore seem that a lengthy very arid period ensued during which time the lake remained dry. At some point in time, the rim would have degraded to a point where it could no longer retain the lake basin, as is apparent at the present time. It is however, uncertain as to the thickness of lake sediments that may have been eroded (destroying any record of sedimentation) since deposition ceased. At the final cessation of deposition, the sediment surface should have been completely flat. Therefore, the considerable relief of the presently observed surface clearly illustrates that a notable degree of erosion has subsequently taken place. Given the late Neogene age determined for Kalkkop in this study, this situation is entirely anticipated. Over the ~180 ka time span of deposition at Kalkkop the climate showed a general drying trend, superimposed on which were notable fluctuations in the form of wetter periods. The presence of subtropical forest elements, however is suggestive of a climate that was, at least intermittently, considerably wetter than today.

We can conclude that during the late Neogene, the intermountain region represented at Kalkkop was overall, drier than the adjacent coastal belt whose humid climate as inferred from the Miocene Knysna lignite deposits (Carr *et al.,* 2010). The pronounced contrast of the present day (humid forest versus dry Karoo vegetation) however, may not have been as great in the Neogene as seen today. The best age estimate for the time of impact at Kalkkop is ~6.3 Ma (see Chapter 4.2.2). This means that the lacustrine succession has been subject to weathering and erosion for ~6 Ma.

A regional erosion rate of ~ 6 m/ 10^6 has been inferred for the southern coastal region (Erlanger, 2011) and on this basis as much as ~36 m of sediments may have been removed by erosion since deposition ceased. An unknown here is the extent to which the chemically precipitated sediments may have been buried and protected from erosion by clastic sediments washed in from the remains of the crater rim.

The changes in $\delta^{13}C$ and $\delta^{18}O$ isotopes are consistent with what has been discussed above. Figures 43 and 44 represent the pollen types 'trees' (moist) and 'Karoo-type shrubs + grasses' (arid) from various depths in comparison with $\delta^{13}C$ and $\delta^{18}O$. The geochemical data therefore fits with other proxies in this study and they all draw the same conclusion that the Kalkkop evolved during drier conditions.

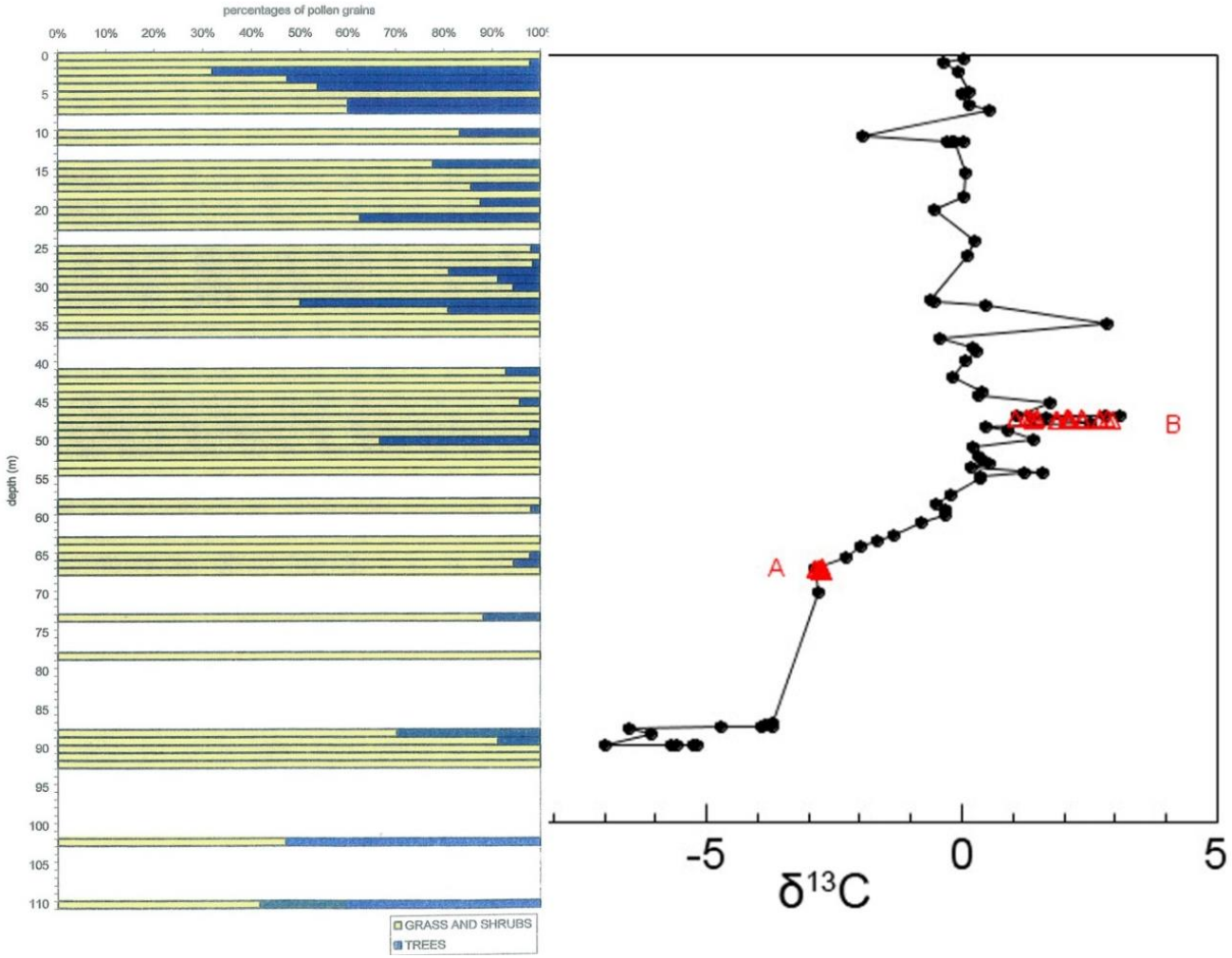

Figure 43: Pollen of grass +karoo-type species vs pollen of trees in KK1 and $\delta^{13}C$ shown at same scale. In the upper part of the succession (8-0 m), the relatively high content trees is misleading as they consist of modern contaminants (*Pinus* and *Euclaptus*) and should be disregarded.

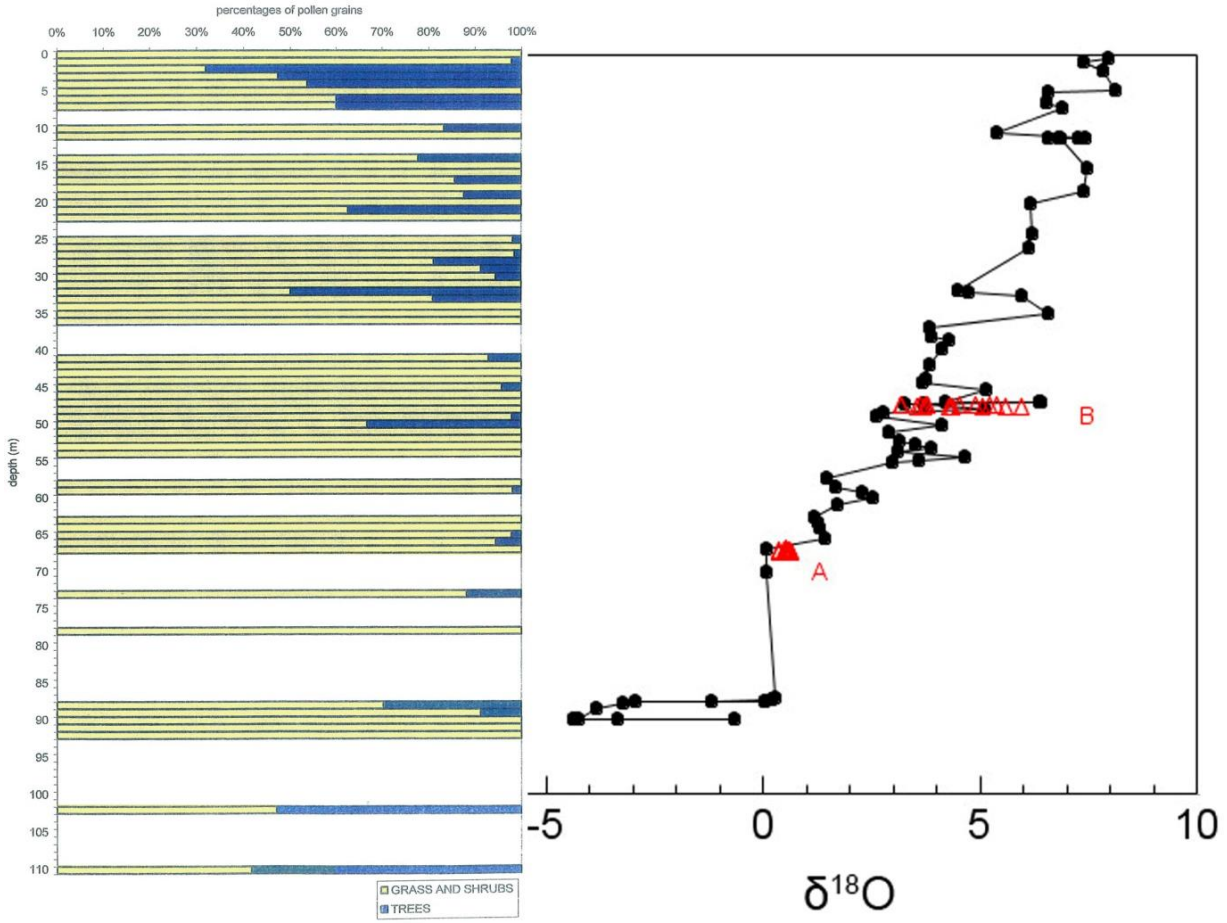

Figure 44: pollen of grass +karoo-type species vs pollen of trees in KK1 and $\delta^{18}O$ shown at same scale. In the upper part of the succession (8-0 m), the relatively high content trees is misleading as they consist of modern contaminants (*Pinus* and *Euclaptus*) and should be disregarded.

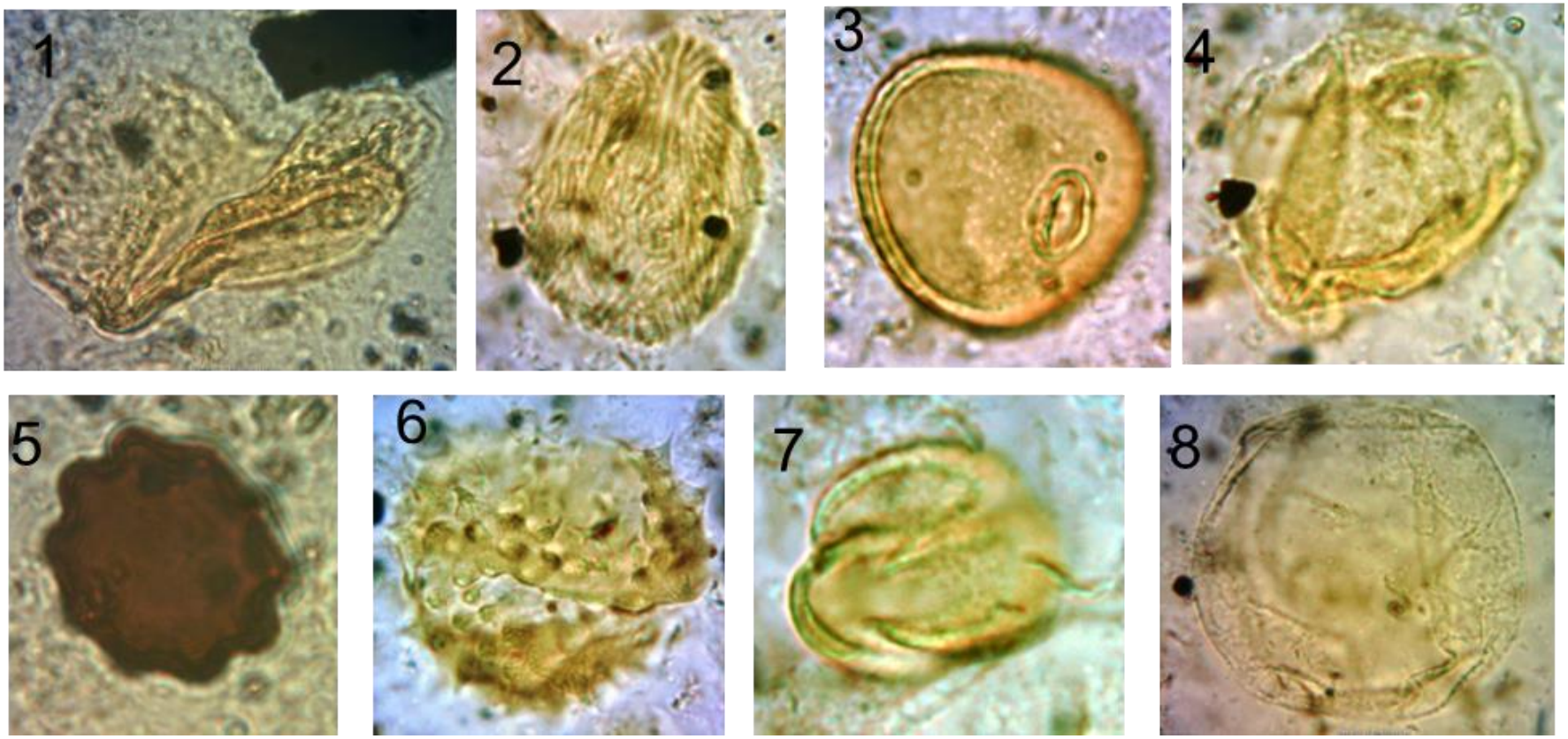

Figure 45 Pollen from the KK1 borehole. 1: Podocarpus (arboreal) 2: Rhus (arboreal); 3: Restionaceae (moist fynbos); 4: 5: fungal spore 6: Asteraceae (fynbos); 7: Azoaceae (succulent); 8: Juncus (water grass).

8. CONCLUSIONS

The major conclusions of this work are as follows.

1. The size of the Kalkkop Crater was previously stated to be ~650 m, but this is only the preserved portion of the structure. From the size of the eroded remnants of the crater rim at Kalkkop, and by analogy with similar features at Tswaing, the original rim- to -rim diameter of the Kalkkop Crater would have been ~1,200 m rather than 650 m, which is similar in size to the present day Tswaing Crater Lake whose rim-to-rim diameter is 1130 m. The impactor diameter (120 m- roughly 10% of crater diameter) would therefore have been much larger than previously thought.

2. A late Quaternary age for Kalkkop (~250 ka) as previously inferred from U-series dating (Reimold *et al.,* 1998) is discounted here on the basis of the highly degraded state of the crater rim in comparison with other impact sites like Tswaing and also due to the unreliability of the U-series dating done on the crater.

3. An age model for the Kalkkop Crater was constructed from the average palaeo-erosion rate of 6.63 m/Ma over the last ~4 Ma from the assumption that the rim was originally at 50 m high, the age of Kalkkop is then suggested to be ~ 6.3 ±1.6 Ma, i.e. latest Miocene.

4. The Kalkkop succession, known from several borehole cores, mainly comprises finely laminated and massive, structure less carbonates (mainly calcite) punctuated by debris flows from the crater rim, providing a long and detailed (seasonal) record of local and regional climate and ecosystems, exceeding the resolution of the marine record. Some of the core is laminated at a sub-millimetre scale which represents seasonal events probably modulated by microbial blooms in the warm season.

5. (i) On the basis of chemical analyses, the samples showed Al_2O_3 < 3.2 wt.%, except for one sample (POM60) with 0.99 wt.% , meaning this sample had significant quantities of clay minerals in it . The MgO content is the highest in samples at top of core and reaches 25 wt.% and this corresponds to about 50% dolomite but there is not enough CaO for there to be this much dolomite.

The increase of MgO on the highest levels of the core with the decrease in CaO suggests that there is a rise in the substitution of Mg for Ca in the carbonate lattice.

(ii) Trace elements Zr, Y, and Nb are present in small concentrations and the parallel REE patterns of Kalkkop and calcrete from heuweltjies from the Western Cape, suggest that the source of the dust is similar (or at least of similar composition), which is the same as the trace elements (Zr, Y and Nb)

6. (i) The strong correlation between the $\delta^{13}C$ and $\delta^{18}O$ in the lower part of the Kalkkop succession suggests non–equilibrium precipitation, high evaporation rate = dry climate.. The lower part of the core precipitated during more arid conditions (evaporitic) whereas recharge of water was more continuous in the upper part of the core.

(iii) During sample processing, the large solid sand-sized grains were not dissolved; meaning all Sr in silicate was not dissolved because the carbonate fraction was dissolved in HCl + nitric acid. The decrease in Sr content with depth may be due to one rainfall event and then later evaporated.

(iii). There a strong positive correlation between $^{87}Sr/^{86}Sr$ ratio and $\delta^{18}O$ and this is due to input of dust along with evaporation increasing the $\delta^{18}O$ of the water. It is possible that the lake started off with a seawater $^{87}Sr/^{86}Sr$ ratio (around 0.709) and has gradually increased as the water strips more radiogenic Sr out of dust that settles in the crater which suggests that the rain water had seawater Sr-isotope ratio.

7. Forest pollen near the top of the succession indicates wetter periods despite the overall drier climate. Presently, these Afromontane taxa are restricted to the humid coastal region with ~800-1000 mm p/a rainfall, suggesting that the currently semi-arid proximal coastal plain (~240 mm p/a) was previously much wetter than at present.

8. Palynology indicates the presence of humid sub-tropical to tropical arboreal species as well as the moist, more temperate genus *Podocarpus*-contrasting with the present semi-arid climate. Some intervals are more dominated by grasses and sclerophyllous *fynbos* taxa, suggesting fluctuating wetter and drier intervals, confirmed by stable isotopes which, along with mineralogy, also illustrate an overall aridification through time.

9. As today, during the late Neogene the intermountain region represented at Kalkkop was apparently, overall, drier than the humid adjacent coastal belt in the Knysna region.

10. The geochemical data therefore fits with other proxies in this study and they all draw the same conclusion that the Kalkkop Crater evolved during drier conditions. The geochemistry does support the old age and the evidence is from

(i) the freshwater snail (*Melanoides)* was found on the upper part of the crater in excavations and this snail is currently confined to the warmer north eastern part of South Africa, and does not occur in the Kalkkop Crater region at all thus suggesting that the climate was still warmer in the Neogene than at present, which would have favoured a saline lake, and the increase in $\delta^{13}C$ may be influenced by lake salinity.

(ii) During the late Neogene, the intermountain region represented at Kalkkop was overall, drier than the adjacent coastal belt whose humid climate as inferred from the Miocene Knysna lignite deposits. And, also pronounced contrast of the present day (humid forest versus dry Karoo vegetation) however, may not have been as great in the Neogene as seen today.

9. REFERENCES

Abell, P.I., 1982, Plio-pleistocene lacustrine stromatolites from Lake Turkana, Kenya: Morphology, stratigraphy and stable isotopes, *Sedimentary Geology*, 32, 1–26

Asikainen, C.A., Francus, P., Brigham-Grette, J., 2006. Sedimentology, clay mineralogy and grain-size as indicators of 65 ka of climate change from El'gygytgyn Crater Lake, Northeastern Siberia. Journal of Paleolimnology, 37, 105–122.

Bell, K., 1989. Carbonates, Genesis and Evolution. Unwin Hyman, London. 618 pp

Bjorlykke, K., 2010. Petroleum Geoscience: From Sedimentary Environments to Rock Physics. Springer-Verlag Berlin Heidelberg, pp 59

Bunbury, J., 2003. Using lake sediments to reveal past climates. Poster, http://www.lpc.uottawa.ca/publications/lake_sediment

Carr, A.S., Boom A., Chase B.M., Roberts D.L., Roberts, Z.E., 2010. Molecular fingerprinting of wetland organic matter using pyrolysis-GC/MS: an example from the southern Cape coastline of South Africa. *Journal of Paleolimnology* 44, 947–961.

Carr, A.S., Boom, A., Dunajko, A., Bateman, M.D., Holmes, P.J., Berrio, J.C.S., 2010. New evidence for the age and palaeoecology of the Knysna Formation, South Africa. *South African Journal of Geology*. 113, 241–256.

Cerling, T, E and Quade, J., 1993. Stable carbon and oxygen isotopes in soil carbonates. In: Swart, P., McKenzie, J.A., and Lohman, K.C. (eds.): *American Geophysical Union Monograph* 78: 217-231

Clemens, J.D., Belcher, R.W., Kisters, A.F.M., 2010. The Heerenveen Batholith, Barberton Mountain Land, South Africa: Mesoarchaean, Potassic, Felsic Magmas Formed by Melting of an Ancient Subduction Complex, *Journal of Petrology*. 51, 1099-1120

Crowley, J. L., Schoene, B., Bowring, S. A., 2007. U-Pb dating of zircon in the Bishop Tuff at the millennial scale. *Geology* 35, 1123-1126.

Coetzee, J.A., 1980. Tertiary environmental changes along the south-western African Coast., *Palaeontology Africana,* 23, 197–203.

De Kock, K.N. and Wolmarans, C.T., 2009. Distribution and habitats of *Melanoides tuberculata* (Müller, 1774) and *M. victoriae* (Dohrn, 1865) (Mollusca: Prosobranchia: Thiaridae) in South Africa. *Water SA*, 35, 713-720

Deepthy, R. and Balakrishnan, S. 2005. Climatic control on clay mineral formation: Evidence from weathering profiles developed on either side of the Western Ghats. Journal of Earth System Science. 114, 545–556

Eugster, H. P., 1967. Hydrous sodium silicates from Lake Magadi, Kenya: Precursors of bedded chert. *Science*, 157, 1177.

Gierlowski-Kordesch E.H., 2010. Chapter1 Lacustrine Carbonates. Developments in Sedimentology.61, 1-101

Goede A., McCulloch M., McDermott F., Hawkesworth C., 1998. Aeolian contribution to strontium and strontium isotope variations in a Tasmanian speleothem. *Chemical Geology,* 149, 37–50

Graustein, W.C., 1989. $^{87}Sr/^{86}Sr$ ratios measure the sources and flow of strontium in terrestrial ecosystems. In: Rundel, P.W., Ehleringer, J.R., Nagy, K.A. Eds., Stable Isotopes in Ecological Research, Ecological Studies. *Springer-Verlag*, 68,491–512.

Faegri, K and Iversen, J., 1989. Textbook of Pollen Analyses. *Blackwell, Oxford*

Faure, G., 1986. Principles of Isotope Geology. 2nd Ed., *J.Wiley & Sons*, New York., p589

Haar, S.H., and Javor B., 1982. Algal mats and stromatolites. In: *Beaches and Coastal Geology. Encyclopedia of Earth Science*. (Ed., Dr.Maurice L.Schwartz). Springer US. p33

Haughton, S.H., Blignaut, J.J.G., Rossouw, P.J., Spies, J.J., Zagt, S., 1953. Results of an investigation into the possible presence of oil in the Karoo rocks in parts of the Union of South Africa. *Department of Mines,* Memoir 45, Geological Survey

Hodgson, D.A., Verleyen, E., Sabbe, K., Squier, A.H., Keely, B.J., Leng, M.J., Saunders, K.M., Vyverman, W., 2005. Late Quaternary climate-driven environmental change in the Larsemann Hills, East Antarctica, multi-proxy evidence from a lake sediment core. *Quaternary Research*, 64, 83-99

Holbourn, A., Kuhnt, W., Schulz, M., Flores, J.C., Andersen, N., 2007. Orbitally-paced climate evolution during the middle Miocene "Monterey" carbon-isotope excursion. *Earth and Planetary Science Letters*. 261, 534–550

Hurlbut, C. S.;Jr. and Klein, C, 1985, Manual of Mineralogy, 20th edition., *John Wiley and Sons*, New York

Huntsman-Mapila, P., Tiercelin, J.J., Benoit, M., Cotton, J., Talbot, M., Hemond, C., Hureau-Mazundier, D., 2007. Major and trace element geochemistry of Lake Tanganyika sediments: implications for late Quaternary climatic variability. *Palaeogeography, Palaeoclimatology, Palaeoecology*. 1-10

Jones, C.E and Jenkyns, H.C., 2001. Seawater strontium isotopes, oceanic anoxic events, and seafloor hydrothermal activity in the Jurassic and Cretaceous. *American Journal of Science*, 301, 112-149

Kaakinen, A., Sonninen, E., Lunkka, J.P., 2006. Stable isotope record in paleosol carbonates from the Chinese Loess Plateau: Implications for late Neogene paleoclimate and paleovegetation. *Palaeogeography, Palaeoclimatology, Palaeoecology*, 237, 359–369

Kampunzu, A.B., Ringrose, S., Huntsman-Mapila, P., Harris, C., Vink, B., 2007. Origins and palaeo-environments of Kalahari duricrusts in the Moshaweng dry valleys (Botswana, Kalahari) as detected by major and trace element composition. *Journal of African Earth Sciences*. 48, 199–221.

Kirchheimer, F., 1932. On Pollen from the Upper Cretaceous Dysodil of Banke, Namaqualand (South Africa). *Transactions Royal Society South Africa*.21, 41-50

Koeberl, C., 1994. African meteorite impact craters: Characteristics and geological importance. *Journal African Earth Sciences* 16, 263-295.

Koeberl, C., Reimold, W.U. and Shirey, S.B. 1994a. Saltpan impact crater, South Africa: Geochemistry of target rocks, breccias, and impact glasses, and osmium isotope systematics.*Geochimica Cosmochimica Acta 56, 2893-2910.*

Koeberl, C., Reimold, W. U., Shirey, S. B. and le Roux, F. G. 1994b. Kalkkop Crater, Cape Province, South Africa: Confirmation of impact origin using osmium isotope systematics. *Geochimica Cosmochimica Acta 58,* 1229-*1234.*

Koeberl, C. and Anderson, R. R., 1996. Manson and company: Impact structures in the United States. In: The Manson Impact Structure, Iowa: Anatomy of an Impact Crater, eds. C. Koeberl and R.R. Anderson, *Geological Society of America*, Special Paper 302, 1-29

Koeberl, C., 2009. El'gygytgyn: a very special meteorite impact crater. Website of the FWF project: P21821-N19 "Studies of the El'gygytgyn Impact Crater". http://lithosphere.univie.ac.at/impactresearch/elgygytgyn-crater/

Kristen, I., Wilkes, H., Vieth, A., Zink, K.G., Plessen, B., Thorpe, J., Partridge, T.C., and Oberhänsli, H., 2010. Biomarker and stable carbon isotope analyses of sedimentary organic matter from Lake Tswaing: evidence for deglacial wetness and early Holocene drought from South Africa. *Journal of Paleolimnology.* 44, 143–160

Kumar, P. S., 2005. Structural effects of meteorite impact on basalt: Evidence from Lonar Crater, India, *Journal of Geophysical Research*. 110

Lamb, A.L., Leng M.J., Sloane, H.J., Telford, R.J., 2005. A comparison of the palaeoclimate signals from diatom oxygen isotope ratios and carbonate oxygen isotope ratios from a low latitude crater lake. *Palaeogeography, Palaeoclimatology, Palaeoecology*, 223, 290–302

Larsen, E.S. (1921) The Microscopic Determination of the Nonopaque Minerals, First edition, USGS Bulletin 679: 52.

Leng, M.J., Marshall, J.D., 2004. Palaeoclimate interpretation of stable isotope data from lake sediment archives. *Quaternary Science Reviews*, 23,811–831

Lee, R.K.L., Owen, R.B., Renaut, R.W., Behrensmeyer, A.K., Potss, R., Sharp, W.D., 2013. Facies, geochemistry and diatoms of late Pleistocene Olorgesailie tufas, southern Kenya Rift. *Palaeogeography, Palaeoclimatology, Palaeoecology*, 374,197-217

Lee-Thorp, J.A and Talma E.S., 2000. Stable light isotopes and past environments in the Southern African Quaternary and Pliocene, In (T.C. Partridge and R. Maud, Ed.s) *The Cenozoic of Southern Africa*, Oxford: Oxford University Press, pp. 236-251.

Le Roex A.P., Bell, D.R., Davis, P., 2003. Petrogenesis of Group I Kimberlites from Kimberley, South Africa: Evidence from Bulk-rock Geochemistry. *Journal of Petrology,* 44, 2261-2286

Li, X., Liu, W., Xu, L., 2012. Carbon isotopes in surface-sediment carbonates of modern Lake Qinghai (Qinghai –Tibet Plateau): Implications for lake evolution in arid areas. *Chemical Geology,* 300-301, 88–96

Liu, W., Li, X., Zhang, L., An, Z., Xu, L., 2009. Evaluation of oxygen isotopes in carbonate as an indicator of lake evolution in arid areas: The modern Qinghai Lake, Qinghai–Tibet Plateau. *Chemical Geology,* 268, 126-136

Lowe, D. R., 1982. Sediment gravity flows: II. Depositional models with special reference to the deposits of high-density turbidity currents. *Journal of Sedimentary Petrology*, Vol. 52, No. 1, pp. 279-297.

Maier, E., and Titschack J., 2010. Spondylus gaederopus: A new Mediterranean climate archive - Based on high-resolution oxygen and carbon isotope analyses. *Palaeogeography, Palaeoclimatology, Palaeoecology,* 291 228 –238

Marean C.W., 2010. Pinnacle Point Cave 13B (Western Cape Province, South Africa) in context: The Cape Floral kingdom, shellfish, and modern human origins. *Journal of Human Evolution.* 59, 425-443.

Mazus, H., 1999. A preliminary report on Palynology, mineralogy, stable isotopes, sedimentology and palaeoenvironmental reconstruction of the Kalkkop Crater, Eastern Cape. *Council for Geoscience*. Report number 1999-0244,

Melosh, H.J., 1989. Impact cratering: A geologic process. *Oxford University Press*, New York. 245

Metwally, A.A.A., 2011. Palynological analysis of the holocene section of a new core from Tswaing Crater, South Africa. MSc Thesis, University of the Witwatersrand.

Midgley J.J., Harris C., Harington A. and Potts A.J. 2012. Geochemical perspective on origins and consequences of Heuweltjie formation in the southwestern cape, South Africa. South African Journal of Geology 115, 577-588.

Mikova J., and Denkova, P., 2007. Modified chromatographic separation scheme for Sr and Nd isotope analysis in geological silicate samples. *Journal of Geosciences*, 52, 221–226

Naylor, M.A., 1980. The origin of inverse grading in muddy debris flow deposits-a review. *Journal of Sedimentary Petrology*. 50, 1111-1116.

Nuhfer, E.B., Anderson, R.Y., Bradbury, J.P., and Dean, W.E., 1993, Modern sedimentation in Elk Lake, Clearwater County, Minnesota, *in*, Bradbury, J.P., and Dean, W.E., eds., Elk Lake, Minnesota: Evidence for Rapid Climate Change in the North-Central United States. *Geological Society of America Special Paper.* 276, 75–96.

Öberg, H., Norström, E., Ryner, M.M., Holmgren K., Westerberg, L.O., Risberg, J., Eddudóttir S.D., Andersen, T.J., Muzuka, A., 2013. Environmental variability in northern Tanzania from AD 1000 to 1800, as inferred from diatoms and pollen in Lake Duluti. *Palaeogeography, Palaeoclimatology, Palaeoecology.* 374, 230–241

Ohlendorf, C., and Sturm. M., 2001. Precipitation and Dissolution of Calcite in a Swiss High Alpine Lake. *Arctic, Antarctic, and Alpine Research*. 33: 410-417.

Park, L.E., Cohen, A.S., 2011. Paleoecological response of ostracods to early Late Pleistocene lake-level changes in Lake Malawi, East Africa. *Palaeogeography, Palaeoclimatology, Palaeoecology* 303, 71–80

Parker, A., Wonnacotta, R.T., Merry. C.L., El-Gelil, Abd., Combrinck, W.L., Combrink, A., 2011. Review of recent research and activities in geodesy in South Africa: 2007 – 2010. *National report to the xxv general assembly Melbourne*, *Australia*

Partridge, T.C, Maud, R.R., 1987. Geomorphic evolution of South Africa since the Mesozoic. *South African Journal of Geology*. 90, 179–208.

Partridge, T.C., Kerr, S.J., Metcalfe, S.E., Scott, L., Talma, A.S., Vogel, J.C., 1993. The Pretoria Saltpan: a 200,000 year Southern African lacustrine sequence. *Palaeogeography, Palaeoclimatology, Palaeoecology,* 101, 317–337

Partridge, T.C., Demenocal, P.B., Lorentz, S.A., Paiker, M.J., Vojel, J.C., 1997. Orbital forcing of climate over south Africa: a 200,000-year rainfall record from the Pretoria saltpan. *Quaternary Science Reviews*, 16, 1125–1133

Partridge, T.C and Scott L., 2000. Lakes and Pans, In: The Cenozoic of Southern Africa. (Eds Partridge, T.C, Maud, R.R), *Oxford Monographs on Geology and Geophysics*, 40, 145-161.

Pedley, M.H., 2005 Tufas and Travertines, In: *Encyclopedia of Sediments and Sedimentary Rocks* (Ed. Middleton G.V), Kluwer Academic Publishers, Dordrecht; 753-754

Pekar, S.F and DeConto, R.M., 2006. High-resolution ice-volume estimates for the early Miocene: evidence for a dynamic ice sheet in Antarctica. *Palaeogeography, Palaeoclimatology, Palaeoecology*, 231, 101–109

Philander, S. G and Fedorov, A. V. 2003. Role of the tropics in changing the response to Milankovich forcing some three million years ago, *Paleoceanography* 18, 1045

Pike, R.J., 1981, Meteorite Craters: Rim Height, Circularity, and Gravity Anomalies. *Lunar and Planetary Science,* XII, 842-844.

Platt, N.H and Wright, V.P., 1991, Lacustrine carbonates: facies models, facies distributions and hydrocarbon aspects. *Special Publications of the International Association of Sedimentologists,* 13, 57-74

Potts, A.J., Midgley J.J., Harris C., 2009. Stable isotope and ^{14}C study of biogenic calcrete in a termite mound, Western Cape, South Africa, and its palaeoenvironmental significance. *Quaternary Research*, 72, 258–264

Prentice, M.L and Matthews, R.K., 1988. Cenozoic ice-volume history: development of a composite oxygen isotope record. *Geology* 16, 963–966

Reimold, W.U., Le Roux, E.G., Koeberl, C. and Shirey, S.B., 1993. Kalkkop Crater, Eastern Cape-A new impact crater in South Africa. *Lunar Planetary Science,* XXIV, 1197-1198.

Reimold W.U., Koeberl C and Reddering J.S., 1998. The 1992 drill core from the Kalkkop impact crater, Eastern Cape Province, South Africa: stratigraphy, petrography, geochemistry and age, *Journal of African Earth Sciences,* 26, 573-592

Reimold, W.U., 1998.Meteorites and Meteorite Craters. *South African Astronomical Observatory* (SAAO).

Ringrose, S., Harris, C., Huntsman-Mapila,P., Vink, B.W., Diskins,S., Vanderpost, C., Matheson,W., 2009, Origins of strandline duricrusts around the Makgadikgadi Pans (Botswana Kalahari) as deduced from their chemical and isotope composition. *Sedimentary Geology*, 219, 262-279

Reineck, H. E and Singh I. B., 1975. Depositional Sedimentary Environments: With Reference to Terrigenous Clastics, Springer-Verlag.

Roberts, D. L., Matthews, T., Herries, A.I.R., Boulter, C., Scott, L., Musekiwa, C., Mthembi, P., Browning, C. Smith, R.M.H., Haarhoff, P., Bateman, M. D., 2011. Regional and Global Context of the Late Cenozoic Langebaanweg (LBW) Palaeontological Site: West Coast of South Africa. *Earth-Science Reviews* 106, 191–214.

Roddy, D. J. and Shoemaker E. M., 1995. Meteor Crater (Barringer Meteorite Crater), Arizona: summary of impact conditions. *Meteoritics* 30: 567.

Round, F. E and Crawford, R. M., 1990. The Diatoms. Biology and Morphology of the Genera. *Cambridge University Press*, UK.

Schmieder, M and Buchner, E., 2008. Dating impact craters: Palaeogeographic versus isotopic and stratigraphic methods-a brief case study, *Geology Magazine*.145, 586-590

Scott, L., 1999. Vegetation history and climate in the Savanna biome South Africa since 190,000 ka: a comparison of pollen data from the Tswaing Crater (the Pretoria Saltpan) and Wonderkrater. *Quaternary International.* 57–58, 215–223

Scott, L., 2000. Pollen, In: The Cenozoic of Southern Africa. (Eds Partridge, T.C, Maud, R.R), *Oxford Monographs on Geology and Geophysics*,40, 339-350.

Shanahan, T.M., McKay, N., Overpeck, J.T., John A. Peck, J.A., Scholz,C. Heil Jr.,C.W., King,J., 2013. Spatial and temporal variability in sedimentological and geochemical properties of sediments from an anoxic crater lake in West Africa: Implications for paleoenvironmental reconstructions. *Palaeogeography, Palaeoclimatology, Palaeoecology*.374, 96-109

Shanahan, T.M., Overpeck J.T., Wheeler C.W., Beek J.W., Pigati J.S., Talbot M.R., Scholz C.A., Peck J, King J.W., 2006. Paleoclimatic variations in West Africa from a record of late Pleistocene and Holocene lake level stands of Lake Bosumtwi, Ghana. *Palaeogeography. Palaeoclimatology. Palaeoecology*., 242, 287–302

Siesser, W.G., 1980. Late Miocene origin of the Benguela Upswelling System off Northern Namibia. *Science* 208, 283–285.

South African Weather Bureau, 1986. Climate of South Africa. *Publication WB*, 40, 474

Taljaard, J.J., 1996. Atmospheric circulation systems, synoptic climatology and weather phenomena of South Africa. Part 6, *Rainfall in South Africa*, 98 pp.

Talma A.S and Netterberg, F., 1983. Stable Isotope abundances in calcretes. *Geological Society, London, Special Publication,* 11, 221-233

Tucker, M.E and Wright, V.P., 1990. Carbonate sedimentology. *Blackwell Scientific Publications, Oxford*. 482pp

Tyson, P.D., 1999. Late-Quaternary and Holocene palaeoclimates of southern Africa: a synthesis. *South African Journal of Geology*. 102, 335–349.

Valero-Garcés B.L., Laird K.R., Fritz S.C., Kelts K., Ito E., Grimm E.C., 1997. Holocene Climate in the Northern Great Plains Inferred from Sediment Stratigraphy, Stable Isotopes, Carbonate Geochemistry, Diatoms, and Pollen at Moon Lake, North Dakota. *Quaternary research*. 48**,** 359–369

Valero-Garcés, B.L., Delgado-Huertas, A., Navas, A., Machín, J., González-Sampériz, P., Kelts,K, 2000. Quaternary palaeohydrological evolution of a playa lake: Salada Mediana, central Ebro Basin, Spain. *Sedimentology* 47, 1135-1156.

Van Geldern, R., Joachimski, M.M., Day, J., Jansen, U., Alvarez, F., Yolkin, E.A., Ma, X.P., 2006. Carbon, oxygen and strontium isotope records of Devonian brachiopod shell calcite. *Palaeogeography, Palaeoclimatology, Palaeoecology*, 240, 47-67

Wittkop, C., Teranes, J., Dean, W.E., and Guilderson, T. 2009. A lacustrine carbonate record of Holocene seasonality and climate. *Geology* . 37, p. 695-698.

Zhao, Y., Zheng, Y., Chen, F., 2009. Trace element and strontium isotope constraints on sedimentary environment of Ediacaran carbonates in southern Anhui, South China. *Chemical Geology*, *265, 3–4*, *345-362*

Zolitschka, B., Schabitz, F., Lucke, A., Corbella, H., Ercolano, B., Fey, M., Haberzettl, T., Janssen, S., Maidana, N., Mayr, C., Ohlendorf, C., Oliva, G., Paez, M.M., Schleser, G.H., Soto, J., Tiberi, P., Wille, M., 2006. Crater lakes of the Pali Aike volcanic field as key sites for paleoclimatic and paleocological reconstructions in Southern Patagonia, Argentina, *Journal of South American earth science*, 21, 294-309

10. APPENDICES

APPENDIX A: KALKKOP CRATER

A1: Surface of the crater

A2: Borehole KK1

A3: Borehole KK1

A4: Rock samples collected on the surface of the Kalkkop Crater

APPENDIX B: KALKKOP BOREHOLE KK1 THIN SECTIONS

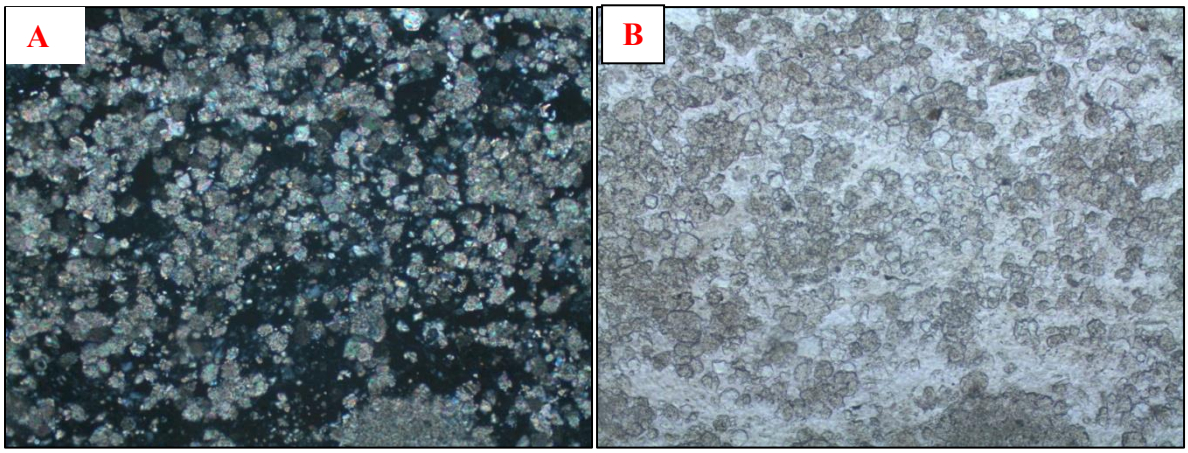

A: 49 3 ppl 1mm fov detail texture xpl. B: 49 3 ppl 1mm fov detail texture

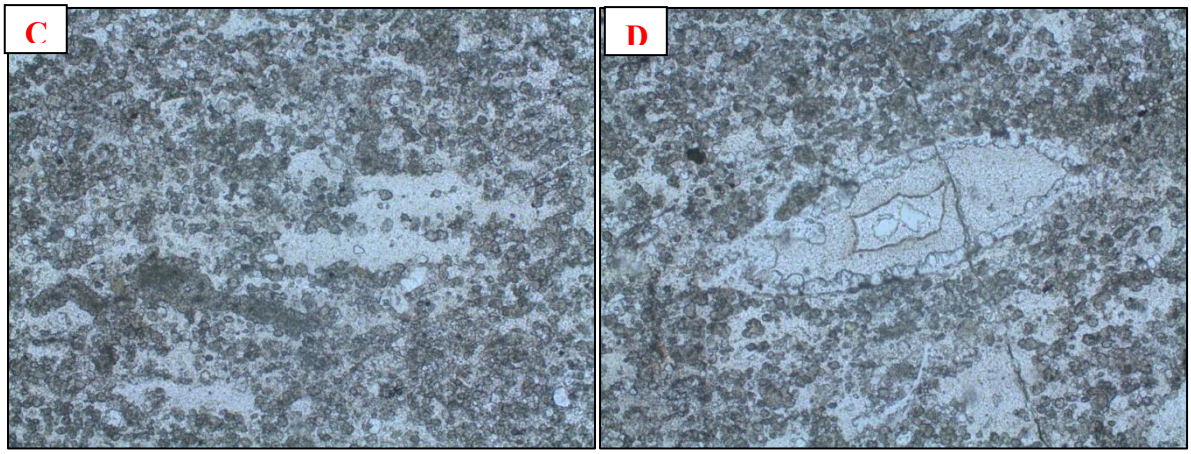

C: 49 3 ppl 2mm fov detail 2, D: 49 3 ppl 2mm fov detail

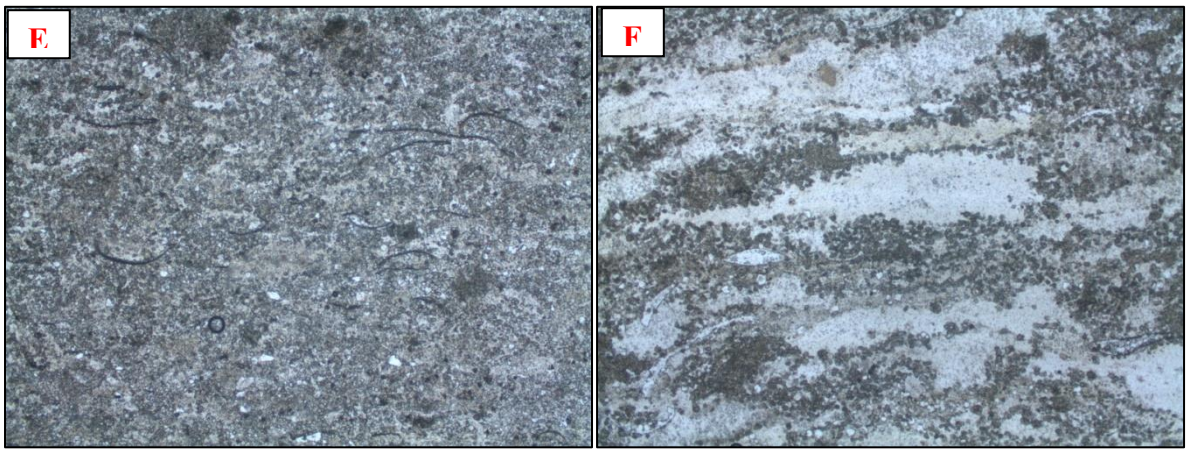

E: 49 3 ppl 4mm fov top is up 2, F: 49 3 ppl 4mm fov top is up layering

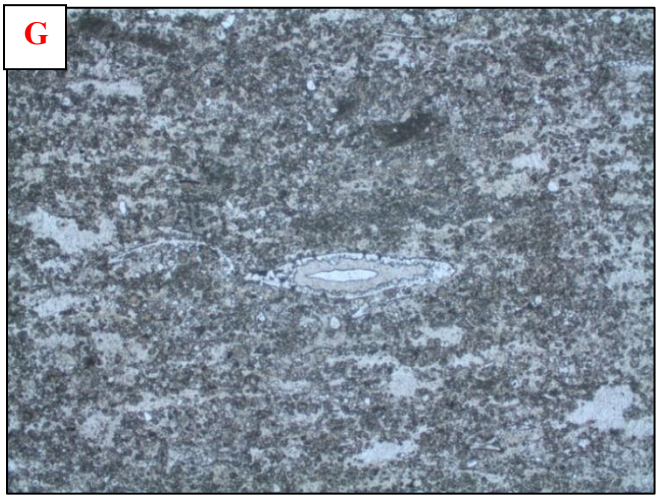

G: 49 3 ppl 4mm fov top is up

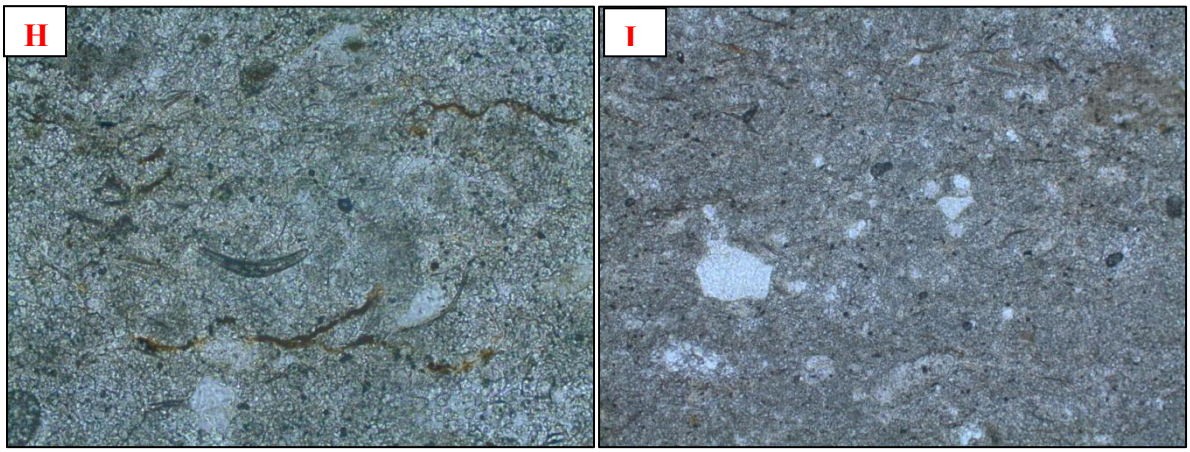

H: 66 83 m ppl 1mm fow top is down, I: 66 83 m ppl 2mm fow top is down

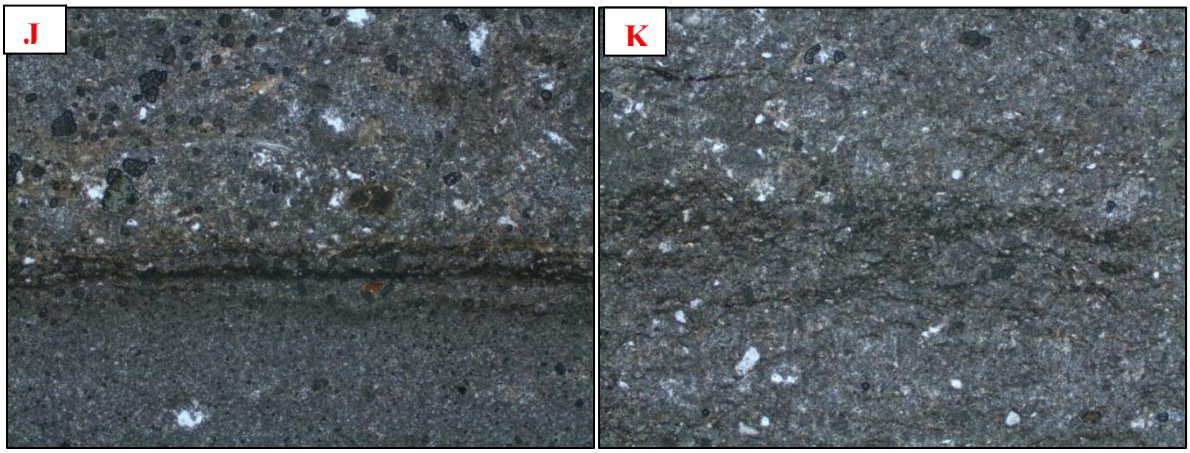

J: 66 83 m ppl 4mm fow top is down layer + chl + bi, K: 66 83 m ppl 4mm fow top is down layering

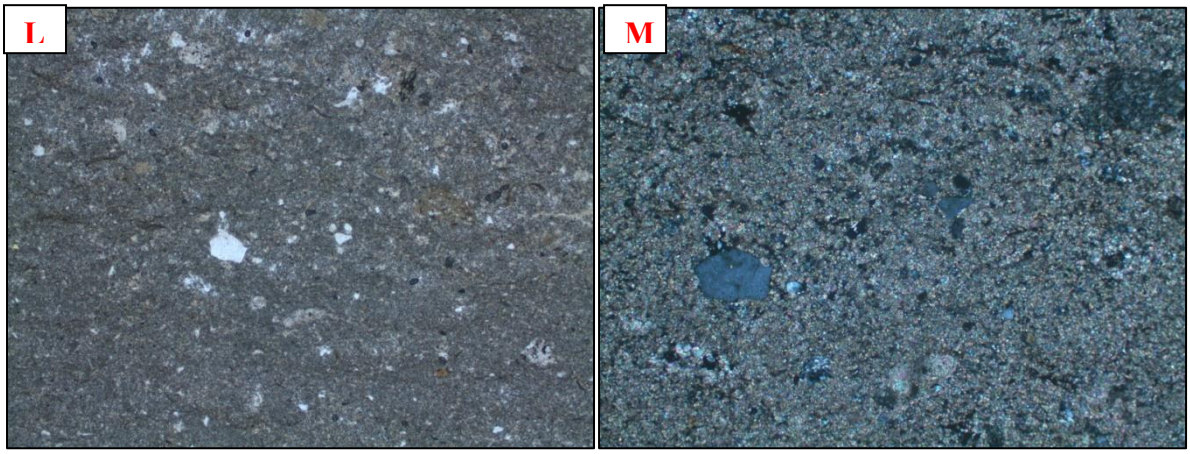

L: 66 83 m ppl 4mm fow top is down, M: 66 83 m xpl 2mm fow top is down

APPENDIX C:

C1: Kalkkop Temperature calculations

Sample	depth	$\delta^{18}O$(‰) PDB	$\delta^{18}O$ SMOW	a -2.8 water	temp -2.8	a 0 water	temp 0 water	a +5	temp +5	a +10	temp +10
BH-KK1	0	-4.27	26.51	1.029392	22.4	1.02651	36.3	1.0214028	66.9	1.016346	108.5
BH-KK2	0	-4.33	26.45	1.02933	22.7	1.026448	36.6	1.0213416	67.3	1.016285	109.1
BH-KK3	0	-4.39	26.39	1.02927	22.9	1.026388	37.0	1.021282	67.7	1.016226	109.7
BH-KK5	0	-3.35	27.46	1.03034	18.2	1.027455	31.5	1.0223436	60.5	1.017282	99.6
BH-KK7	0	-0.67	30.22	1.033112	7.0	1.030219	18.7	1.0250937	43.9	1.020019	76.9
POM01/0.4M	0.4	7.93	39.08	1.041998	-21.7	1.03908	-13.3	1.0339104	4.0	1.028792	25.1
POM02/0.9M	0.9	7.37	38.51	1.041429	-20.2	1.038513	-11.6	1.033346	6.1	1.02823	27.8
POM03/2.2M	2.2	7.81	38.97	1.041882	-21.4	1.038965	-13.0	1.0337962	4.4	1.028678	25.7
POM04/4.8M	4.8	8.11	39.27	1.042187	-22.2	1.039268	-13.9	1.0340979	3.3	1.028979	24.3
POM05/5.1M	5.1	6.57	37.68	1.040597	-17.8	1.037683	-9.0	1.0325204	9.3	1.027409	31.8
POM07/6.35M	6.35	6.53	37.64	1.040557	-17.7	1.037644	-8.9	1.0324812	9.4	1.02737	32.0
POM08/7.22M	7.22	6.90	38.02	1.040938	-18.8	1.038023	-10.1	1.0328588	7.9	1.027746	30.1
POM 45	10.5	5.38	36.45	1.039363	-14.2	1.036453	-5.0	1.0312963	14.2	1.026191	38.0
POM 46	11.12	7.40	38.54	1.041453	-20.2	1.038537	-11.7	1.0333697	6.0	1.028254	27.7
POM 47	11.2	6.80	37.92	1.040837	-18.5	1.037923	-9.7	1.0327593	8.3	1.027647	30.6
POM 48	11.23	7.23	38.36	1.04128	-19.7	1.038364	-11.1	1.0331981	6.6	1.028083	28.5
POM 49	11.3	6.56	37.67	1.040585	-17.8	1.037672	-8.9	1.032509	9.3	1.027398	31.8
POM 50	11.33	6.84	37.96	1.040879	-18.6	1.037965	-9.9	1.0328006	8.2	1.027688	30.4
POM 51	15.3	7.45	38.59	1.041506	-20.4	1.038589	-11.8	1.0334223	5.8	1.028306	27.4
POM09/18.4M	18.44	7.38	38.52	1.041433	-20.2	1.038517	-11.6	1.0333503	6.1	1.028235	27.8
POM10/20M	20	6.13	37.23	1.040144	-16.5	1.037231	-7.5	1.032071	11.0	1.026962	34.0
POM11/24.3M	24.3	6.19	37.29	1.040204	-16.7	1.037292	-7.7	1.0321312	10.8	1.027022	33.7
POM12/26.2M	26.2	6.10	37.19	1.040106	-16.4	1.037194	-7.4	1.032034	11.2	1.026925	34.2
POM13/31.8M	31.8	4.47	35.52	1.038426	-11.3	1.035518	-1.8	1.0303662	18.1	1.025265	43.0
POM14/32.2M	32.2	4.72	35.78	1.038687	-12.1	1.035778	-2.7	1.0306251	17.0	1.025523	41.6
POM1532.5M	32.5	5.96	37.05	1.039961	-15.9	1.037049	-6.9	1.0318897	11.8	1.026781	34.9
POM16/35M	35	6.55	37.66	1.040575	-17.7	1.037661	-8.9	1.0324986	9.3	1.027387	31.9
POM17/37M	37	3.83	34.86	1.037762	-9.2	1.034856	0.5	1.0297075	21.0	1.02461	46.7
POM18/38.11M	38.11	3.86	34.89	1.037796	-9.3	1.03489	0.4	1.029741	20.8	1.024643	46.5
POM19/38.7M	38.7	4.26	35.30	1.038204	-10.6	1.035297	-1.0	1.0301465	19.1	1.025047	44.2
POM20/39.8M	39.8	4.10	35.14	1.038044	-10.1	1.035137	-0.4	1.0299871	19.8	1.024888	45.1
POM21/42M	42	3.84	34.87	1.037771	-9.3	1.034865	0.5	1.0297166	20.9	1.024619	46.6
POM22/43.8M	43.8		30.91	1.033805	4.4	1.03091	15.8	1.0257811	40.2	1.020703	71.8
POM23/44.4M	44.4	3.67	34.70	1.037604	-8.7	1.034698	1.1	1.0295506	21.7	1.024454	47.6
POM 52	45.3	5.11	36.18	1.039086	-13.3	1.036176	-4.0	1.0310213	15.3	1.025917	39.4
POM 53	46.9	4.21	35.25	1.038153	-10.5	1.035246	-0.8	1.0300954	19.3	1.024996	44.5
POM 54	46.94	6.37	37.48	1.04039	-17.2	1.037476	-8.3	1.0323149	10.1	1.027204	32.8
POM 55	47	6.40	37.50	1.040417	-17.3	1.037504	-8.4	1.0323426	10.0	1.027232	32.6
POM 56	47.26	3.70	34.72	1.037625	-8.8	1.03472	1.0	1.0295721	21.6	1.024475	47.5
POM 57	48.41	2.78	33.78	1.036681	-5.7	1.033779	4.5	1.0286354	25.9	1.023543	53.0
POM26/49M	49	2.62	33.61	1.036513	-5.2	1.033611	5.1	1.0284684	26.7	1.023377	54.0
POM 58	52.76	3.48	34.50	1.037407	-8.1	1.034502	1.8	1.029355	22.6	1.024259	48.7
POM 59	53.3	3.87	34.90	1.03781	-9.4	1.034904	0.4	1.0297557	20.8	1.024658	46.4
POM 60	54.4	4.64	35.69	1.038603	-11.9	1.035695	-2.4	1.030542	17.4	1.02544	42.0
POM 61	54.9	3.57	34.59	1.037492	-8.4	1.034587	1.5	1.0294394	22.2	1.024343	48.2
POM35/59.3M	59.3	2.26	33.24	1.036139	-3.9	1.033238	6.5	1.0280972	28.4	1.023008	56.3
POM36/60M	60	2.53	33.51	1.036416	-4.8	1.033514	5.5	1.0283718	27.1	1.023281	54.6
POM39/63.2	63.2	1.27	32.22	1.03512	-0.4	1.032222	10.4	1.0270867	33.4	1.022002	62.8
POM40/64.1M	64.1	1.29	32.24	1.035139	-0.5	1.032241	10.4	1.0271051	33.3	1.02202	62.7
POM41/65.4M	65.4	1.41	32.36	1.035263	-0.9	1.032364	9.9	1.0272278	32.7	1.022143	61.9
POM42/67M	67	0.09	31.00	1.033896	4.0	1.031001	15.4	1.0258718	39.7	1.020793	71.2
POM43/70.1M	70.1	0.07	30.98	1.033875	4.1	1.03098	15.5	1.0258512	39.8	1.020773	71.3
POM 62	87.03	0.27	31.19	1.034086	3.3	1.031191	14.6	1.0260604	38.7	1.020981	69.8
POM 63	87.19	0.18	31.10	1.033994	3.7	1.031099	15.0	1.0259688	39.2	1.02089	70.5
POM 64	87.48	-1.20	29.67	1.032559	9.1	1.029668	21.2	1.0245454	47.1	1.019473	81.1
POM 65	87.51	0.04	30.95	1.033844	4.2	1.03095	15.6	1.0258206	40.0	1.020742	71.5
POM 66	87.63	-2.93	27.88	1.030771	16.4	1.027884	29.4	1.0227705	57.8	1.017707	95.8
POM 67	87.69	-3.25	27.56	1.03044	17.8	1.027555	31.0	1.0224428	59.9	1.017381	98.7
POM44/88.4M	88.4	-3.85	26.94	1.029821	20.5	1.026938	34.1	1.0218286	64.0	1.01677	104.4

C2: Kalkkop Groundwater analyses

Sample	%cc	$\delta^{13}C$ PDB	$\delta^{18}O$ SMOW	a -2 water	temp -2	a - 3water	temp - 3water	a -4	temp -4	a -5	temp -5	a -6	temp - 6
SO1	86.0	-1.78	24.84	1.0269	34.3	1.0279	29.2	1.0290	24.4	1.0300	19.7	1.0310	15.3
SO2	83.0	-3.45	25.17	1.0272	32.7	1.0283	27.7	1.0293	22.9	1.0303	18.3	1.0314	13.9
SO3	84.8	1.45	26.86	1.0289	24.6	1.0299	19.9	1.0310	15.5	1.0320	11.3	1.0331	7.2
SO4	81.7	-0.88	25.45	1.0275	31.3	1.0285	26.3	1.0296	21.6	1.0306	17.1	1.0316	12.8
SO5	78.1	-0.77	25.55	1.0276	30.8	1.0286	25.9	1.0297	21.1	1.0307	16.7	1.0317	12.4
SO6	41.2	-1.29	25.31	1.0274	32.0	1.0284	27.0	1.0294	22.2	1.0305	17.7	1.0315	13.4
SO7	55.5	1.55	27.27	1.0293	22.7	1.0304	18.1	1.0314	13.8	1.0324	9.6	1.0335	5.6
SO8	71.5	1.49	25.57	1.0276	30.7	1.0287	25.8	1.0297	21.1	1.0307	16.6	1.0318	12.3
SO9	3.7	-8.97	18.29	1.0203	74.5	1.0214	67.2	1.0224	60.3	1.0234	53.8	1.0244	47.7
SO10	13.9	-2.02	23.47	1.0255	41.6	1.0266	36.1	1.0276	30.9	1.0286	26.0	1.0297	21.2
SO11	28.2	2.45	29.42	1.0315	13.4	1.0325	9.3	1.0336	5.3	1.0346	1.5	1.0356	-2.2
SO12	81.5	-0.59	27.46	1.0295	21.8	1.0305	17.3	1.0316	13.0	1.0326	8.9	1.0337	4.9
SO13	15.3	-1.51	24.54	1.0266	35.9	1.0276	30.7	1.0287	25.8	1.0297	21.1	1.0307	16.6
SO14	6.1	-5.80	19.37	1.0214	66.8	1.0224	59.9	1.0235	53.5	1.0245	47.4	1.0255	41.6
SO15	30.8	-0.69	26.25	1.0283	27.4	1.0293	22.6	1.0304	18.1	1.0314	13.7	1.0324	9.6
SO16	1.0	-14.58	16.30	1.0183	90.3	1.0194	82.0	1.0204	74.2	1.0214	66.9	1.0224	60.0

APPENDIX D:

D1: Borehole KK2

D2: Borehole KK3